OUKA
Osaka University Knowledge Archive

Title	A study on the thermal-hydraulic structure in subcooled flow boiling
Author(s)	Rouhollah, Ahamdi
Citation	大阪大学, 2013, 博士論文
Version Type	VoR
URL	https://hdl.handle.net/11094/24962
rights	
Note	

Osaka University Knowledge Archive : OUKA

https://ir.library.osaka-u.ac.jp/

Osaka University

Doctoral Dissertation

A study on the thermal-hydraulic structure in subcooled flow boiling

Rouhollah Ahmadi

January 2013

Graduate School of Engineering,
Department of Mechanical Engineering
Osaka University

Copyright

by

Osaka University

2013

A Study on the Thermal-Hydraulic Structure in Subcooled Flow Boiling

(サブクール流動沸騰の熱流動構造の研究)

APPROVED BY
SUPERVISING COMMITTEE:

Committee:

Isao Kataoka , Supervisor

Fumiteru Akamatsu

Tomio Okawa

Kenji Yoshida

A Study on the Thermal-Hydraulic Structure in Subcooled Flow Boiling

(サブクール流動沸騰の熱流動構造の研究)

by

Rouhollah Ahmadi

Dissertation

Presented to the Faculty of the Graduate School of Engineering of

Osaka University

in Partial Fulfillment

of the Requirements

for the Degree of

Doctor of Philosophy in Mechanical Engineering

Osaka University

January 2013

Dedication

To my kind parent

and

To my patient spouse

who have encouraged and inspired me during this project.

Abstract

A Study on the Thermal-Hydraulic Structure in Subcooled Flow Boiling

(サブクール流動沸騰の熱流動構造の研究)

Rouhollah Ahmadi, PhD

Osaka University, 2012

Supervisor: Isao Kataoka

Prediction of the void fraction profile in the subcooled flow boiling region is of considerable practical importance in evaluating the two-phase flow instabilities in boiling channels and the neutron moderation and fuel burnup in nuclear reactor cores. In this study, bubble dynamics in water subcooled flow boiling was investigated through visualization using a high-speed camera. The test section is a vertical rectangular channel, and a copper surface used as a heated surface. Main experimental parameters are the pressure, mass flux, liquid subcooling and surface wettability. However, considering the high-temperature and radiation environments in nuclear reactors, the surface of low contact angle is more practicable used as the heated surface. On the surface with low contact angle, several experiments were conducted under low void fraction conditions close to the onset of nucleate boiling. It is observed that no bubbles stayed at the nucleation sites at which they were formed. Depending on the experimental conditions, the following two types of bubble behavior were observed after nucleation: (1) lift-off

from the heated surface followed by collapsing rapidly in subcooled bulk liquid due to condensation, and (2) sliding along the vertical heated surface for a long distance. Since the bubble lift-off was observed only when the wall superheat was high, the boundary between the lift-off and the sliding could be determined in terms of the Jakob number. Based on the bubble behavior in high wettable surface, discussion was made for the possible mechanisms governing the bubble dynamics. Using visual investigation, mechanism of net vapor generation is developed for low pressure and moderate pressure condition.

In low pressure condition, at high liquid subcooling close to the condition of the onset of nucleate boiling, all the bubbles were lifted off the heated surface immediately after the nucleation to disappear quickly in the subcooled bulk liquid due to condensation. It was found that the void fraction did not increase significantly unless the liquid subcooling became low enough for some bubbles to be reattached to the heated surface after the lift-off. When the reattachment took place, the bubble lifetime was substantially elongated since the bubbles slid up the vertical heated surface for a long distance after the reattachment. It was concluded that in the atmospheric pressure conditions tested in this work, the bubble reattachment to the heated surface was a key phenomenon to cause the sharp increase of the void fraction at the point of net vapor generation.

Observations in moderate pressure show that as bubbles nucleate on the heated surface, they depart from nucleation sites and slide on the heated surface. In the course of sliding, some bubbles grow and travel to the downstream flow and some bubbles collapse in subcooled liquid. Near the condition of ONB, because only few small bubbles nucleate on the heated surface, vaporization rates and therefore void fractions remain in low value. It is found that when the condition of OSV is reached, the vaporization rates vigorously increase while condensation rates remain low. The measurement results reveal that, the

volume of the collapsing bubbles is a small fraction of whole bubbles volume, owing to their small size. In contrast, the production of few big sliding bubbles in a wide ranges of bubble size make the vigorous increase of vaporization rates, right after the condition of OSV. In following, it is revealed that the big sliding bubbles are mainly formed in the wake region of the preceding sliding bubbles. Therefore, the significant increase of the void fraction at OSV is contributed to the formation of big sliding bubbles which is induced by the wake-effect of the preceding sliding bubbles.

Finally, the influence of contact angle on bubble dynamics and void evolution is explored in visual investigation. Close to ONB condition, it is observed that bubble behavior is essentially different as surface contact angle is changed. Bubbles stick to nucleation site in hydrophobic surface, and they depart from nucleation site in hydrophilic surface. In hydrophobic surface, bubble departure as a preliminary triggering mechanism is observed at NVG condition. In atmospheric pressure condition, it is observed that in some nucleation sites bubble departure follows by bubble reattachment to contribute void fraction increase sharply when the condition of OSV reaches. In elevated pressure, bubble departure coincides with the wake-effect of the preceding sliding bubble to cause void fraction significantly increases at OSV.

Acknowledgements

The author would like to express deepest sense of gratitude to Professor Tomio Okawa for continuous guidance and numerous discussions throughout this work, without which this work could not be completed. A special appreciation is also due to Professor Isao Kataoka and Professor Kenji Yoshida for their support during performing experiments. Thanks are expressed to the Laboratory staffs and members of Interphase Heat and Mass Transfer of Osaka University and especially Tatsuya Ueno who has done pleasant corporation in this project.

I am very thanks also the Ministry of Science, Research and Technology of Iran due to its financial supports of my study and life expense throughout this course.

Table of Contents

List of Tables

List of Figures

Nomenclatures

A	cross-sectional area (m^2)
A_h	heated surface area (m^2)
d	diameter (m)
$d_{b,p}$	preceding bubble diameter (m)
D_H	equivalent hydraulic diameter
$\overline{f}$	mean bubble release frequency (1/s)
G	mass flux (kg/m^2s)
h	heat-transfer coefficient
h_{fg}	latent heat of vaporization (J/kg)
Ja	Jakob number
k	thermal conductivity (W/m·K)
l	depth (m)
n	nucleation site density ($1/cm^2$)
N_b	the number of bubbles
N_{im}	the number of images
N_s	the number of nucleation sites
Nu	Nusselt number
P	pressure (Pa)
Pe	Peclet number
Pr	Prandtl number
q_w	heat flux (W/m^2)
R	radius (m)
Re	Reynolds number

St	Stanton number
T	temperature (K)
t_0	recording time (s)
u	velocity (m/s)
V	volume (m^3) or voltage
w	width (m)
x_{eq}	thermal-equilibrium vapor quality
y	distance from the wall (m)
Y_b^+	dimensionless distance from the wall to bubble tip
z	axial coordinate (m)

Greek symbols

α	void fraction
Γ_C	condensation rate (kg/m^3s)
Γ_{Net}	net vaporization rate (kg/m^3s)
$\Gamma_{Net,NWA}$	non-wake-affected net vaporization rate (kg/m^3s)
$\Gamma_{Net,WA}$	wake-affected net vaporization rate (kg/m^3s)
Γ_V	vaporization rate (kg/m^3s)
γ_C	amount of condensation (kg)
γ_V	amount of vaporization (kg)
ΔT_{sub}	liquid subcooling (K)
ΔT_w	wall superheated (K)
δ_{shl}	superheated layer thickness (m)
Π_{att}	reattachment probability
φ	contact angle (degree)

ρ	density (kg/m^3)
σ	surface tension (N/m)
τ_w	wall shear stress
ω	threshold factor

Superscript

a	apparent

Subscripts

0	visualization section
1	calculated by Eq. 1
2	calculated by Eq. 2
b	bubble
bulk	bulk
f	disappearance from the visualization section
g	vapor phase
h	heated area
l	liquid
last	disappearance from the visualization section
lift	lift-off
lta	local time-averaged
max	maximum
mean	mean value
min	minimum

NWA	non-wake-affected
sat	saturation
std	standard deviation
thr	threshold
v	vapor
WA	wake-affected
x	horizontal
y	vertical

Abbreviation

NVG	net vapor generation
ONB	onset of nucleate boiling
OSV	onset of significant void

CHAPTER 1 INTRODUCTION

1.1 Literature Review

Subcooled liquid, in two-phase heat and mass transfer process, is a state of a liquid when the temperature is below the boiling point at a given pressure. When subcooled liquid is injected to a heated channel, liquid temperature and wall temperature rise gradually in the axial direction in the single-phase region. Formation of the first bubbles or the onset of nucleate boiling (ONB) is then permitted at the location where the liquid temperature in the close proximity to the heated wall becomes high enough [1,2]. It is known that void fraction is low just downstream of the location of ONB, and a rapid increase in the void fraction commences further downstream from the ONB point [3] (see Fig. 1.1). This phenomenon is commonly regarded as the net vapor generation (NVG) or the onset of significant void (OSV). Although the void fraction upstream of the location of OSV is small and usually neglected, the presence of bubbles alters the mechanisms of the heat transfer and pressure loss in this region [3,4]. Accurate prediction of the void fraction in subcooled flow boiling is of considerable importance in the design and operation of nuclear power plants since it influences various parameters including the core flow rate, fuel burnup and the inception of two-phase flow instabilities [5]. Kroger and Zuber showed that the ability to predict the PNVG is of essential importance in predicting the void fraction in subcooled flow boiling accurately [6]. Furthermore, it is considered that the mechanism to cause the OSV is in close relation to the bubble behavior between the locations of ONB and OSV. For instance, it is frequently postulated

that the bubbles remain on the heated surface between the locations of ONB and OSV, but they are eventually detached from the heated surface at the location of OSV to cause a rapid increase in the void fraction [7–9]. It can hence be said that the bubble dynamics in the region between the locations of ONB and OSV are of importance for the mechanistic determinations of the heat transfer rate, pressure loss and the void fraction in subcooled flow boiling.

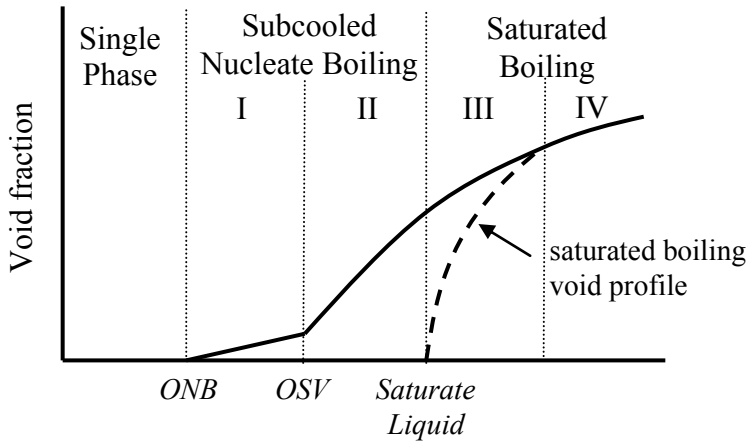

Fig. 1.1 Void fraction status in subcooled nucleate boiling

Bubble behavior in subcooled flow boiling was studied photographically by many researchers. In early work by Gunther [10], it was observed that bubbles grew and collapsed while sliding along the heated surface under the influence of main flow. In the experiments by Bibeau and Salcudean [11], bubbles slid along the heated surface before being ejected into the subcooled bulk liquid. Since the bubbles were collapsed due to condensation, they did not travel far downstream after nucleation. Zeitoun and Shoukri [12] also observed that the bubbles tended to be detached from the heated surface. They

developed an empirical correlation for the mean bubble diameter as a function of the Reynolds number, Jakob number and the boiling number. Thorncroft et al. [13] observed the bubble behavior in subcooled flow boiling using FC-87 as a working fluid. In their experiments for upflow configuration, bubble slid along the heated surface and typically did not lift off. In contrast, in downward flow configuration, bubbles were lifted off the heated surface directly from the nucleation site or after sliding for a certain distance. Situ et al. [14,15] carried out forced convection subcooled water boiling experiments using a vertical annular channel as the test section. They measured the bubble lift-off diameter, but reported that some bubbles slid along the heated surface and did not lift off the surface within the visualization region. Okawa et al. [16] studied the bubble behavior in subcooled flow boiling of water using mass flux and subcooling as the main experimental parameters. In their experiments, bubbles slid along the vertical heated surface for a long distance or lifted off the surface after sliding several bubble diameters. It was reported that sliding bubbles were observed under the condition of high mass flux and low liquid subcooling. It is also reported that the behavior of vapor bubbles produced at the nucleation cavity is dependent on the surface wettability and in some case bubble stick to its nucleation site [17].

The above literature survey reveals that bubbles in subcooled upward flow boiling may stick to nucleation site or slide on the heated surface or may lift off from the heated surface. If bubble stick to nucleation site, it in fact hinders bubble generation on the nucleation site for the period of attachment. In this case, bubble departure from nucleation site is a preliminary condition to bubble generation be continues. The experimental data by Thorncroft et al. [13] indicate that the sliding of vapor bubbles significantly enhance the heat transfer from the heated surface. Furthermore, the bubble lifetime is considerably different between the sliding and lift-off bubbles since bubbles

are usually collapsed rapidly due to condensation if they are lifted off the heated surface. The bubble dynamics would hence be in close relation to axial evolution of the void fraction in subcooled boiling region.

Because of the importance in predicting the void fraction in the subcooled boiling region, many correlations have been developed so far for the PNVG as reviewed extensively by Lee and Bankoff [18] and Warrier and Dhir [19]. In the development of the PNVG correlations, it is frequently postulated that the bubbles are attached to the heated surface just downstream of ONB and the rapid increase of the void fraction is permitted when the bubble departure from the nucleation site or the bubble lift-off from the heated surface occurs [7, 9, 20 and 21].

The point at which bubbles can depart from the wall before they suffer condensation (OSV) has been proposed to be either hydrodynamically controlled or thermally controlled. Among the early proposals for thermally controlled departure are those by Griffith et al. [22], Bowring [20], Dix [23], and Levy [7]. The first study on the OSV issue was performed by Griffith et al. [22]. They were the first to propose the idea that boiling in the channel could be divided into two distinct regions: a highly subcooled boiling region followed by a slightly subcooled region. The transition between the two regions was identified by the presence of a blanket of attached vapor bubbles on the heating surface. Also, at OSV, the evaporation rate was assumed to be exactly balanced by the condensation rate. By examining the available experimental data, Griffith et al. [22] identified the OSV point as the location where the heat transfer coefficient was five times the single-phase heat transfer coefficient, i.e.,

$$T_{sat} - T_{bulk} = \frac{q_w}{5h_l} \tag{1}$$

Where, h_l is the heat-transfer coefficient of single-phase liquid which flowing is at the same total mass flow rate.

A few years later, Bowring [20] introduced the idea that the OSV was related to the detachment of the bubbles from the heated surface. The beginning of the slightly subcooled region was fixed at the OSV point. He developed a simple empirical correlation to predict the subcooling at which OSV would most likely occur,

$$T_{sat} - T_{bulk} = \frac{\eta q_w}{G / \rho_l} \tag{2}$$

Where $\eta \times 10^6 = 14.0+0.1P$ (10<P<136 bar); P is the system pressure in bars and G, q_w and ρ_l expressed in SI units.

Another empirical correlation was developed by Dix [23]. Based on experimental observations, he argued that there existed a bubble layer on the wall and that OSV occurred when the bubbles reached a critical size and were ejected from this bubble layer into the liquid core. His empirical correlation was expressed as

$$T_{sat} - T_{bulk} = 0.00135 \frac{q_w}{h_l} \left(\mathrm{Re}_l \right)^{0.5} \tag{3}$$

The above three criteria are based on the assumption that at OSV the wall heat flux is balanced by heat removal due to liquid subcooling .

Levy [7] introduced a hydrodynamically based model. The point of bubble departure from the heated surface (NVG) is determined from a bubble force balance and the single-phase liquid turbulent temperature distribution away from the heated wall. He

considered the following forces: surface tension force, buoyancy force, and wall shear force. He speculated that bubble detachment occurred when the forces (buoyancy and drag) that tend to detach the bubble from the wall overcomes the forces (surface tension) that tend to hold the bubble to the wall. The main point of the paper by Levy is a new method of calculating the liquid subcooling at the point of bubble departure. This is different from Bowring's method [20]. Levy suggests also a certain relationship between the true local vapor weight fraction and the corresponding thermal equilibrium value. Finally, he neglects buoyancy force anfd by applying an accepted slip correlation he calculates the void fraction in subcooled boiling.

$$T_{sat} - T_{bulk} = q_w \left[\frac{1}{h_l} - \frac{\Pr Y_b^+}{\rho_l c_{pl} \sqrt{\frac{\tau_w}{\rho_l}}} \right] \tag{4}$$

Where Y_b^+ is the dimensionless distance from the wall to the bubble tip. Staub [8] added the effect of buoyancy to the Levy model.

Saha and Zuber [21] postulated that both the hydrodynamic and the heat-transfer mechanisms may apply. Thus in the low mass flow region, the heat diffusion controls the condensation process and the departure process is heat-transfer- limited, signified by the Nusselt number:

$$Nu = \frac{q_w D_H}{k_l \left(T_{sat} - T_{bulk} \right)} \tag{5}$$

Whereas for high flow rates both the heat transfer and the hydrodynamics are controlling, signified by the Stanton number:

$$St = \frac{q_w}{Gc_{pl}\left(T_{sat} - T_{bulk}\right)} \tag{6}$$

The data from various sources in rectangular, annular and circular tubes as well as for some freon data were plotted against the Peclet number, where:

$$Pe = \frac{Nu}{St} = \frac{GD_H c_{pl}}{k_l} \tag{7}$$

Saha and Zuber developed the following criteria for hydrodynamic and thermal control region:

$$Nu_{OSV} = 455 \;\; or \;\; T_{sat} - T_{bulk} = 0.0022\left(\frac{q_w D_h}{k_l}\right) \;\; for \;\; Pe < 70,000 \tag{8.1}$$

$$St_{OSV} = 0.0065 \;\; or \;\; T_{sat} - T_{bulk} = 154\left(\frac{q_w}{Gc_{pl}}\right) \;\; for \;\; Pe > 70,000 \tag{8.2}$$

The data used by Saha and Zuber [21] covered the following range of parameters for water: P = 0.1 to 13.8 MPa; G = 95 to 2760 kg/m^2 s; and q_w = 0.28 to 1.89 MW/m^2.

The correlations for PNVG commonly contain empirical constants, and their values are determined using the experimental data of the void fraction distribution. Therefore, although these correlations are useful to estimate the PNVG, it would not necessarily be guaranteed that the bubble departure or the bubble lift-off is the key phenomenon to cause NVG.

1.2 Technical Objective

In view of the present insufficient understanding of the mechanisms governing the bubble dynamics and the onset of NVG in subcooled flow boiling, the visualization studies in various condition of thermal flow seems to be clarify some aspects of subcooled flow boiling.

The first aim of this work is to identify the thermal-hydraulic conditions that affect bubble dynamics or bubble behavior in subcooled flow boiling. Based on the experimental results of bubble behavior, discussion can be made to investigate possible mechanisms to determine the bubble dynamics.

In order to develop a mechanistic explanation for the significant increase of the void fraction at OSV, moreover attention to bubble behavior the vaporization and condensation process should also sufficiently be understood in subcooled flow boiling. Hence, visual analysis of bubble generation during subcooled boiling using a high-speed camera is carried out to find the key phenomena causing the significant void increment at OSV.

Considering the high-temperature and radiation environments in nuclear reactors, the surface of low contact angle is more practicable used as the heated surface [24,25]. However, this study aims to realize effect of surface property on bubble generation and bubble behavior in subcooled flow boiling, as a final objective.

1.3 Research Outlines

This paper consists of seven chapters and the contents of each chapter are as follows:

Chapter 2 provides information related to experimental activities. In particular, this chapter deals with the experimental facilities, instrumentations and experimental procedures.

Chapter 3 reports experimental data measured at boiling incipience in subcooled flow boiling. Bubble dynamics and bubble behaviors are visually investigated and then parametrically categorized.

Chapter 4 reports an investigation on triggering mechanism of NVG under atmospheric pressure condition. Using visualization method vaporization and condensation of bubbles is investigated in subcooled region to find key phenomenon causes the significant void evolution at the location of OSV.

Chapter 5 presents proposed mechanism of NVG under moderate pressure condition. In elevated pressure, bubbles after formation on nucleation sites depart from their sites and slide on the heated surface. Therefore, different mechanism is developed in this chapter to explain the increase of void at OSV.

Chapter 6 reports experimental data of subcooled flow boiling tested on the various contact angle of heated surface. In this chapter influence of surface wettability on bubble behavior and void evolution at OSV is investigated.

Finally, in chapter 7 conclusions obtained in this dissertation are summarized.

References

[1] Y.Y. Hsu, On the size range of active nucleation cavities on a hating surface, Journal of Heat Transfer 84 (1962) 207–216.

[2] T. Sato, H. Matsumura, On the conditions of incipient subcooled boiling with forced convection, Bull. JSME 726 (1964) 392–398.

[3] J.G. Collier, J.R. Thome, Convective Boiling and Condensation, third ed., Oxford University Press, Oxford, 1994. pp. 325–374.

[4] N. Basu, G.R. Warrier, V.K. Dhir, Wall heat flux partitioning during subcooled flow boiling: part 1–model development, Journal of Heat Transfer 124 (2005) 131–140.

[5] S.C. Lee, S.G. Bankoff, Prediction of the onset of flow instability in transient subcooled flow boiling, Nuclear Engineering and Design 139 (1) (1993) 149-159.

[6] P.G. Kroeger, N. Zuber, An analysis of the effects of various parameters on the average void fractions in subcooled boiling, International Journal of Heat and Mass Transfer 11 (2) (1968) 211-233.

[7] S. Levy, Forced convection subcooled boiling prediction of vapor volumetric fraction, International Journal of Heat and Mass Transfer 10 (1967) 951–965.

[8] F.W. Staub, The void fraction in subcooled boiling–prediction of the initial point of net vapor generation, Journal of Heat Transfer 90 (1968) 151–157.

[9] J.T. Rogers, M. Salcudean, Z. Abdullah, D. McLeod, D. Poirier, The onset of significant void in up-flow boiling of water at low pressure and velocities, International Journal of Heat and Mass Transfer 30 (1987) 2247–2260.

[10] F.C. Gunther, photographic study of surface-boiling heat transfer to water with force convection, Journal of Heat Transfer 73 (1951) 115–123.

[11] E.L. Bibeau, M. Salcudean, A study of bubble ebullition in forced-convective subcooled nucleate boiling at low pressures, International Journal of Heat and Mass Transfer 37 (1994) 2245–2259.

[12] O. Zeitoun, M. Shoukri, Bubble behavior and mean diameter in subcooled flow boiling, Journal of Heat Transfer 118 (1996) 110–116.

[13] Thorncroft, G.E., Klausner, J.F., Mei, R., An experimental investigation of bubble growth and detachment in vertical upflow and downflow boiling, International Journal of Heat and Mass Transfer 41 (1998) 3857–3871.

[14] R. Situ, Y. Mi, M. Ishii, M. Mori, Photographic study of bubble behaviors in forced convection subcooled boiling, International Journal of Heat and Mass Transfer 47 (2004) 3659–3667.

[15] R. Situ, T. Hibiki, M. Ishii, M. Mori, Bubble lift-off size in forced convective subcooled boiling flow, International Journal of Heat and Mass Transfer 48 (2005) 5536–5548.

[16] T. Okawa, T. Ishida, I. Kataoka, M. Mori, Bubble rise characteristics after the departure from a nucleation site in vertical upflow boiling of subcooled water, Nuclear Engineering and Design 235 (2005) 1149–1161.

[17] T. Okawa, T. Harada, Y. Kotsusa, Photographic study on bubble motion in subcooled pool boiling, Journal of Engineering for Gas Turbines and Power 132 (2010) art. no. 102922.

[18] S.C. Lee, S.G. Bankoff, A comparison of predictive models for the onset of significant void at low pressures in forced-convection subcooled boiling, Journal of Mechanical Science and Technology 12 (3) (1998) 504-513.

[19] G.R. Warrier, V.K. Dhir, Heat transfer and wall heat flux partitioning during subcooled flow nucleate boiling–a review, Journal of Heat Transfer 128 (12) (2006) 1243-1256.

[20] R.W. Bowring, Physical model based on bubble detachment and calculation of steam voidage in the subcooled region of a heated channel, OECD Halden Reactor Project Report HPR-10, 1962.

[21] P. Saha, N. Zuber, Point of net vapor generation and vapor void fraction in subcooled boiling, Proceedings of the 5th International Heat Transfer Conference, Tokyo, 1974, pp. 175-179.

[22] Griffith, P. J., Clark, A., and Rohsenow, W. M. Void Volumes in Subcooled Boiling Systems. ASME paper 58-HT-19, 1958.

[23] G.E. Dix, Vapor void fraction for forced convection with subcooled boiling at low flow rates, Ph.D. Thesis, University of California, Berkeley, CA, 1971.

[24] Y. Hirose, T. Hayashi, T. Hazuku, T. Takamasa, T., Experimental study on contact angle of water droplet in high-temperature condition, Proceedings of the 14th International Conference on Nuclear Engineering, Miami, Florida, USA, 2006, Paper No. 89614.

[25] T. Takamasa, T. Hazuku, K. Okamoto, L. Mishima, M. Furuya, Radiation induced surface activation on Leidenfrost and quenching phenomena, Experimental Thermal and Fluid Science 29 (2005) 267–274.

CHAPTER 2 EXPERIMENTAL SETUP

Experimental apparatus was setup in order to study bubble dynamics and investigate mechanism of net vapor generation in upward subcooled flow boiling.

2.1 Experimental Equipment

Configuration of the experimental loop is depicted schematically in Fig. 2.1. In this study, filtrated and deionized tap water was used as a working fluid. Prior to the experiment, the water was kept boiling at least for an hour in a storage tank containing heaters for degassing. To remove air from the loop, it was vacuumed and filled with argon gas for several times. The loop was then vacuumed to supply the degassed water from the storage tank by means of pressure difference. A canned motor pump was used to drive the working fluid through the experimental loop. The electric power supplied to the pump and the openings of several needle valves were controlled to adjust the mass flow rate at desired values; a turbine flow meter was used right after the pump to measure the total mass flow rate. The fluid was preheated using two 5 kW sheath heaters to set the inlet subcooling, and then injected to a test section. It should be noted that a small part of liquid was delivered to a bypass line as an auxiliary system to control the system pressure. The bypass line consisted of a stainless steel round tube, and it was heated ohmically by passing a DC current to generate steam-water two-phase flow inside of it. The DC power supplied 0-60V and 0-1000A, and it was controlled to adjust the system

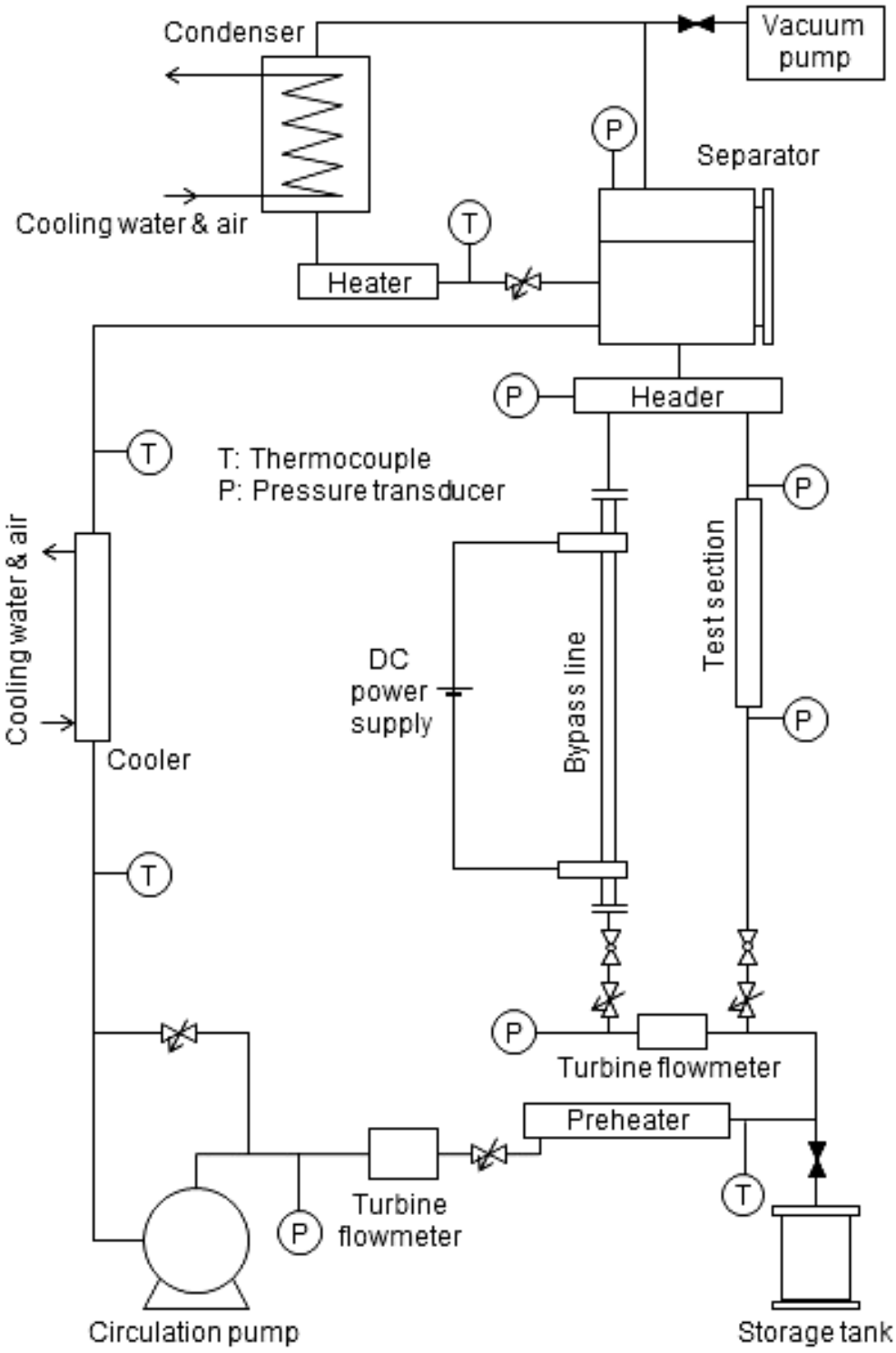

Fig. 2.1 Schematic diagram of the experimental loop

pressure. The flow rate in the bypass line was measured using a turbine flow meter. The remaining liquid entered the test section whose configuration is described later. After exiting the bypass line or the test section, the steam-water mixture entered the separator through an outlet header. Vapor phase was then sent to a condenser. The heat transfer rate in the condenser was also controlled to maintain the system pressure at desired values. The fluid temperature was reduced to a subcooling state at the cooling section before returning to the circulation pump. Temperatures and pressures were measured using K-type thermocouples and pressure transducers at the locations shown schematically in Fig. 2.1.

2.1 Test Section

A schematic diagram of the test section is depicted in Figure 2.2. A main body of the test section was made of stainless steel. A copper block containing two 1.2 kW cartridge heaters was set on the main body to construct the flow channel. The cross sectional flow area was rectangular in shape of 10 × 20 mm. As delineated in the top view in Fig. 2.2, the copper block was covered by a stainless steel jacket. The end face of the copper block of 10 mm in width was regarded as the heated surface. The copper block and the jacket were connected smoothly by means of electron beam welding to avoid significant nucleation in the connecting region. The total heated length was 400 mm. The test section had two measuring sections at 100 and 300 mm from the bottom of the heated section. At each measuring section, three thermocouples were embedded in the copper block to determine the wall superheat ΔT_w; the measurement points were 5, 15 and 25 mm from the heated surface. The fluid temperature was also measured using K-type

thermocouples. In addition, two sets of glass windows were mounted at the measuring sections for visual observation of bubbles using a high-speed camera. For the visualization, bubbles were backlight using a metal halide lamp.

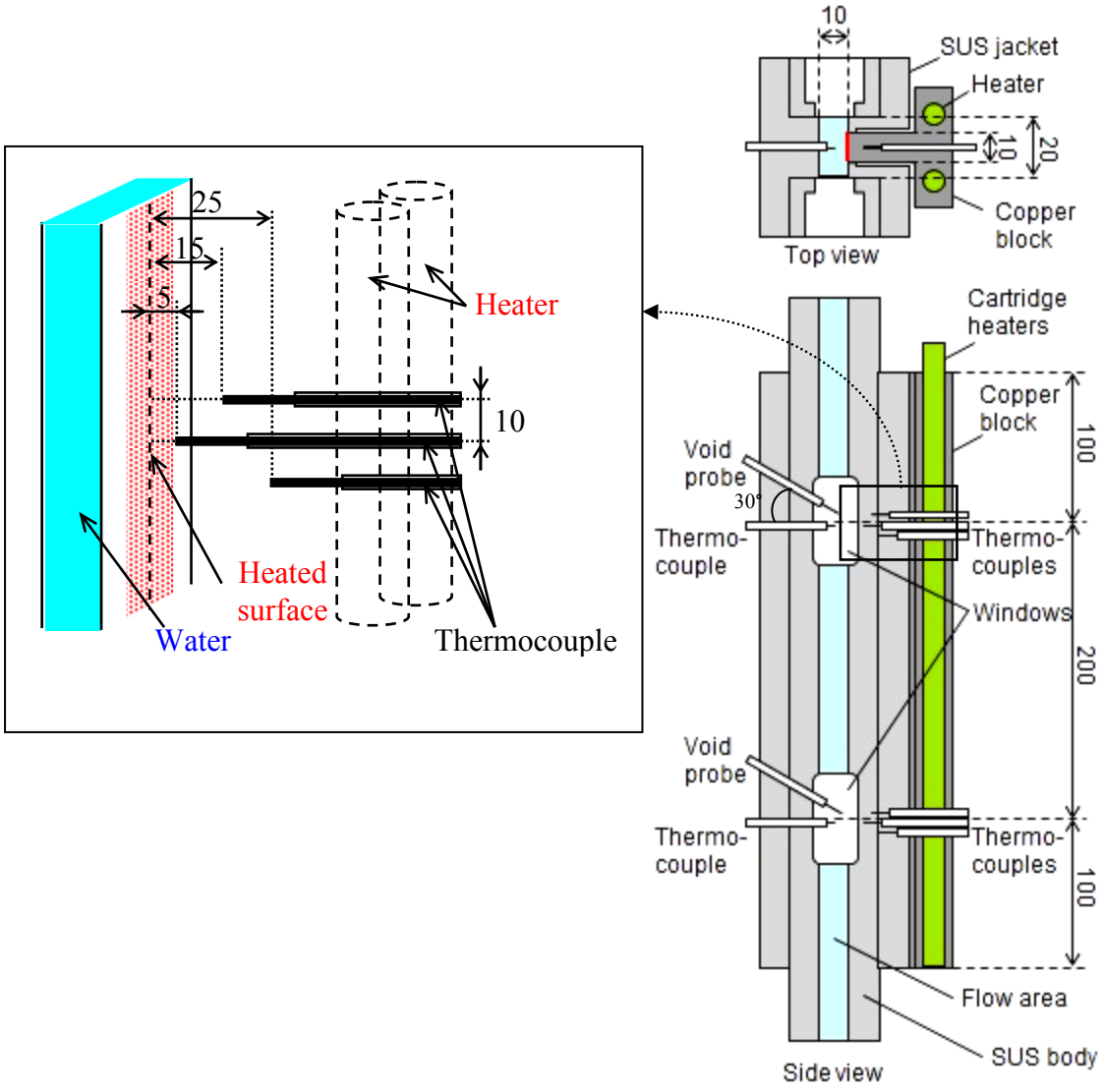

Fig. 2.2 Schematic diagram of the experimental test section

2.3 Instrumentation

In this project, measurements were performed at the upper measuring section which was shown in Fig. 2.2. The main experimental parameters were the pressure, the liquid subcooling, the mass flux, the heat flux, the wall temperature and the void fraction.

Temperatures and pressures were measured using K-type thermocouples and pressure transducers. The test section pressure P was calculated from the pressures measured at the inlet and outlet of the test section assuming a linear profile between the two measurement points. The liquid subcooling ΔT_{sub} was determined from the liquid temperature at the outlet of the preheater and the heat applied in the test section. A turbine flow meter accurate to within ±120 mLPM was used to measure the total mass flow rate, and the flow rate in the bypass line was measured using a turbine flow meter accurate to within ±7.5 mLPM. The data measured with these two turbine flow meters were used to calculate the mass flow rate in the test section G. The heat flux q_w was calculated from the temperature gradient measured using the thermocouples embedded in the heating block. The measurement accuracies of P, ΔT_{sub}, G and q_w were estimated less than 10 kPa, 2 K, 10 kg/m^{2}s and 20 kW/m^2, respectively.

Thermocouples

Thermocouples used in the experiment are of K-type (Chromel Alumel). Grounded sheath thermocouples of outer diameter 0.04 inch were used to measure the temperature of flowing water at different junctions of the loop, namely the tanks, inlet and outlet of the preheater and cooler. Thermal profile on the test surface was measured by three sheath thermocouples of diameter 0.01 inch imbedded into the copper block.

Pressure Transducers

Pressure Transmitters used in the experiments are of KH15 model. This is the detecting unit which used semiconductor strain gauge and the pressure transmitter which built-in electronic circuit and pressure is converted into electricity signal of 4-20 mA DC, 0-5 V DC or 1-5 V DC, and transmit it. The minimum and maximum limit of pressure transducers mounted in top and bottom of rectangular test section are 0 and 2.0 MPa pressure gauge, respectively.

Fig. 2.3 Pressure transducer

Contact angle measuring

An instrument of PG-X (FIBRO system AB) model was used to measure contact angle as a way to measure surface wettability. The integrated micro pump is designed for a standard liquid where the droplet size can be set in steps of 0.5 µL. Degassed and distilled water was injected to a small tube to place a single drop of water on the copper surface. A digital image of the droplet profile was analyzed to derive at the static contact angle.

Fig. 2.4 Contact angle measurement instrument PG-X model

Optical void probe

The local void fraction is measured using an optical void probe. The sensor tip of the void probe is 0.08 mm in diameter. As shown in the side view in Fig. 2.2, the void probe is set at an inclination angle of 30º from the horizontal and traversed using a micrometer. The optical void sensor is an ideal instrument to monitor the amount of vapor bubbles presented in a liquid. It is used to detect the volumetric fraction of vapor phase, called void fraction, at a point in liquid flow. The local void fraction is measured based on the principle of light reflection. If sensor surrounded with liquid the signal light emits and reflects back to the sensor; if vapor bubble covers sensor, the signal light scattered out.

High speed camera

In this study a PHORTON FASTCAM-MAX 120K is used as high speed camera to capture bubble creation. Bubbles were backlight using a metal halide lamp for visual observation of bubbles behavior within a high-speed camera. The visualization area of the high-speed camera was set depending to experimental condition. The maximum frame rate and the maximum shutter speed of the high-speed camera are 120,000 fps and 1/250,000 sec.

Turbine flow meter

The FTO flowmeter is an in-line volumetric flow metering device utilizing a blade rotor to generate flow information. The FTO has the ability to measure very low liquid or gas flows under high temperature and pressure conditions with accuracy and reliability. A precision orifice within the meter, directs all of the measured fluid tangentially (See Fig. 2.5) past the underside of a paddle blade rotor. The rotor rotates in a plane in line with the fluid's motion in the same manner as an undershot water wheel. The rotor is freely suspended and of low mass, so it rotates with a speed relative to the velocity of the flowing medium within the meter. The pickoff is located externally and adjacent to the rotor. The pickoff, in conjunction with an amplifier, senses the rotation of the rotor and provides an output pulse whose frequency is correlated with the fluid flow rate. The sum of the output pulses corresponds to the total volume of the fluid being measured. These pulses can be fed into digital totalizers, frequency to DC converters, or any of the many frequency indicating, recording, and control devices available within the field.

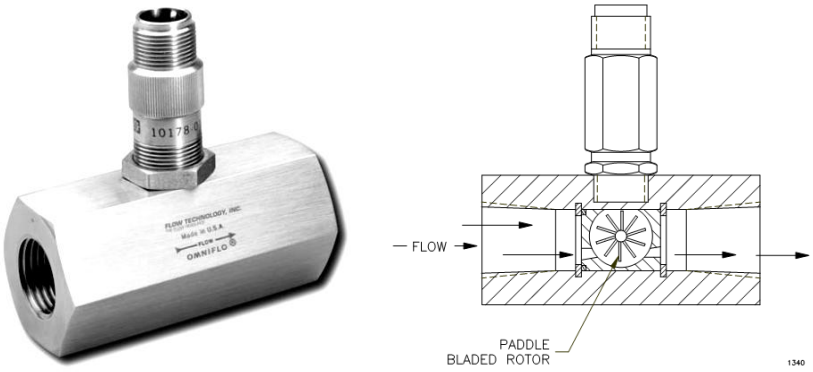

Fig. 2.5 Flow meter FTO model

2.4 Experimental Procedure

In this project, many experiments are performed in subcooled flow boiling condition to identify influence of system pressure, mass flow rate, subcooled temperature, heat flux and surface contact angle on bubble behavior and void evolution. The first parameter measured before any experiment is surface contact angle. In all of the experiments, experimental data is acquired when system is in thermo-hydraulic steady state. In this way, in according with designated experimental condition, mass flow rate is adjusted by regulating of pump power and the opening of the inlet valves. A control system set the inlet liquid temperature of test section at desired value by regulating preheater power according to inlet liquid temperature of preheater. Using the cooler system the inlet liquid temperature of preheater can be adjusted, easily. In consequence, in order to keep pressure at desire value two parts of experimental loop, i.e. the condenser and the bypass line, maybe work together. The rate of condensation of vapor phase accumulated in the separator vessel is controlled manually by injecting specified mixture of air and water in the condenser jacket. On the other hand, the amount of the vaporization rate in the bypass line is adjusted by applying certain heat power to the bypass line. When pressure and inlet temperature are kept in the desired value the power supply of rectangular test section can be set to the experimental designed value of heat flux.

2.4.1 Contact angle measurement

According to definition, the advancing contact is when the contact line is moving in the direction from liquid to vapor and the receding contact angle for the opposite [1]. Static advancing contact angle of the heated surface was measured before any experiments. In order to measure contact angle, heater block was dismantled from rectangular test section. A liquid droplet applied on a solid substrate will interact with the surface. This interaction can be described as wetting, when the liquid droplet spreads across the surface without penetration. An instrument with PG-X (FIBRO system AB) model was used to measure contact angle as a way to measure surface wettability. Degassed and distilled water was injected to a small tube to place a single drop of water on the copper surface. A digital image of the droplet profile was analyzed manually to derive the static contact angle. In this way, as shown in Fig. 2.6 three points of droplet border are selected along the droplet contour. Using these three points the advancing contact angle can be measured, easily.

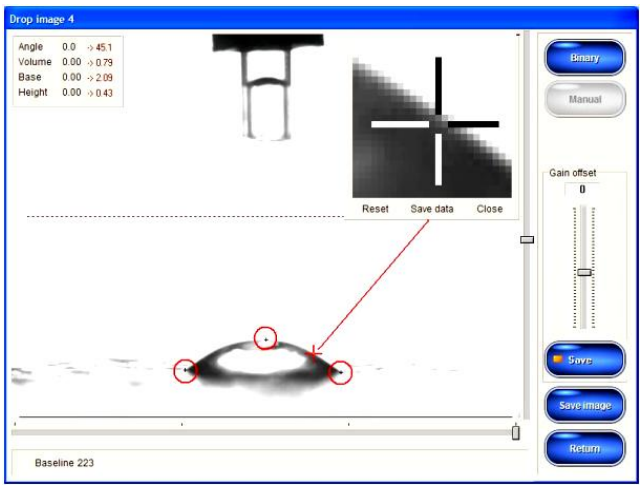

Fig. 2.6 Manual measurement of contact angle

2.4.2 Void fraction measurement

The optical void probe is used to obtain local time-averaged void fraction. The position of void probe tip can be adjusted from the close to the heated surface toward center of channel using micrometer. The micrometer is calibrated by measuring distance of the void probe tip from heated surface using scaled images. In all the present study, the time period of void probe signal is set in 100 μs. To obtain local time-averaged void fraction, 300,000 void data is recorded in 30 second and then it is analyzed. To attain lateral void distribution, local time-averaged void is measured in the position close to the heated surface toward center channel step by step until no signal is detected by the probe.

The reflection of the emitted laser towards the void probe tip is used to measure void fraction. The signal shows different voltage values when the probe tip is in the liquid or in the gas. Fig. 2.7 shows an example of short time of void probe signal against time. The probe distance from heated wall is y=0.33 mm. To calculate local void fraction is more appropriate to set a threshold of voltage data. In this method, the average time that probe sensor is covered by the vapor bubble to the total time, can be a good estimate of local time-averaged void fraction α_{lta}. Thus, the calculated void fraction is affected by the threshold. The threshold of voltage signals, V_{thr}, is defined by

$$V_{thr} = V_{\min} + \omega(V_{\max} - V_{\min}) \tag{1}$$

Here, V_{min} and V_{max} are the minimum and maximum measured voltage values and ω is the factor to determining thresholds. In a typical experimental condition, ω and local void fraction α_{lta} are shown in Fig. 2.8a.

In the Fig. 2.8a, local void fraction of five places of void probe tip (y= 0.1, 0.33, 0.78, 1.28, 2.18 mm) is shown versus ω. In this measurement system, when the void probe tip is in the water, voltage is low (ω = 0, α_{lat} = 100%), and when it is covered completely with steam the output voltage is in higher range (ω = 1, α_{lat} = 0). This figure illustrates that when ω is located between 0.2 and 0.8, α_{lat} does not change so much. Therefore, threshold factor is between 0.2 and 0.8.

The local time-averaged void fractions α_{lat} are used in calculating of average void fraction in the heated channel. By assuming ω = 0.5, an example of profile distribution of local time-averaged void fraction is shown in Fig. 2.8b, for a typical experimental condition. By integral of the average local void fraction distribution, average void fraction can be calculated easily.

It should be noted in some experimental condition with low void fraction, measurement of void fraction using optical void probe is impossible. In this case, void fraction can be calculated using image analysis method. In each condition several snapshots of bubble generation are randomly selected, and total volume of the vapor bubbles is measured in each snapshot. The average of vapor volume obtained in all images dividing by heated channel volume observed in the images is average void fraction. In some experimental condition that both methods of void measurement are possible, the comparison of void fraction obtained by image analysis process with void fraction measured by optical void probe at threshold factor ω=0.5, show fairly well consistency. Please see void results in chapter 3.

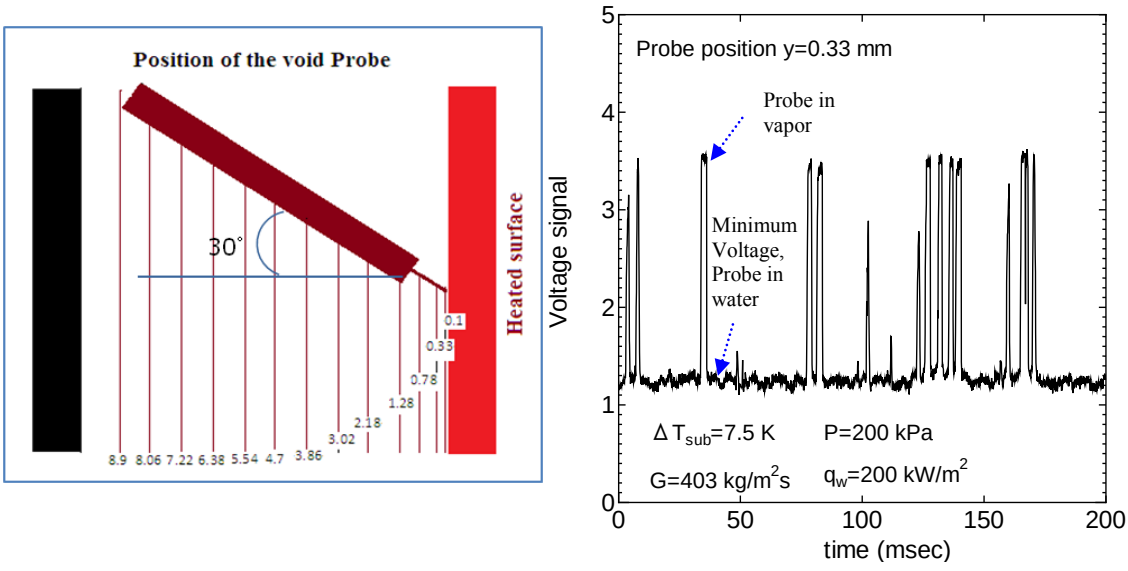

Fig. 2.7 Void probe position map and an example of void probe signal

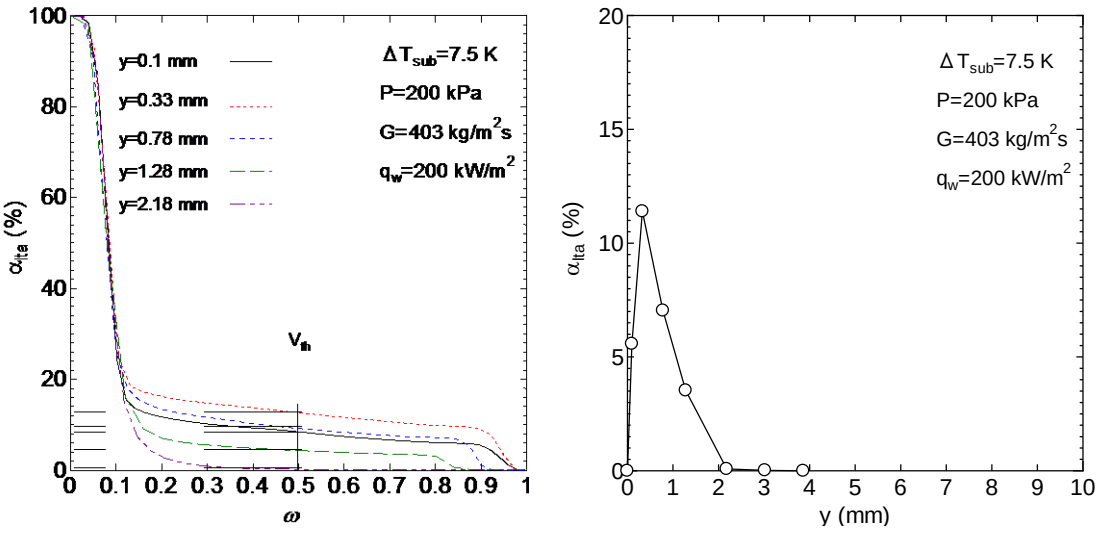

(a) (b)

Fig. 2.8 (a) Example of local time-averaged void fraction against factor of threshold voltage, (b) example of time-averaged void fraction distribution

2.5 Data Acquisition and Processing

The data generated by the thermocouples, the pressure transducers, the flowmeters and the power applied to the cartridge heaters were recorded continuously every 1 second by a Workbench Data Shuttle PC data acquisition system. These raw data is an input of FORTRAN program to obtain average value of experimental parameters. Bubble generation, collapsing, growth and departure is recorded by a high speed video camera linked to a PC. Because of limitation of memory of PC, a part of this video is selected and kept in the PC. Moreover, signals of optical void probe are acquired by an interface program in PC, and then are analyzed by FORTRAN program.

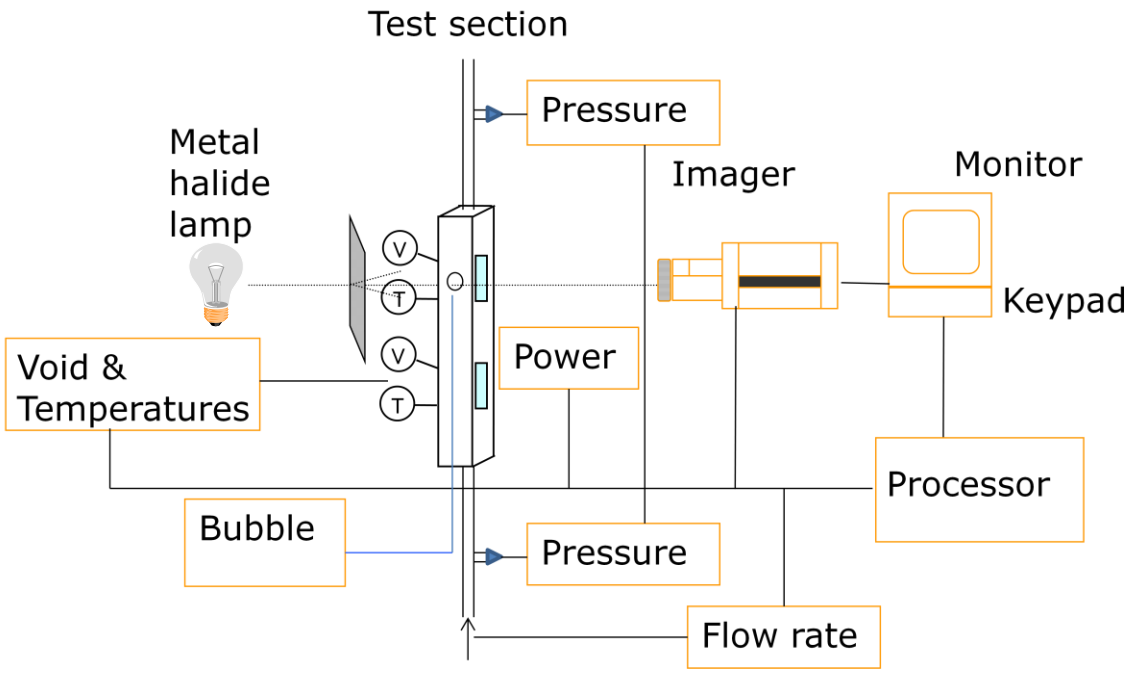

Fig. 2.9 Schematic of experimental setup

References

[1] S.G. Kandlikar, M. Shoji, V.K. Dhir, Handbook of Phase Change: Boiling and Condensation, Taylor & Francis, London, 1999.

CHPTER 3 BUBBLE DYNAMICS AT BOILING INCIPIENCE

3.1 Introduction

When subcooled liquid is injected to a heated channel, liquid temperature and wall temperature rise gradually in the axial direction in the single-phase region. Formation of the first bubbles or the onset of nucleate boiling (ONB) is then permitted at the location where the liquid temperature in the close proximity to the heated wall becomes high enough [1,2]. It is known that void fraction is low just downstream of the location of ONB, and a rapid increase in the void fraction commences further downstream from the ONB point [3]. This phenomenon is commonly regarded as the net vapor generation (NVG) or the onset of significant void (OSV). Although the void fraction upstream of the location of OSV is small and usually neglected, the presence of bubbles alters the mechanisms of the heat transfer and pressure loss in this region [3,4]. Furthermore, it is considered that the mechanism to cause the OSV is in close relation to the bubble behavior between the locations of ONB and OSV. For instance, it is frequently postulated that the bubbles remain on the heated surface between the locations of ONB and OSV, but they are eventually detached from the heated surface at the location of OSV to cause a rapid increase in the void fraction [5–7]. It can hence be said that the bubble dynamics in the region between the locations of ONB and OSV are of importance for the mechanistic determinations of the heat transfer rate, pressure loss and the void fraction in subcooled flow boiling.

Bubble behavior in subcooled flow boiling was studied photographically by many researchers. In early work by Gunther [8], it was observed that bubbles grew and

collapsed while sliding along the heated surface under the influence of main flow. In the experiments by Bibeau and Salcudean [9], bubbles slid along the heated surface before being ejected into the subcooled bulk liquid. Since the bubbles were collapsed due to condensation, they did not travel far downstream after nucleation. Zeitoun and Shoukri [10] also observed that the bubbles tended to be detached from the heated surface. They developed an empirical correlation for the mean bubble diameter as a function of the Reynolds number, Jakob number and the boiling number. Thorncroft et al. [11] observed the bubble behavior in subcooled flow boiling using FC-87 as a working fluid. In their experiments for upflow configuration, bubble slid along the heated surface and typically did not lift off. In contrast, in downward flow configuration, bubbles were lifted off the heated surface directly from the nucleation site or after sliding for a certain distance. Situ et al. [12,13] carried out forced convection subcooled water boiling experiments using a vertical annular channel as the test section. They measured the bubble lift-off diameter, but reported that some bubbles slid along the heated surface and did not lift off the surface within the visualization region. Okawa et al. [14] studied the bubble behavior in subcooled flow boiling of water using mass flux and subcooling as the main experimental parameters. In their experiments, bubbles slid along the vertical heated surface for a long distance or lifted off the surface after sliding several bubble diameters. It was reported that sliding bubbles were observed under the condition of high mass flux and low liquid subcooling.

The above literature survey reveals that bubbles in subcooled upward flow boiling may slide along or lift off the heated surface. The experimental data by Thorncroft et al. [11] indicate that the sliding of vapor bubbles significantly enhance the heat transfer from the heated surface. Furthermore, the bubble lifetime is considerably different between the two types of bubble behavior since bubbles are usually collapsed rapidly due to

condensation if they are lifted off the heated surface. The bubble dynamics would hence be in close relation to axial evolution of the void fraction in subcooled boiling region, which is of importance in evaluating the inception of two-phase instability of boiling systems and the fuel burnup in nuclear reactors. However, the detailed mechanisms to determine the bubble dynamics have not been elucidated. The main purpose of this chapter is to identify the thermal-hydraulic conditions that affect the bubble dynamics in subcooled flow boiling. The bubble behavior is therefore observed in varied conditions of pressure, mass flux and liquid subcooling. Considering the high-temperature and radiation environments in nuclear reactors, the surface of low contact angle is used as the heated surface [15,16]. Based on the present experimental results, discussion is also made to investigate possible mechanisms to determine the bubble dynamics.

3.2 Experimental description

In the present experiments, measurements were performed at the upper measuring section. The main experimental parameters were the pressure, the liquid subcooling and the mass flux. The test section pressure P was calculated from the pressures measured at the inlet and outlet of the test section assuming a linear profile between the two measurement points. The liquid subcooling ΔT_{sub} was determined from the liquid temperature at the outlet of the preheater and the heat applied in the test section. The measurement accuracies are declared in Chapter 2. The experimental ranges of P, ΔT_{sub} and G were 96 to 860 kPa, 4 to 30 K, and 169 to 1170 kg/m^{2}s, respectively. Main experimental conditions and results are summarized in Table 3.1. The heat flux q_w was calculated from the temperature gradient measured using the thermocouples embedded in

the heating block. In each experimental condition, the wall heat flux q_w was increased step by step until the first bubbles were formed within the visualization window to determine the ONB condition and to record the bubble behavior at ONB using the high-speed camera. Throughout the experiments, a data acquisition system attached to a personal computer recorded the temperatures, pressures and mass fluxes every 1 second. The visualization area of the high-speed camera was about 10 × 10 mm with the spatial resolution of about 0.02 mm/pixel. The frame rate and the shutter speed were set to 6000 fps and 0.167 ms, respectively.

Table 3.1 Main experimental conditions and results at ONB (*L: Lift-off, S: Sliding, B: Both)

Run	P (kPa)	G (kg/m^{2}s)	q_w (kW/m^2)	ΔT_{sub} (K)	ΔT_w (K)	Bubble behavior*	N	$D_{b,mean}$ (mm)	$D_{b,std}$ (mm)	Ja
1	100	169	160	11.2	13.8	L	13	1.70	0.22	41.22
2	100	169	170	14.2	12.8	L	2	3.90	0.20	38.22
3	100	170	189	20.6	13.3	L	11	1.60	0.17	40.62
4	98	260	200	15.4	13.9	L	18	1.90	0.65	41.86
5	100	325	200	12.5	13.7	L	8	1.90	0.24	40.76
6	100	325	220	15.9	14.7	L	7	1.20	0.31	43.89
7	98	392	166	8.4	11.4	L	8	2.06	0.33	35.23
8	97	384	224	12.7	15.8	L	22	1.72	0.32	49.69
9	101	388	289	18.3	16.4	L	16	1.00	0.18	49.76
10	96	393	318	19.6	18.4	L	75	0.87	0.38	58.61
11	111	495	173	6.5	12.5	B	47	0.31	0.11	34.60
12	108	497	207	10.3	13.2	L	37	0.33	0.07	37.46
13	113	489	269	16.4	12.9	L	18	0.40	0.05	35.29
14	110	484	312	17.9	15.7	L	75	0.38	0.11	44.28
15	198	325	132	10.1	6.7	S	10	0.25	0.05	10.86
16	201	386	81	4.2	4.9	S	8	0.28	0.06	7.93
17	200	383	149	6.6	8.5	S	5	0.20	0.03	13.72
18	203	382	166	10.4	7.6	S	7	0.20	0.03	12.13
19	201	386	213	14.2	9.1	S	25	0.20	0.03	14.70
20	201	386	229	16.9	7.8	S	4	0.15	0.03	12.58

Table 3.1 (*Continued)*

Run	P (kPa)	G (kg/ m^2s)	q_w (kW /m^2)	ΔT_{sub} (K)	ΔT_w (K)	Bubble behavior*	N	$D_{b,mean}$ (mm)	$D_{b,std}$ (mm)	Ja
21	192	785	230	12.3	8.2	S	8	0.15	0.03	13.89
22	186	790	308	16.9	10.6	S	30	0.12	0.02	18.31
23	196	780	437	23.5	12.9	B	20	0.13	0.01	21.47
24	245	1070	419	20.2	11.5	B	17	0.14	0.02	15.55
25	230	1080	465	23.7	11.7	B	13	0.14	0.02	16.89
26	238	1170	611	29.7	14.4	B	19	0.16	0.04	20.08
27	415	358	126	6.6	6.4	S	20	0.17	0.02	5.34
28	415	363	178	11.1	7.4	S	17	0.15	0.01	6.19
29	421	361	217	15.2	7.9	S	20	0.14	0.02	6.53
30	406	762	123	4.4	5.9	S	30	0.14	0.01	5.01
31	404	768	158	6.3	6.9	S	32	0.13	0.01	5.87
32	407	764	207	9.8	7.0	S	14	0.11	0.01	5.97
33	405	761	272	13.4	8.1	S	21	0.11	0.01	6.90
34	403	761	328	17.4	8.8	S	23	0.11	0.01	7.53
35	432	1140	257	12.3	5.7	S	24	0.07	0.01	4.63
36	406	1170	301	14.1	7.1	S	17	0.07	0.01	6.05
37	400	1170	357	16.7	7.8	S	33	0.07	0.01	6.78
38	397	1170	442	20.7	9.0	S	24	0.07	0.01	7.88
39	801	381	92	4.7	4.0	S	12	0.07	0.02	1.85
40	799	376	128	7.5	4.7	S	17	0.06	0.01	2.19
41	802	377	172	12.0	6.0	S	30	0.06	0.01	2.77
42	799	380	213	14.8	6.0	S	30	0.06	0.01	2.78
43	808	384	252	19.1	5.6	S	30	0.06	0.01	2.57
44	824	774	92	4.0	3.5	S	24	0.04	0.01	1.60
45	829	785	148	7.3	4.4	S	30	0.03	0.01	1.96
46	827	794	212	12.0	4.1	S	20	0.03	0.01	1.81
47	815	798	280	15.1	5.4	S	30	0.03	0.01	2.47
48	815	803	321	17.4	6.0	S	20	0.03	0.01	2.73
49	860	1072	138	5.6	4.1	S	15	0.03	0.01	1.75
50	827	1075	146	6.0	4.3	S	20	0.03	0.01	1.91
51	809	1091	198	8.7	5.0	S	20	0.03	0.01	2.28
52	806	1100	275	12.8	5.6	S	30	0.03	0.01	2.59
53	797	1094	345	16.1	6.5	S	30	0.02	0.00	3.03
54	798	1122	414	19.3	5.2	S	20	0.02	0.00	2.42

3.3 Experimental results

3.3.1 ONB condition and comparison

A number of correlations have been developed for the ONB condition in subcooled flow boiling. Considering a tiny hemispherical bubble nucleus sitting at a cavity mouth, Sato and Matsumura [2] hypothesized that the bubble nucleus does not grow if the minimum temperature of the surrounding liquid is lower than the bubble temperature. They used the Young-Laplace equation and the Clasius-Clapeyron equation to calculate the bubble temperature, and a linear profile was assumed for the liquid temperature distribution near the heated surface. They finally showed that the following condition should be satisfied at the location of ONB:

$$q_w = \frac{k_l h_{fg} \rho_v \Delta T_w^2}{8\sigma T_{sat}} \tag{1}$$

where k is the thermal conductivity, h_{fg} is the latent heat of vaporization, ρ is the density, σ is the surface tension, T_{sat} is the saturation temperature, and the subscripts l and v denote the liquid and vapor phases, respectively. The effect of the contact angle φ on the shape of bubble nucleus was taken into consideration in the following correlation by Davis and Anderson [17]:

$$q_w = \frac{k_l h_{fg} \rho_v \Delta T_w^2}{8(1+\cos\varphi)\sigma T_{sat}} \tag{2}$$

This correlation is identical to Eq. 1 if φ is set to 90º. The following empirical correlation by Bergles and Rohsenow [18] is also widely used to estimate the ONB condition in water subcooled flow boiling:

$$q_w = 0.0018P^{1.156}(1.8\Delta T_w)^{2.83/P^{0.0234}} \tag{3}$$

It is noted that the original expression is rewritten in the SI units in Eq. 3. The above correlations assume that the cavities of wide spectrum in sizes are available on a heated surface and they can work as active nucleation sites. However, even if many cavities are available, some of them may not work as active nucleation sites due to flooding particularly when the surface is hydrophilic. In view of this, Basu et al. [19] included a correction factor F in the ONB criterion as

$$q_w = \frac{F^2 h_{fg}\rho_v k_l \Delta T_w^2}{2\sigma T_{sat}} \tag{4}$$

The functional form of F was determined empirically using the ONB data for the heated surfaces of various contact angles within 1 to 85º:

$$F = 1 - \exp\left[-\left(\frac{\pi\varphi}{180}\right)^3 - 0.5\left(\frac{\pi\varphi}{180}\right)\right] \tag{5}$$

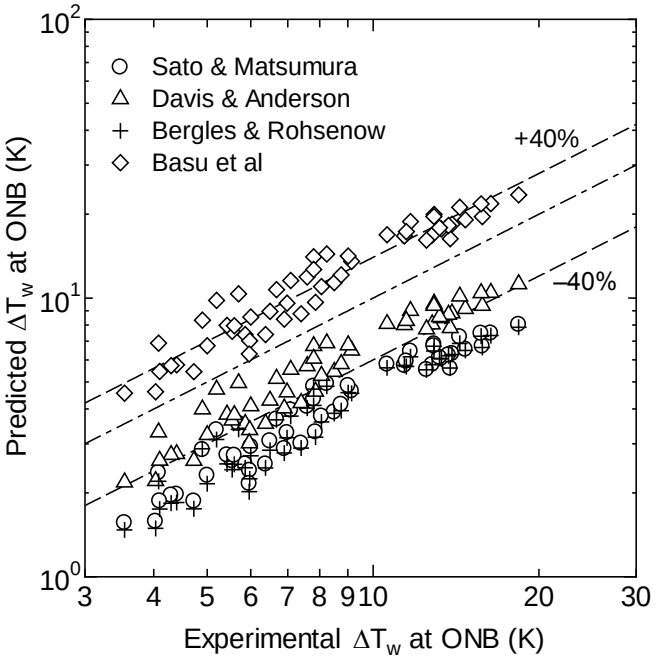

Fig. 3.1Comparison of the predicted and experimental values of ΔT_w at ONB

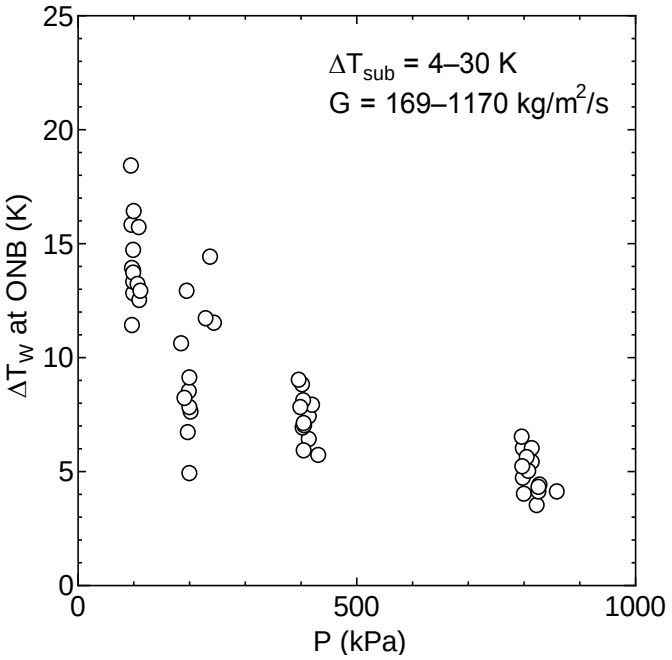

Fig. 3.2 Dependence of the wall superheat at ONB on the pressure

The values of ΔT_w measured at ONB are compared with the predictions by the above four correlations in Fig. 3.1 Since the heated surface of low contact angle was used in the present work, the correlations proposed by Davis and Anderson [17] and Basu et al. [19] in which the effect of surface wettability is taken into consideration provide better predictions comparing with the other two correlations. Although the correlation by Basu et al. [19] tends to overestimate the present data, it should be noted that the value of ΔT_w calculated by Eqs. 4 and 5 is highly susceptible to the contact angle when the value of contact angle is small. In fact, Eqs. 4 and 5 predict the present experimental data within the error of ±40% if the value of φ is slightly increased to 24º. It may therefore be considered that the ONB was delayed in the present experiment due to flooding as supposed by Basu et al. [19]. In the nuclear reactor core, the contact angle of the heated surface is expected to be reduced because of the high-temperature and radiation environments [15,16]. It can be confirmed that the effect of the surface wettability should be taken into consideration to estimate the location of ONB accurately when the contact angle is low. It may also be interesting to note that the correlations shown above suggest that a decrease of P leads to a reduction of vapor phase density and consequently to an increase in ΔT_w at ONB. The relation between P and ΔT_w at ONB in the present experiments is presented in Fig. 3.2. It can be confirmed that ΔT_w at ONB tended to increase with a decrease in P particularly near the atmospheric pressure.

3.3.2 Bubble dynamics

In the widely-used model for OSV by Levy [5], it is postulated that the void fraction starts to rise sharply when the frictional force acting on a bubble in the vertical

direction overcomes the surface tension force to hold it. In the present experiments, however, bubbles did not stay at the nucleation sites even at the boiling incipience. Two typical types of bubble behavior observed in this work are depicted in Figs. 3.3 and 3.4, respectively. As shown in Fig. 3.3, some bubbles lifted off the heated surface after sliding for a certain distance. Since the bubbles were propelled into the subcooled bulk liquid

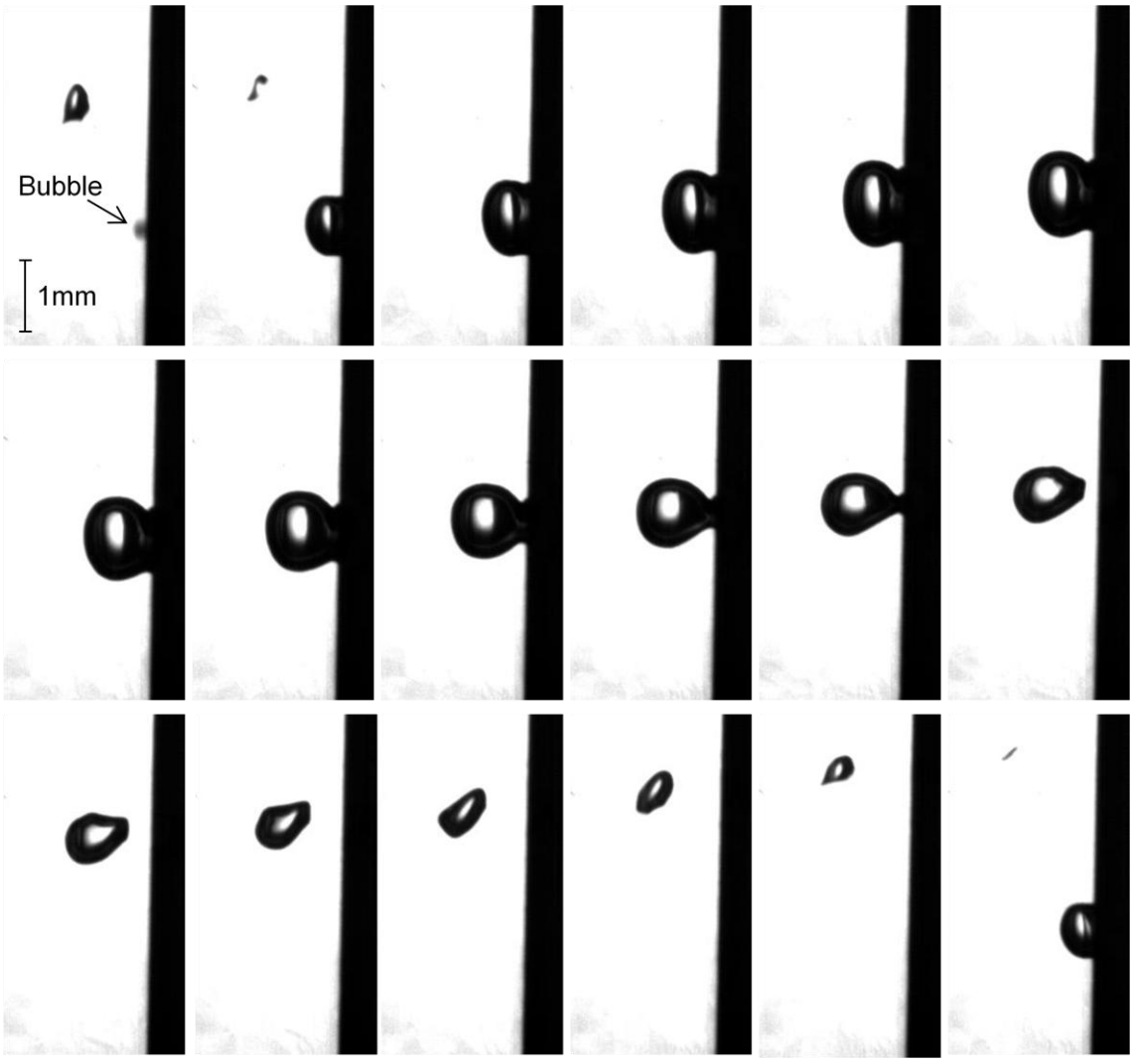

Fig. 3.3 Bubble lift-off from the heated surface observed in Run 8 (time interval is 0.67 ms)

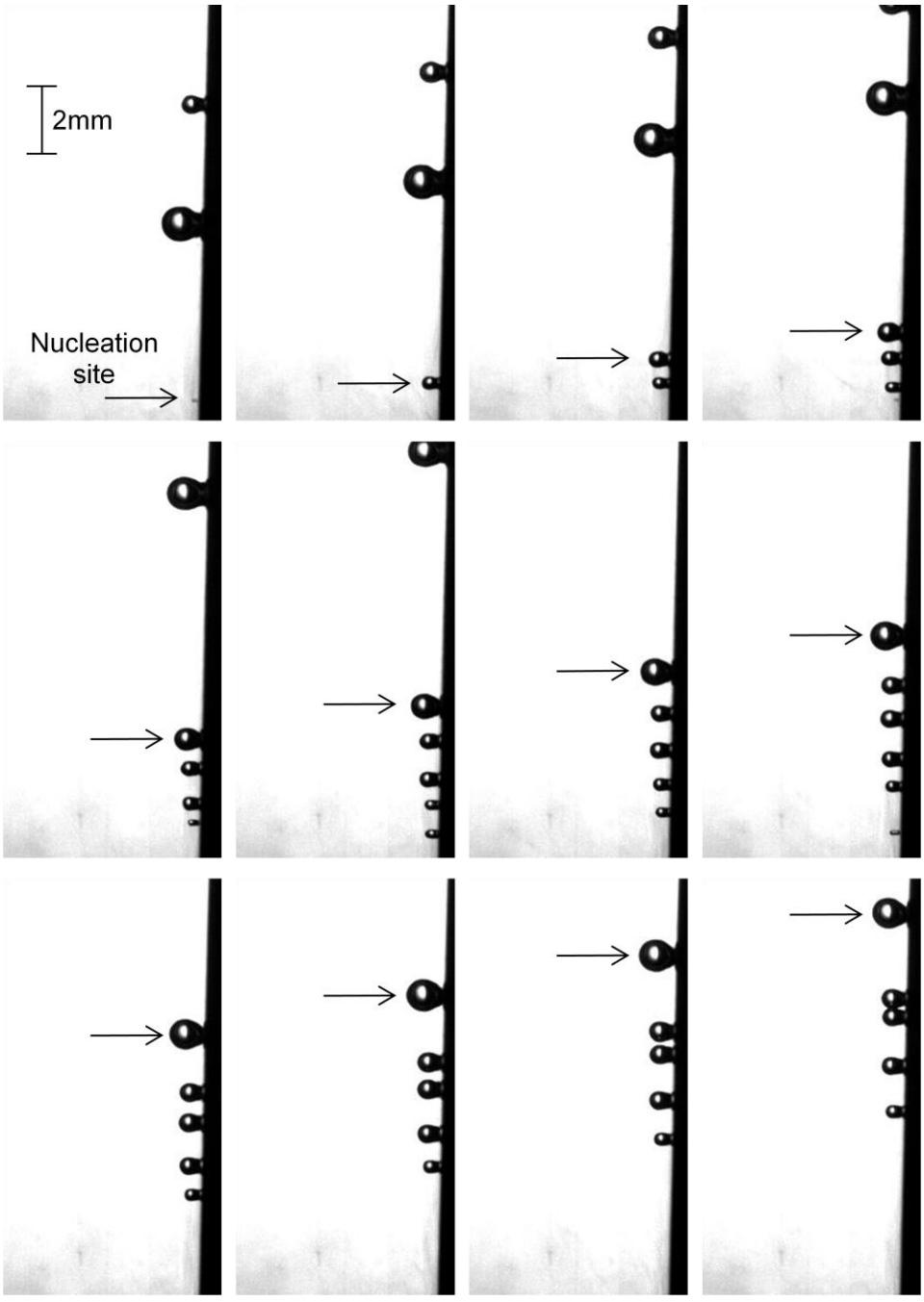

Fig. 3.4 The bubble sliding along the heated surface for a long distance observed in Run 15 (time interval is 3.33 ms)

after the lift-off, they were collapsed due to condensation within a short time after nucleation. As shown in Fig.3.4, in a different experimental condition, bubbles slid along the heated surface for a long distance. Since the bubbles stayed close to the heated surface, the bubble lifetime was significantly elongated. Although the bubbles mostly left the visualization region as shown in Fig. 3.4, disappearance of bubbles during sliding was also observed in the experiments at high liquid subcooling.

Bubble behavior observed in each experimental condition is also shown in Table 3.1. Here, the two types of bubble behavior depicted in Figs. 3.3 and 3.4 are referred as lift-off (L) and sliding (S), respectively. In some experimental conditions, both the two types of bubble behavior were observed simultaneously depending on the nucleation site. The term of 'both' was applied to this case in the table (B). Since the bubble size was considerably different between the two types, the arithmetic mean bubble diameter $D_{\mathrm{b,mean}}$ is also listed in Table 3.1. Here, the bubble size measurement was conducted at the moment of lift-off for the lift-off bubbles and at the moment of the departure from the nucleation sites for the sliding bubbles, and D_{b} was estimated from the maximum bubble dimensions in the horizontal and vertical directions $D_{\mathrm{b,x}}$ and $D_{\mathrm{b,y}}$ through $D_{\mathrm{b}}^3 = D_{\mathrm{b,x}} D_{\mathrm{b,y}}^2$ assuming that the bubble dimension in depth was equal to $D_{\mathrm{b,y}}$; N and $D_{\mathrm{b,std}}$ in the table denote the number of bubbles analyzed to derive $D_{\mathrm{b,mean}}$ and the standard deviation of D_{b}, respectively. The values listed in the last column in Table 3.1 are the Jakob number Ja defined by

$$Ja = \frac{\rho_l c_{pl} \Delta T_w}{\rho_v h_{fg}} \tag{6}$$

where c_{p} is the specific heat.

In order to investigate the parametric trend, the observed bubble behavior is plotted on the *P*–*G* map in Fig. 3.5a. It can be seen that the bubble lift-off occurred only under the low pressure conditions less than 250 kPa, and only sliding bubbles were observed at the higher pressures within the present experimental conditions. Since multiple types of bubble behavior were observed at the low pressures, the effects of *G* and ΔT_{sub} are further explored in Fig. 3.5b for the two pressure ranges of *P* = 96–113 kPa (single symbols) and 186–245 kPa (double symbols). Although the effect of ΔT_{sub} could not be fully tested, it can be seen that the bubble lift-off was more frequently observed at high liquid subcooling if the values of *P* and *G* were in the same ranges (see the single symbols at around *G* = 500 kg/m^{2}s and the double symbols at around *G* = 800 kg/m^{2}s). Since the effect of the pressure on the bubble behavior was significant, the dependence of $D_{b,mean}$ on *P* is explored in Fig. 3.6. It can clearly be seen that $D_{b,mean}$ tended to decrease with increased value of *P*.

3.4 Discussion

The experimental results presented in this chapter indicated that the system pressure is significantly influential in the size and behavior of bubbles in water subcooled flow boiling. In the equilibrium state, the bubbles observed in the present work would be small enough to slide along the vertical heated surface under the influence of shear-induced lift force [20]. It is hence considered that the bubble lift-off was promoted in the non-equilibrium state experienced right after the nucleation. Mikic et al. [21] analyzed the bubble growth rate for a spherical bubble growing attached to a surface.

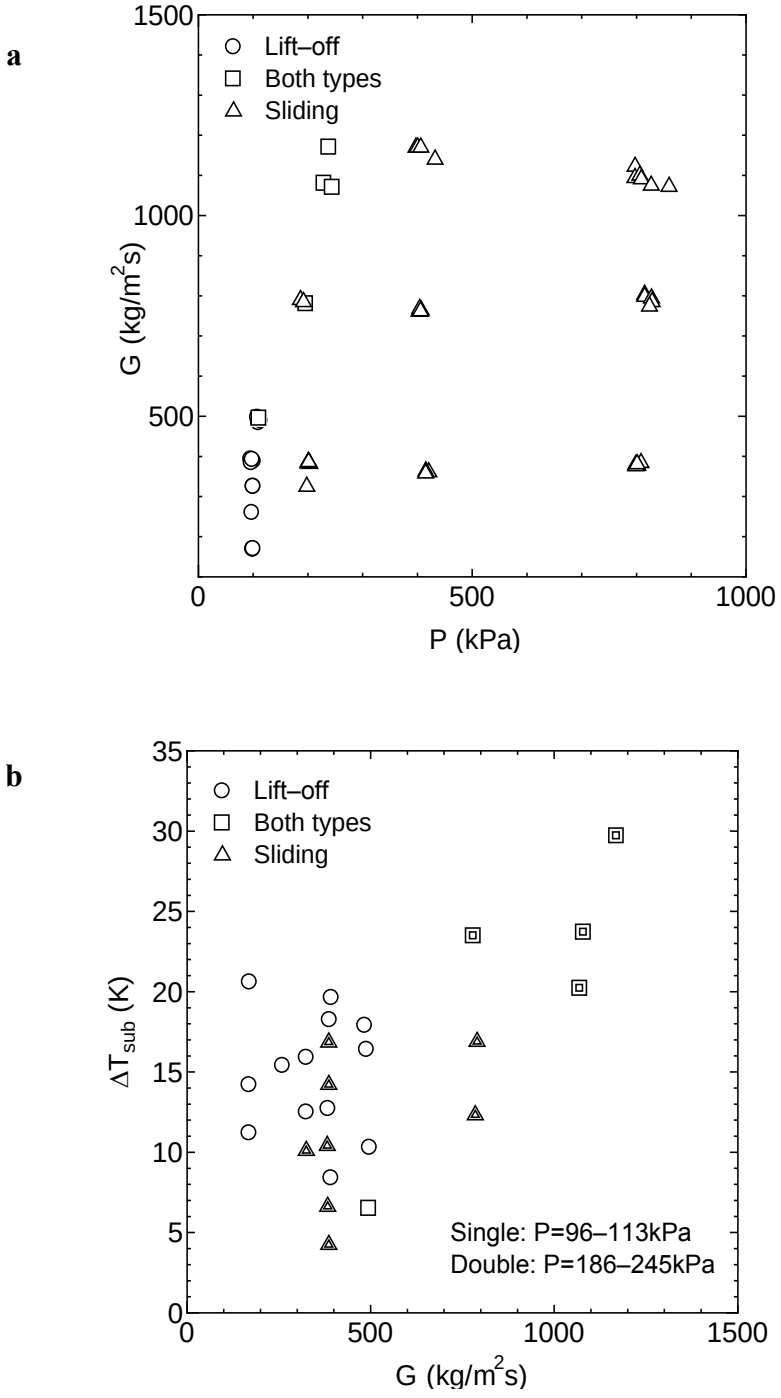

Fig. 3.5 Observed bubble behavior plotted on (a) *P*–*G* map, and (b) *G*–ΔT_{sub} map.

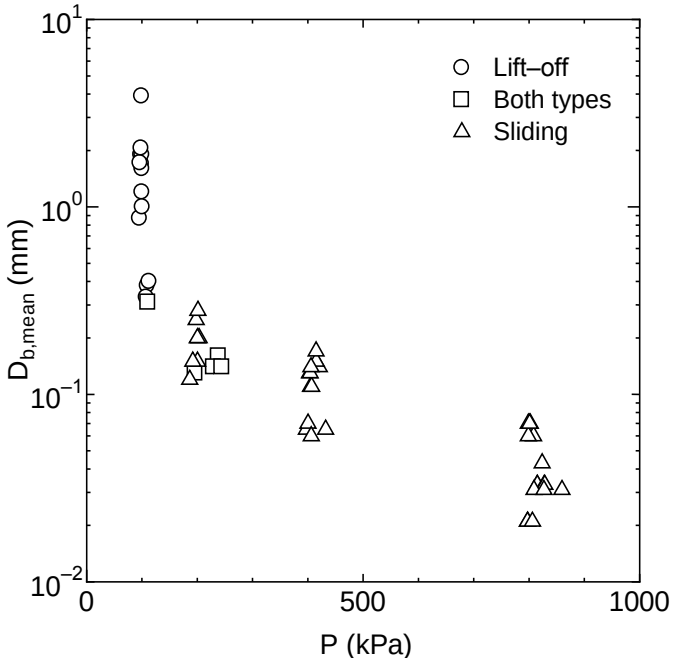

Fig. 3.6 Effect of the pressure on the mean bubble diameter

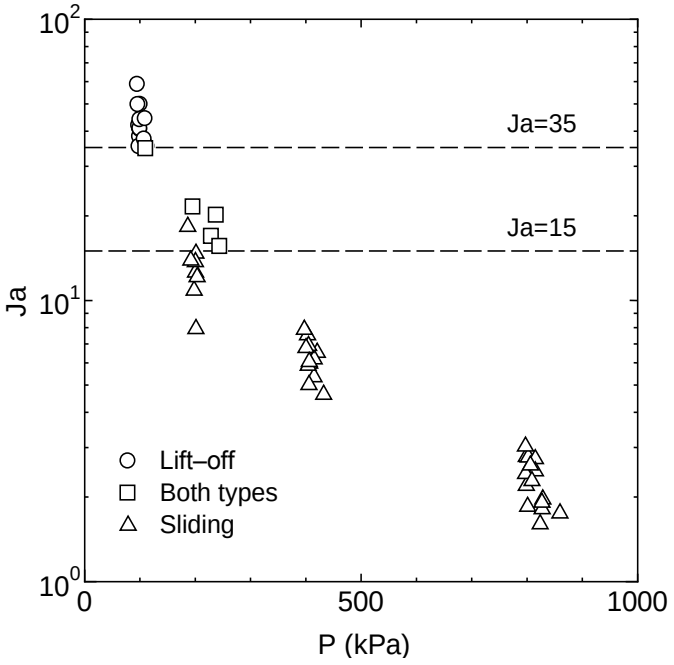

Fig. 3.7 Effect of the pressure on the Jakob number

In the present experiment, the bubble growth period was generally so long that the growth rate may be approximated by

$$R_b = Ja\sqrt{\frac{12}{\pi}\frac{k_l}{\rho_l c_{pl}}t} \tag{7}$$

where R_b is the bubble radius. Although all the thermal-hydraulic properties of water are dependent on the pressure, the vapor density is most sensitive. If one recalls the ONB correlation (e.g. Eq. 1), the value of ΔT_w tends to increase with decreased value of P or ρ_v. Furthermore, since ρ_v is included in the denominator of Eq. 6, the sensitivity of Ja on P is more noticeable. The relation between P and Ja measured in this work is displayed in Fig. 3.7. It can be confirmed that the value of Ja at ONB decreases sharply with an increase in P as expected. It should be noted that the situation in subcooled flow boiling is more complex than that postulated by Mikic et al. [21]. In fact, since they considered a growing bubble in a pool of uniformly superheated liquid, the effects of liquid subcooling and mass flux were not taken into account. It would however be expected from the above equation that the bubble growth rate is significantly dependent on the vapor density and tends to be greater at low pressures.

If the bubble is attached to the surface, the bubble size in the equilibrium state may be comparable to the superheated layer thickness δ_{shl}, within which the liquid temperature is higher than the saturation temperature. In view of this, the dimensionless bubble diameter is defined by $D_{b,mean}/\delta_{shl}$, and plotted against Ja in Fig. 3.8. Here, δ_{shl} is simply estimated by the following equation, assuming the linear temperature profile near the heated wall [1,2].

$$\delta_{\mathrm{th}} = \frac{k_{\mathrm{l}} \Delta T_{\mathrm{w}}}{q_{\mathrm{w}}} \tag{8}$$

It can be seen that the value of $D_{\mathrm{b,mean}}/\delta_{\mathrm{shl}}$ is of the order of 1 at low Jakob numbers, but it increases noticeably with an increase in *Ja*. This suggests that, at low pressures of high Jakob number, a considerable portion of a bubble was exposed to subcooled liquid. It is therefore considered that the bubble growth rate was determined as a consequence of a significant competition between the vaporization at the wall side and the condensation at the bulk liquid side of the bubble. Furthermore, Figs. 3.7 and 3.8 indicate that the bubble behavior observed in this work can roughly be characterized using the Jakob number as

$$\begin{cases} \text{lift-off} & Ja > 35 \\ \text{both types} & 15 < Ja < 35 \\ \text{sliding} & Ja < 15 \end{cases} \tag{9}$$

Time variations of bubble dimensions $D_{\mathrm{b,x}}$, $D_{\mathrm{b,y}}$ and D_{b} were measured for several lift-off bubbles. A typical result is presented in Fig. 3.9. First, it can be seen that the bubble grows rapidly in the initial stage, but the growth rate decreases gradually and the value of D_{b} becomes fairly constant at around 1.2 ms after nucleation. In this case, the unsteady growth force may promote the bubble detachment from the surface [22,23]. Second, although $D_{\mathrm{b,y}}$ is greater than $D_{\mathrm{b,x}}$ in the early stage, they become in the same order at the moment of lift-off. This implies that the bubble changed from flattened to more rounded in shape before the detachment from the surface. It is therefore considered that the local liquid flow induced by the change of the bubble shape would also be one of the causes of the bubble lift-off. The surface tension force is considered to be a main

cause of the shape change [24]. Third, it may be interesting to note that the bubble volume started to decrease before the lift-off. Figure 3.10 displays the process of bubble lift-off observed in Run 8. Here, the same images are shaded and overlapped with the next images to highlight the time-evolution of bubble dimensions. It can be seen that the reduction of the bubble volume prior to the lift-off occurs at the sidewall rather than the top of the bubble. It appears that the condensation is most significant on the downside of the bubble, which may be consistent with Lucic and Mayinger [25] who reported that the maximum of the local Nusselt number was located in this area based on the measurements using the holographic interferometry technique. In consequence, since local liquid flow directing toward the bubble base may cut out the connection between the bubble and the wall, the net condensation prior to the lift-off is also expected to contribute the bubble detachment.

Under the condition of high *Ja*, the bubbles grow rapidly after nucleation and overcome the condensation to become large bubbles. The bubble size can be much greater than the thickness of the superheated layer that is formed in the liquid phase before nucleation. In this situation, the effects of unsteady growth force, change in bubble shape, and net condensation may become prominent. Although further study is necessary to fully understand the bubble behavior, it is considered that the Jakob number is a particularly important parameter to characterize the size and behavior of the bubbles at ONB in subcooled flow boiling.

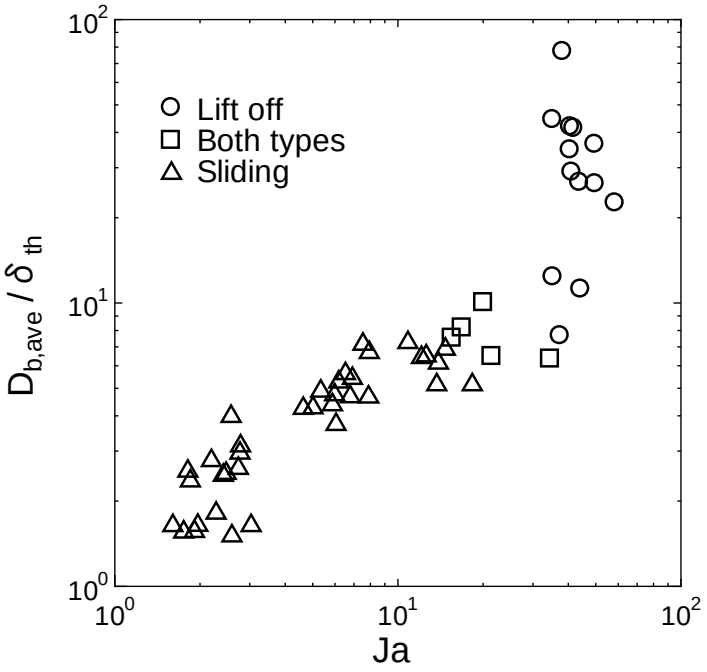

Fig. 3.8 Dependence of the dimensionless bubble diameter on the Jakob number

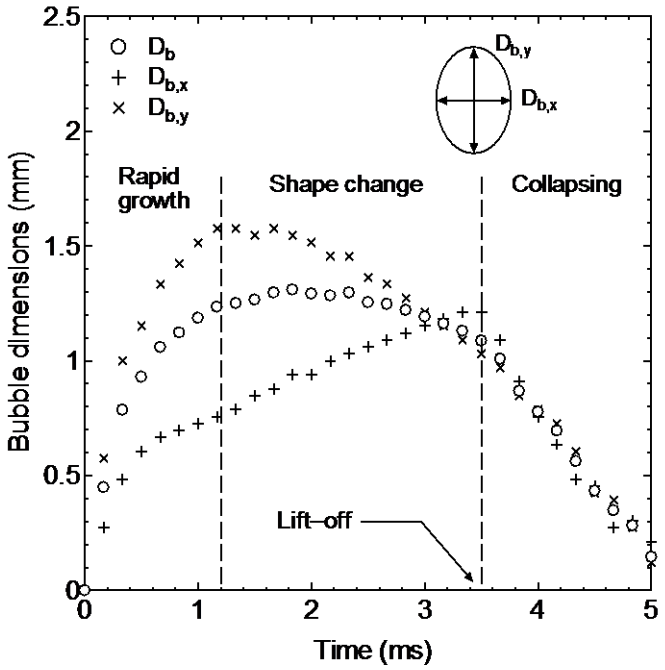

Fig. 3.9 Time evolutions of the dimensions of a lift-off bubble observed in Run 8

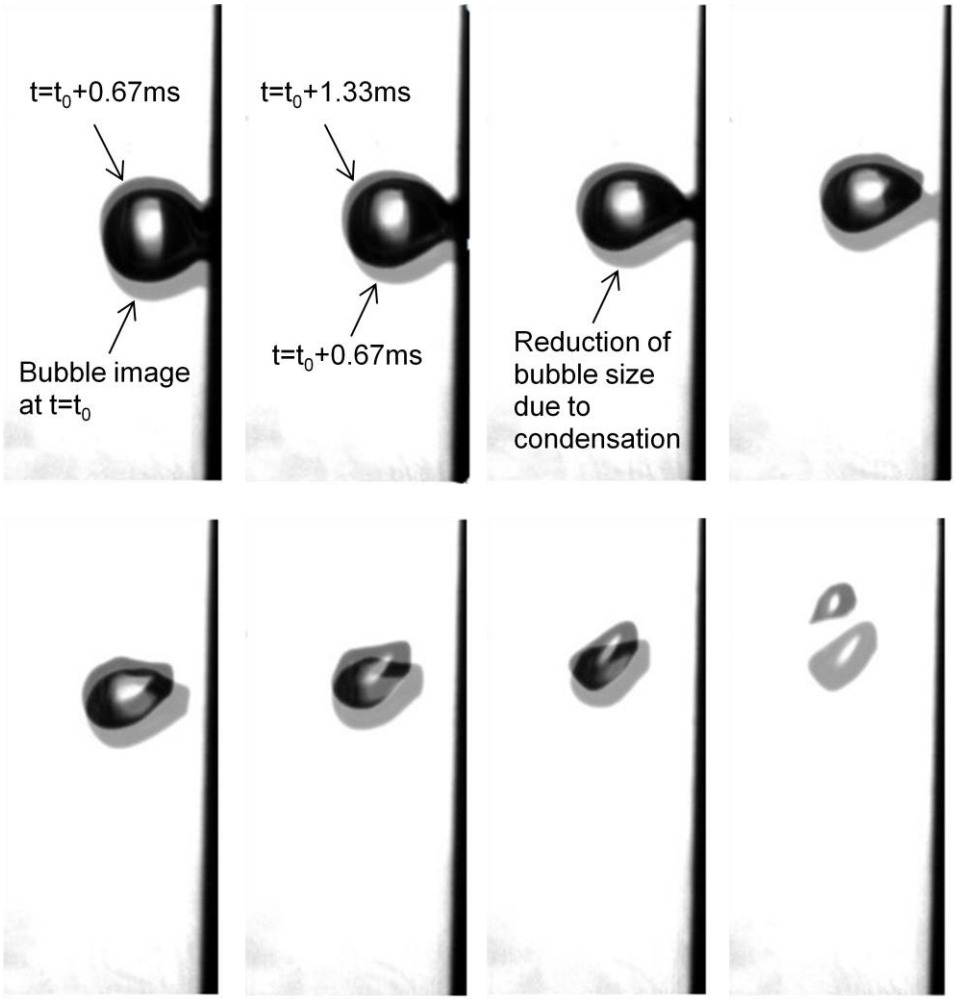

Fig. 3.10 Overlapped bubble images during the lift-off process observed in Run 8 (time interval is 0.67 ms)

3.5 Conclusion

Experiments were carried out to explore the bubble dynamics at the onset of nucleate boiling in water subcooled flow boiling. The flow direction was vertical upward and the surface of small contact angle was used as the heated surface. The pressure, mass flux and liquid subcooling were used as the main experimental parameters. The main conclusions of the present work are summarized as follows:

(1) The size and behavior of bubbles were significantly dependent on the pressure. The difference of the typical bubble diameter was greater than one order of magnitude between the experiments performed under the atmospheric and elevated pressures. In the experiments under the atmospheric pressure, most bubbles lifted off the heated surface within a short time after nucleation. Since the bubbles were collapsed rapidly in subcooled bulk liquid after the lift-off, the bubble lifetime was generally short. In contrast, bubbles usually slid along the vertical heated surface in the experiments under the elevated pressures. In this case, most bubbles traveled long distance, although some bubbles condensed to disappear during sliding in the experiments of high liquid subcooling.

(2) The wall superheat at the onset of nucleate boiling was higher in the experiments under the atmospheric pressure mainly due to low vapor density. In consequence, the Jakob number based on the wall superheat decreased with an increase in the pressure. It was shown that the boundary between the lift-off and sliding in the present experiments can be determined in terms of the Jakob number. It was also indicated that the bubble size scaled by the superheated layer thickness tended to increase with increased value of the Jakob number.

(3) The unsteady growth force, the time variation of the bubble shape and the condensation at the sidewall of the bubble were considered as the possible mechanisms to cause the bubble lift-off. It was considered that the bubble behavior observed in this work could be characterized in terms of the Jakob number since the three effects mentioned above are intensified with an increase in this dimensionless parameter.

References

[1] Y.Y. Hsu, On the size range of active nucleation cavities on a hating surface, Journal of Heat Transfer 84 (1962) 207–216.

[2] T. Sato, H. Matsumura, On the conditions of incipient subcooled boiling with forced convection, Bull. JSME 726 (1964) 392–398.

[3] J.G. Collier, J.R. Thome, Convective Boiling and Condensation, third ed., Oxford University Press, Oxford, 1994. pp. 325–374.

[4] N. Basu, G.R. Warrier, V.K. Dhir, Wall heat flux partitioning during subcooled flow boiling: part 1–model development, Journal of Heat Transfer 124 (2005) 131–140.

[5] S. Levy, Forced convection subcooled boiling prediction of vapor volumetric fraction, International Journal of Heat and Mass Transfer 10 (1967) 951–965.

[6] F.W. Staub, The void fraction in subcooled boiling–prediction of the initial point of net vapor generation, Journal of Heat Transfer 90 (1968) 151–157.

[7] J.T. Rogers, M. Salcudean, Z. Abdullah, D. McLeod, D. Poirier, The onset of significant void in up-flow boiling of water at low pressure and velocities, International Journal of Heat and Mass Transfer 30 (1987) 2247–2260.

[8] F.C. Gunther, photographic study of surface-boiling heat transfer to water with force convection, Journal of Heat Transfer 73 (1951) 115–123.

[9] E.L. Bibeau, M. Salcudean, A study of bubble ebullition in forced-convective subcooled nucleate boiling at low pressures, International Journal of Heat and Mass Transfer 37 (1994) 2245–2259.

[10] O. Zeitoun, M. Shoukri, Bubble behavior and mean diameter in subcooled flow boiling, Journal of Heat Transfer 118 (1996) 110–116.

[11] Thorncroft, G.E., Klausner, J.F., Mei, R., An experimental investigation of bubble growth and detachment in vertical upflow and downflow boiling, International Journal of Heat and Mass Transfer 41 (1998) 3857–3871.

[12] R. Situ, Y. Mi, M. Ishii, M. Mori, Photographic study of bubble behaviors in forced convection subcooled boiling, International Journal of Heat and Mass Transfer 47

(2004) 3659–3667.

[13] R. Situ, T. Hibiki, M. Ishii, M. Mori, Bubble lift-off size in forced convective subcooled boiling flow, International Journal of Heat and Mass Transfer 48 (2005) 5536–5548.

[14] T. Okawa, T. Ishida, I. Kataoka, M. Mori, Bubble rise characteristics after the departure from a nucleation site in vertical upflow boiling of subcooled water, Nuclear Engineering and Design 235 (2005) 1149–1161.

[15] Y. Hirose, T. Hayashi, T. Hazuku, T. Takamasa, T., Experimental study on contact angle of water droplet in high-temperature condition, Proceedings of the 14th International Conference on Nuclear Engineering, Miami, Florida, USA, 2006, Paper No. 89614.

[16] T. Takamasa, T. Hazuku, K. Okamoto, L. Mishima, M. Furuya, Radiation induced surface activation on Leidenfrost and quenching phenomena, Experimental Thermal and Fluid Science 29 (2005) 267–274.

[17] E.J. Davis, G.H. Anderson, The incipience of nucleate boiling in forced convection flow, AIChE Journal 12 (1966) 774–780.

[18] A.E. Bergles, W.M. Rohsenow, The determination of forced-convection surface-boiling heat transfer, Journal of Heat Transfer 1 (1964) 365–372.

[19] N. Basu, G.R. Warrier, V.K. Dhir, Onset of nucleate boiling and active nucleation site density during subcooled flow boiling, Journal of Heat Transfer 124 (2002) 717–728.

[20] A. Tomiyama, H. Tamai, I. Zun, S. Hosokawa, Transverse migration of single bubbles in simple shear flows, Chemical Engineering Science 57 (2002) 1849–1858.

[21] B.B. Mikic, W.M. Rohsenow, P. Griffith, On bubble growth rates, International Journal of Heat and Mass Transfer 13 (1970) 657–666.

[22] G.E. Thorncroft, J.F. Klausner, R. Mei, Bubble forces and detachment models, Multiphase Science and Technology 13 (2001) 35–76.

[23] T. Okawa, T. Harada, Y. Kotsusa, Photographic study on bubble motion in subcooled pool boiling, Journal of Engineering for Gas Turbines and Power 132

(2010) art. no. 102922.

[24] T. Okawa, K. Hayashi, A. Tomiyama, Numerical verification of a simplified model for vapor bubble lift-off from a hydrophilic heated flat-wall, Nuclear Engineering and Design 240 (2010) 3942–3948.

[25] A. Lucic, F. Mayinger, Transport phenomena in subcooled flow boiling, Heat Mass Transfer 46 (2010) 1159–1166.

CHAPTER 4 NET VAPOR GENERATION MECHANISM UNDER ATMOSPHERIC PRESSURE CONDITION

4.1 Introduction

Accurate prediction of the void fraction in subcooled flow boiling is of considerable importance in the design and operation of nuclear power plants since it influences various parameters including the core flow rate, fuel burnup and the inception of two-phase flow instabilities [1]. In flow boiling in a heated channel, the boundary between the single-phase region and the subcooled boiling region is determined by the onset of nucleate boiling (ONB), which is permitted at the location where the bulk liquid temperature is still lower than the saturation temperature but the wall temperature becomes high enough. It is however known that the void fraction near the point of ONB is low and a rapid increase in the void fraction commences at a certain point located further downstream of ONB [2]. This point is commonly regarded as the point of net vapor generation (PNVG) or the point of the onset of significant void (POSV) since the void fraction upstream of this point is very low and usually neglected. Kroger and Zuber showed that the ability to predict the PNVG is of essential importance in predicting the void fraction in subcooled flow boiling accurately [3].

Because of the importance in predicting the void fraction in the subcooled boiling region, many correlations have been developed so far for the PNVG as reviewed extensively by Lee and Bankoff [4] and Warrier and Dhir [5]. In the development of the PNVG correlations, it is frequently postulated that the bubbles are attached to the heated surface just downstream of ONB and the rapid increase of the void fraction is permitted

when the bubble departure from the nucleation site or the bubble lift-off from the heated surface occurs [6-9]. However, the correlations for PNVG commonly contain empirical constants, and their values are determined using the experimental data of the void fraction distribution. Therefore, although these correlations are useful to estimate the PNVG, it would not necessarily be guaranteed that the bubble departure or the bubble lift-off is the key phenomenon to cause NVG. In fact, several investigators visualized the bubble behavior in water subcooled flow boiling to observe that the bubbles did not stay at the nucleation sites even under the conditions close to ONB [10-14]. In preceding chapter, it was found that the bubble behavior at ONB was significantly dependent on the pressure; the bubbles were lifted off the heater surface immediately after the nucleation near the atmospheric pressure whilst they slid along the vertical heated surface for a long distance at elevated pressures. It was found that the wall superheat at ONB tended to increase sharply with a decrease in the system pressure, suggesting that bubble growth rate was greater at low pressure. It was hence discussed that the distinct difference observed in the bubble behavior could be attributed to significant influence of the pressure on the bubble growth rate immediately after the nucleation.

In order to develop a mechanistic and reliable correlation for the PNVG, the processes to cause the rapid increase of the void fraction in subcooled flow boiling should sufficiently be understood. Hence, in this work, both the void fraction measurement using a void probe and the observation of bubble behavior using a high-speed camera are performed at the same experimental conditions. The occurrence of NVG is first determined from the void fraction data. The movie data are then analyzed in detail to identify the key phenomena to cause the NVG.

4.2 Experimental Description

The present heated surface was rather hydrophilic due to oxidization and its mean contact angle was measured 18º. The upper measuring section was only used for the measurement of thermal-flow properties as well as the local void fraction. The measurement procedure for P ΔT_{sub}, G and q_w was discussed in Chapter 2 and 3. As was discussed in Chapter 2, local void fraction is measured using an optical void probe. The sensor tip of the void probe was 0.08 mm in diameter. As shown in the side view in Fig. 2.2, the void probe was set at an inclination angle of 30º from the horizontal and traversed using a micrometer. In addition, two sets of glass windows were mounted at the measuring sections for visual observation of bubbles using a high-speed camera. In the present experiments, the visualization area of the high-speed camera is about 15 mm high and 10 mm wide with the spatial resolution of about 0.03 mm/pixel. The frame rate and the shutter speed were set to 6000 fps and 0.167 ms, respectively.

The main experimental parameters were the pressure, liquid subcooling, mass flux and the heat flux. Listed in Tables 4.1 to 4.3 are the three sets of experimental conditions tested in this work, which are hereafter referred to as Exp. Nos. 1 to 3, respectively. The values of the wall superheat ΔT_w, thermal-equilibrium vapor quality x_{eq} and mean void fraction α are also listed in the tables; precise definitions of α will be given later. In each set of experiments, ΔT_{sub} was reduced step by step to measure the void fraction distribution in the lateral direction by traversing the optical void probe and then record the bubble behavior using the high-speed camera. In each set of experiments, it was tried to keep P, G and q_w constant. It should however be noted that a noticeable increase in P was unavoidable when the liquid temperature approached the saturation temperature due

to limitation of the condenser performance as can be seen in the tables. Throughout the experiments, a data acquisition system attached to a personal computer recorded the temperatures, pressures and mass fluxes every 1 second.

Table 4.1 Main experimental conditions and results in Exp. No. 1

Run	P (kPa)	G (kg/m^{2}s)	q_w (kW/m^2)	ΔT_{sub} (K)	ΔT_w (K)	x_{eq} (%)	$\langle\alpha\rangle_1$ (%)	$\langle\alpha\rangle_2$ (%)
101	103	390	217	16.3	9.5	-3.14	0	-
102	102	392	219	15.2	10.6	-2.88	0	-
103	103	392	213	14.4	10.4	-2.71	0	-
104 (ONB)	102	393	213	13.3	11.5	-2.49	0.001	-
105	102	395	210	12.2	12.0	-2.30	0.001	-
106	101	395	212	11.2	12.7	-2.07	0.020	-
107 (NVG)	101	389	215	9.6	14.3	-1.88	0.020	-
108	100	387	224	7.6	15.0	-1.40	0.377	0.477
109	101	384	227	6.6	15.1	-1.09	0.443	0.789
110	103	409	229	4.9	13.4	-0.65	1.170	1.240
111	115	409	229	3.7	13.3	-0.38	-	2.307
112	128	407	227	2.3	13.0	-0.06	-	3.715

Table 4.2 Main experimental conditions and results in Exp. No. 2

Run	P (kPa)	G (kg/m^{2}s)	q_w (kW/m^2)	ΔT_{sub} (K)	ΔT_w (K)	x_{eq} (%)	$\langle\alpha\rangle_1$ (%)	$\langle\alpha\rangle_2$ (%)
201	114	462	226	19.7	5.9	-3.43	0	-
202	113	462	216	17.4	6.6	-3.03	0	-
203	113	461	222	16.3	8.3	-2.82	0	-
204	113	460	217	15.4	8.6	-2.65	0	-
205 (ONB)	113	461	215	14.3	9.4	-2.44	0.000	-
206	113	461	222	13.2	10.9	-2.23	0.001	-
207	112	463	224	12.2	11.9	-2.03	0.005	-
208 (NVG)	113	460	221	11.3	11.8	-1.88	0.032	0.058
209	113	461	218	10.5	11.7	-1.73	0.101	0.147
210	115	460	222	9.8	11.9	-1.59	0.201	0.282
211	115	458	220	8.7	12.0	-1.39	0.235	0.356
212	117	460	217	7.3	12.6	-1.13	0.498	0.747
213	120	456	218	6.4	12.4	-0.93	-	1.050
214	128	458	223	5.4	12.5	-0.70	-	1.805
215	140	459	221	3.8	12.6	-0.46	-	2.755

Table 4.3 Main experimental conditions and results in Exp. No. 3

Run	P (kPa)	G (kg/m^{2}s)	q_w (kW/m^2)	ΔT_{sub} (K)	ΔT_w (K)	x_{eq} (%)	$\langle\alpha\rangle_1$ (%)	$\langle\alpha\rangle_2$ (%)
301	111	529	269	19.5	8.8	-3.38	0	-
302	112	532	265	18.1	9.4	-3.14	0	-
303	111	533	265	16.7	10.7	-2.88	0	-
304 (ONB)	112	534	263	16.0	11.1	-2.73	0.000	-
305	112	536	267	15.0	12.3	-2.56	0.000	-
306	113	538	269	14.3	13.2	-2.42	0.001	-
307	114	539	268	13.4	13.5	-2.24	0.015	0.001
308 (NVG)	114	539	265	12.8	13.6	-2.13	0.020	0.026
309	114	532	269	11.7	14.1	-1.93	0.083	0.161
310	114	535	271	10.7	14.5	-1.74	0.158	0.294
311	116	528	266	9.1	14.3	-1.43	-	0.548
312	121	529	274	8.2	14.4	-1.26	-	0.968
313	131	531	274	7.2	14.0	-1.04	-	1.523
314	148	532	273	5.2	13.9	-0.72	-	2.482

4.3. Experimental results

4.3.1. Determination of the NVG condition

The void fraction was measured using the void probe as described in the previous chapter but the movie data were additionally used in several experimental conditions. The typical bubble behavior observed at ONB is presented in Fig. 4.1. In this case, only one nucleation site was activated within the visualization section, and all the bubbles produced at this site were lifted off the vertical heated surface immediately after the nucleation to disappear quickly in the subcooled bulk liquid as reported in our previous paper [13]. In consequence, no bubbles hit the probe tip although a number of bubbles were produced. Therefore, in order to measure the volume-averaged void fraction in the visualization section $<\alpha>$ accurately, $<\alpha>$ was calculated from the movie data using the following equation.

$$\langle \alpha \rangle = \frac{1}{V_0 N_{\mathrm{im}}} \sum_{\mathrm{i}=1}^{N_{\mathrm{im}}} \sum_{\mathrm{j}=1}^{N_{\mathrm{b,i}}} V_{\mathrm{b,ij}} \tag{1}$$

where V_0 is the volume of the visualization section, N_{im} is the number of images analyzed, $N_{\mathrm{b,i}}$ is the number of bubbles included in the i-th image, and $V_{\mathrm{b,ij}}$ is the volume of the j-th bubble included in the i-th image. In calculating V_{b}, it was simply assumed that the sphere-equivalent bubble diameter was equal to the arithmetic average of the maximum dimensions of the bubble image in the horizontal and vertical directions.

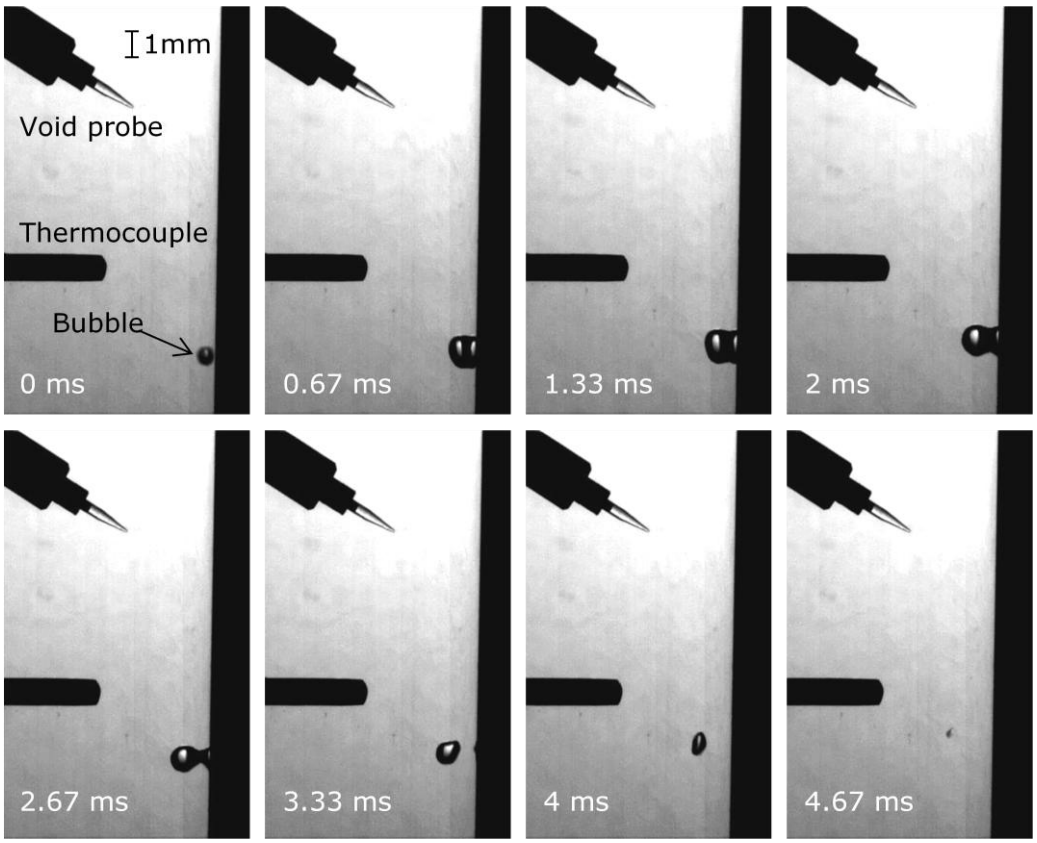

Fig. 4.1 Typical bubble behavior observed at ONB (Run 104)

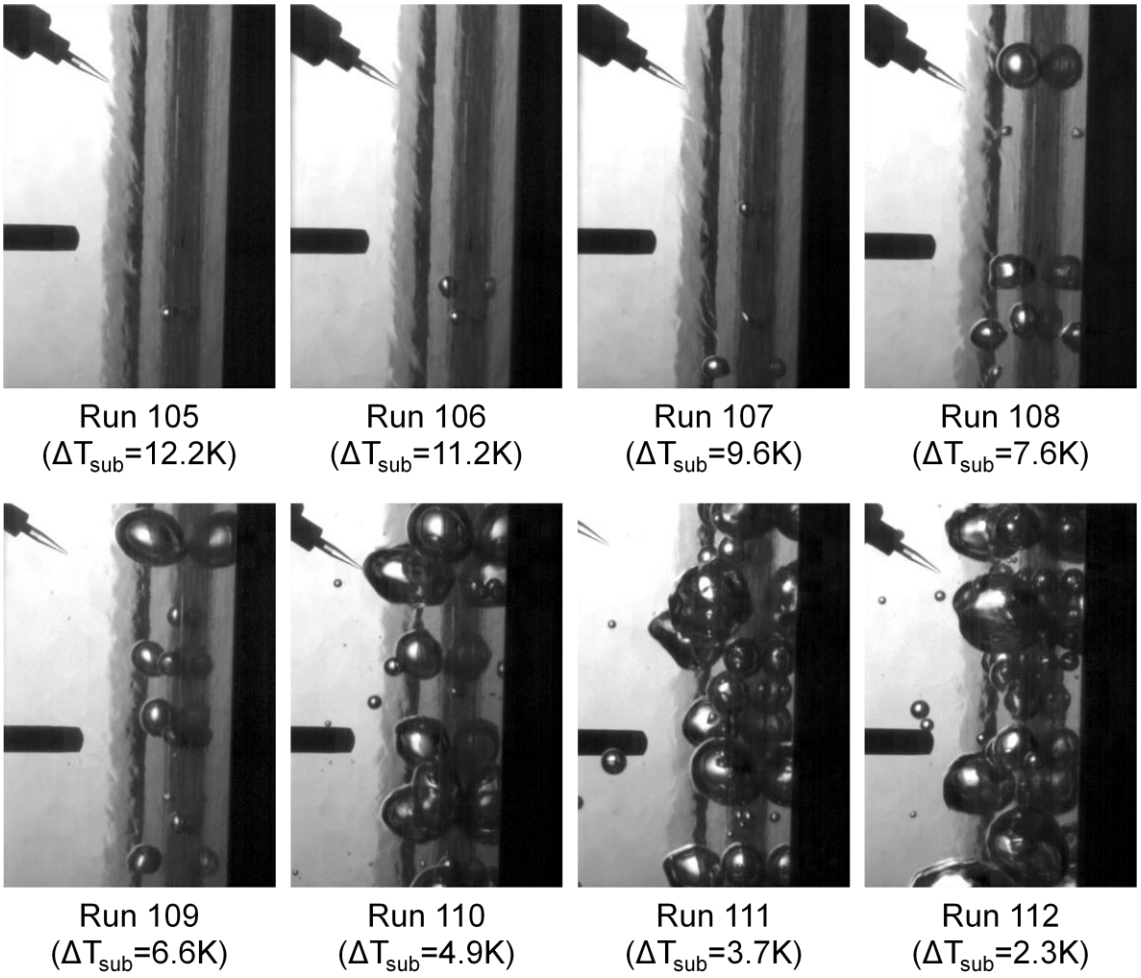

Fig. 4.2 Snapshots of bubbles at different values of subcooling in Exp. No. 1

The snapshots obtained at several values of ΔT_{sub} in Exp. No. 1 are displayed in Fig. 4.2. At low values of ΔT_{sub}, the measurement of void fraction from the movie data was not possible due to considerable overlapping of bubbles. It was however expected that the local time-averaged void fraction α_{lta} was not influenced by the relative position of the probe tip with the active nucleation sites significantly. Hence, the values of $<\alpha>$ were estimated from the probe data in these cases. The void profiles measured using the void probe are depicted in Fig. 4.3. Here, y denotes the distance from the heated surface.

It can be seen that the peak void fraction and the bubble layer thickness increased with a decrease in ΔT_{sub} as in the experiments conducted by previous investigators [14, 15]. From the void profiles in Fig. 4.3, the values of $<\alpha>$ were calculated by

$$\langle \alpha \rangle = \frac{l_h}{A_0} \int_0^{w_0} \alpha_{lta} \, dy \tag{2}$$

where A_0 and w_0 are the cross-sectional area (200 mm^2) and the width (10 mm) of the rectangular channel and l_h is the depth of the heated area (10 mm). It was confirmed in several experimental conditions of moderate void fraction that the values of $<\alpha>$ calculated by Eqs. 1 and 2 coincide each other fairly well (see Tables 4.1-3 and Fig. 4.4; here, $<\alpha>_1$ and $<\alpha>_2$ denote the values of $<\alpha>$ calculated using Eqs. 1 and 2, respectively.).

In Fig. 4.4, the values of $<\alpha>$ are plotted against the thermal-equilibrium quality x_{eq} to decide the NVG conditions. It can be confirmed that the void fraction was negligibly small under the conditions close to ONB and ΔT_{sub} should further be reduced to initiate the net vapor generation. From the evident change of the slopes, the conditions of NVG were decided as indicated with the arrows in Figs. 4.4a-c. Lee and Bankoff [4] compared various NVG correlations using 8 sets of low pressure data for water to report that the one developed by Saha and Zuber [8] showed the best performance. In view of this, the NVG conditions in the present work were compared with the predictions by the Saha-Zuber correlation. It was confirmed that the values of ΔT_{sub} at NVG determined in this work agreed with the predictions fairly well within the error of ±2 K.

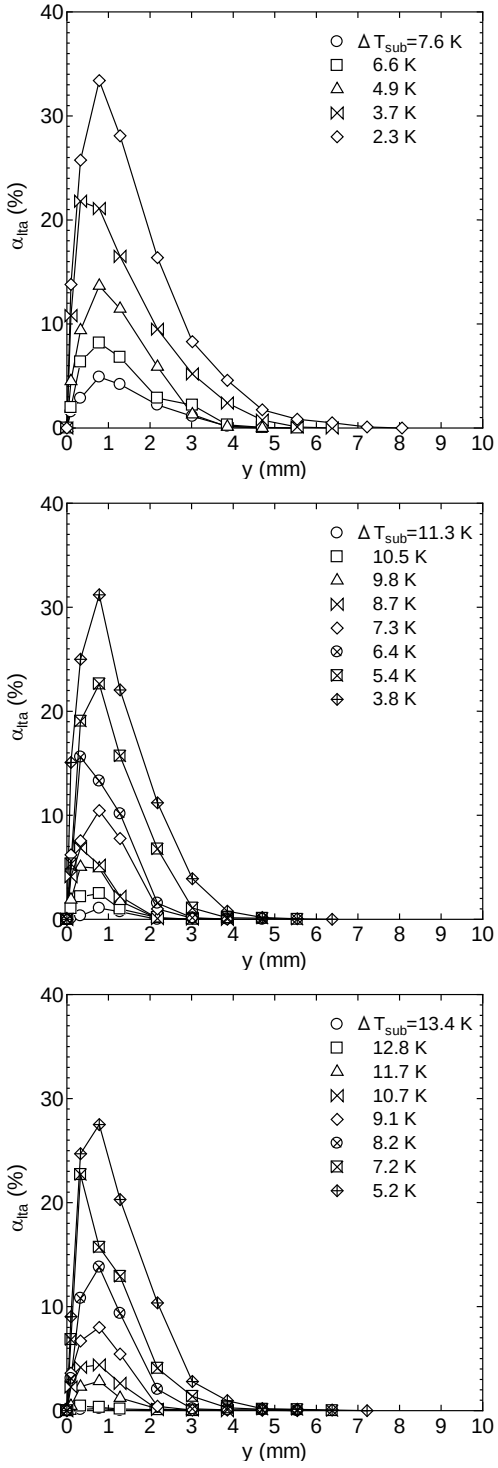

Fig. 4.3 Dependence of the lateral void fraction distribution on the liquid subcooling; (a) Exp. No. 1, (b) Exp. No. 2, and (c) Exp. No. 3

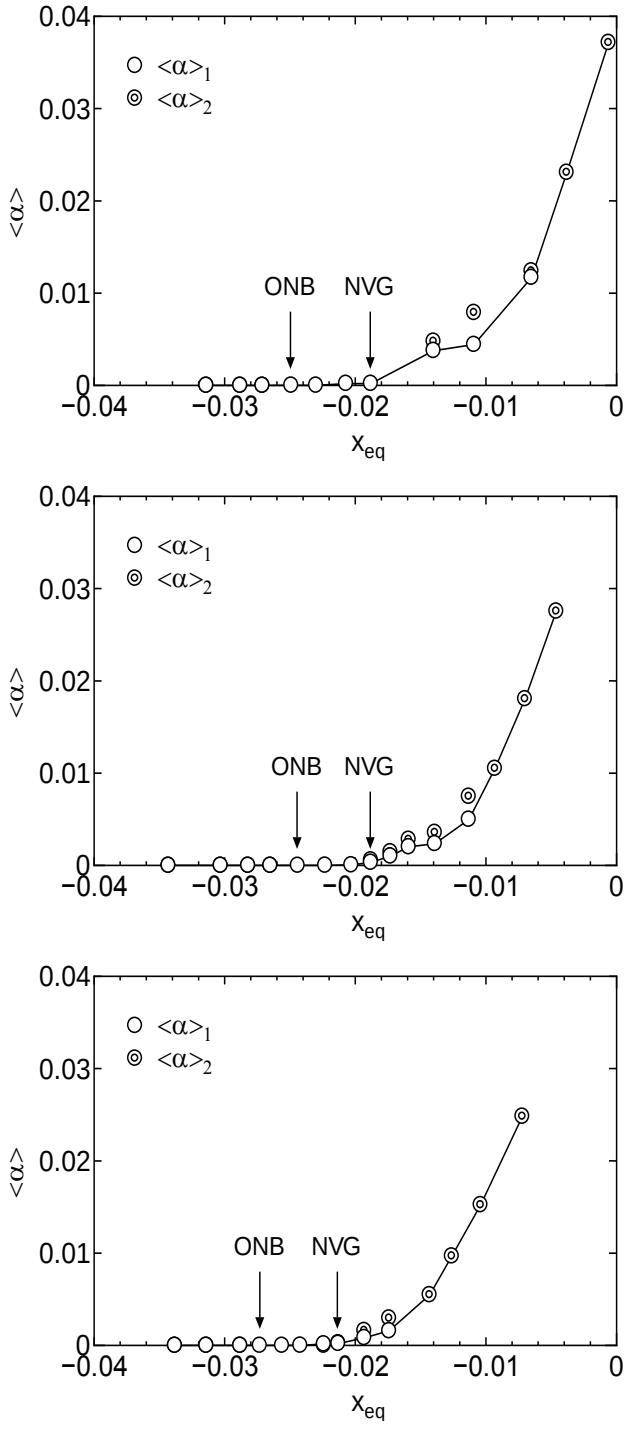

Fig. 4.4 Dependence of the mean void fraction at the measuring section on the thermal-equilibrium vapor quality; (a) Exp. No. 1, (b) Exp. No. 2, and (c) Exp. No. 3

4.3.2. Key phenomena causing NVG

In the present experiments, bubbles were detached from the heated surface and propelled into the subcooled bulk liquid even at the ONB as shown in Fig. 4.1. Therefore, neither the bubble departure from the nucleation site nor the bubble lift-off from the heated surface is considered to be the mechanism triggering the NVG. Here, a fundamental investigation is carried out on the condition under which a rapid increase in the void fraction commences. If the steady state is postulated, the continuity equation of the one-dimensional two-fluid model for the vapor phase is given by

$$\frac{\mathrm{d}}{\mathrm{d}z}(\alpha\rho_{\mathrm{g}}u_{\mathrm{g}}) = \Gamma_{\mathrm{V}} - \Gamma_{\mathrm{C}} \tag{3}$$

where z is the axial coordinate, α is the void fraction, ρ is the density, u is the velocity in the vertical direction, Γ_{V} is the vaporization rate, Γ_{C} is the condensation rate, and the subscript g refers the vapor phase. If ρ_{g} and u_{g} are assumed to be constant for simplicity and z is replaced by x_{eq}, Eq. 3 is rewritten as

$$\frac{\mathrm{d}\alpha}{\mathrm{d}x_{\mathrm{eq}}} = \frac{Gh_{\mathrm{fg}}A_0}{q_{\mathrm{w}}l_{\mathrm{h}}\rho_{\mathrm{g}}u_{\mathrm{g}}}(\Gamma_{\mathrm{V}} - \Gamma_{\mathrm{C}}) \tag{4}$$

The above equation confirms that the net vaporization rate ($\Gamma_{\mathrm{V}} - \Gamma_{\mathrm{C}}$) is of primary importance for α to increase sharply with an increase in x_{eq}. It was observed in the present experiments that at high liquid subcooling, all the vapor bubbles disappeared in close proximity to the nucleation site due to condensation. In this case, $\Gamma_{\mathrm{V}} \approx \Gamma_{\mathrm{C}}$ holds and consequently Eq. 4 does not permit a rapid increase in α with x_{eq}.

Important bubble behavior observed in Run 108 is presented in Fig. 4.5. Under this experimental condition, most bubbles disappeared quickly as shown in Fig. 4.1 but some bubbles could travel for a long distance to arrive at the top of the visualization section. One such example is indicated with circles in the figure. Although the bubble was once lifted off the vertical heated surface immediately after the nucleation (1–3 ms), it was reattached to the surface at 4 ms and then slid along the surface for a long distance. During the sliding stage, the bubble size increased asymptotically due to the heat supplied from the wall. It is evident that the occurrence of the bubble reattachment followed by the formation of sliding bubble disturbed the balance between Γ_V and Γ_C ($\Gamma_V > \Gamma_C$).

The bubble reattachment was observed more frequently at lower values of ΔT_{sub}. The time-elapsed bubble images obtained in Run 111 are shown in Fig. 4.6. It can be seen that the two bubbles formed successively at the same nucleation site were reattached to the heated surface to travel upward for a long distance. Figures 4.7a-c show the bubble reattachment probabilities Π_{att} that was simply defined as the number of reattached bubbles divided by the total number of bubbles; here, the measurement of Π_{att} was performed for the bubbles produced at the nucleation site first activated at ONB. It is also noted that Π_{att} could be measured only at high and moderate values of liquid subcooling due to significant bubbles' overlapping at low subcooling. It can be seen in Figs. 4.7a-c that Π_{att} is zero at the low values of x_{eq} close to ONB, and the conditions under which Π_{att} takes positive values correspond to those of NVG very well.

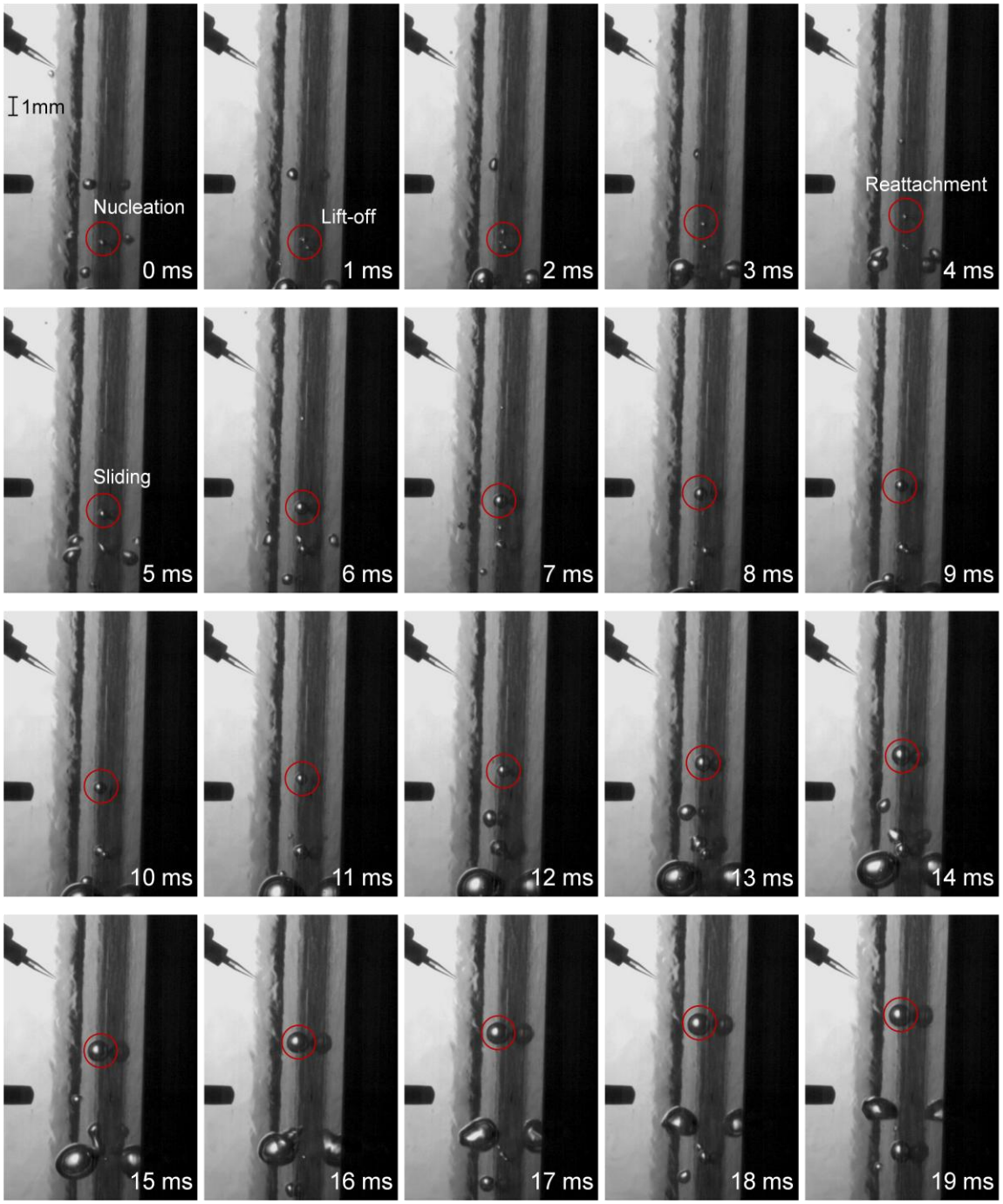

Fig. 4.5 Process of the bubble reattachment to the heated surface after the lift-off (Run 108)

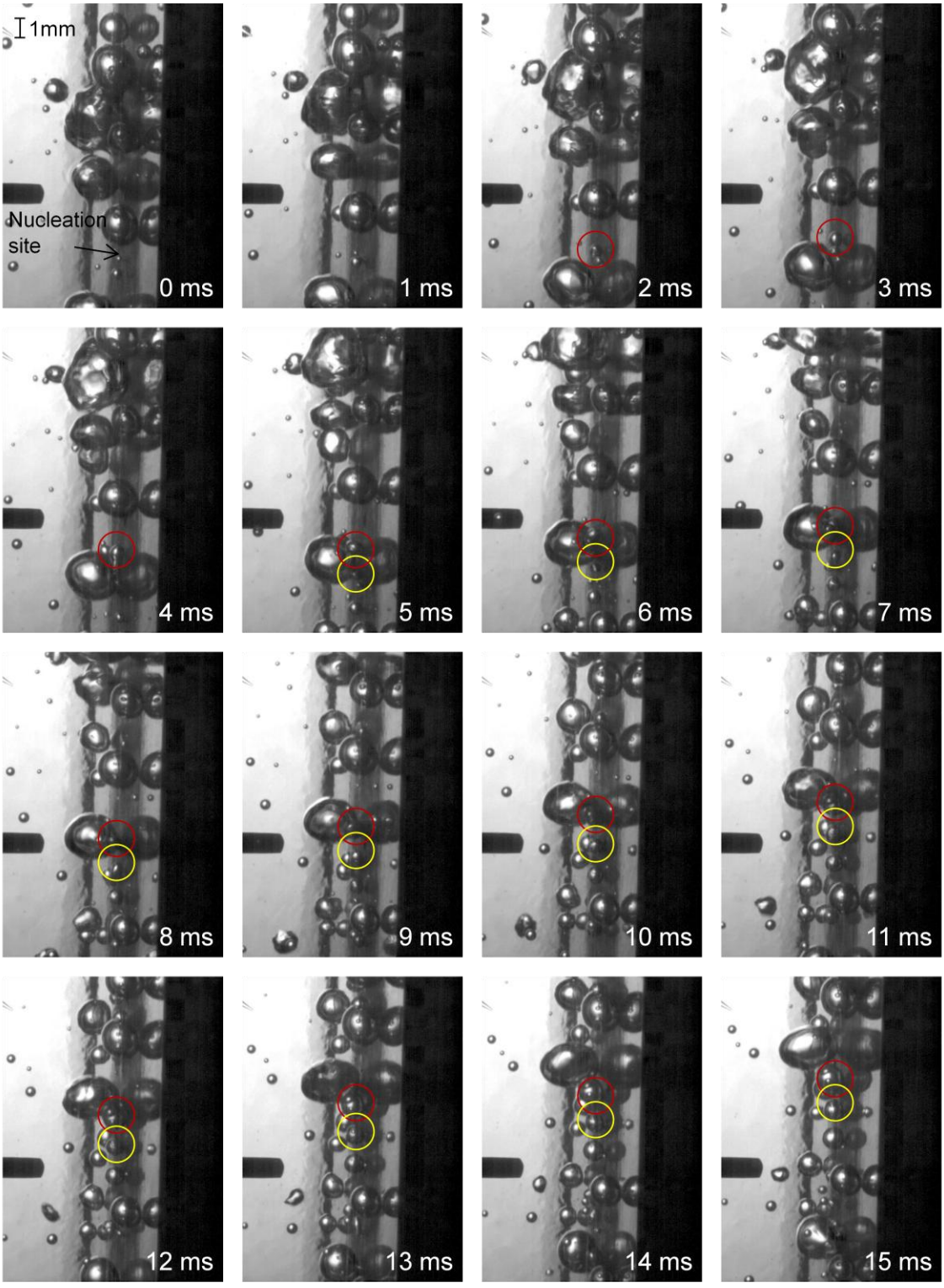

Fig. 4.6 Process of the bubble reattachment at lower subcooling (Run 111)

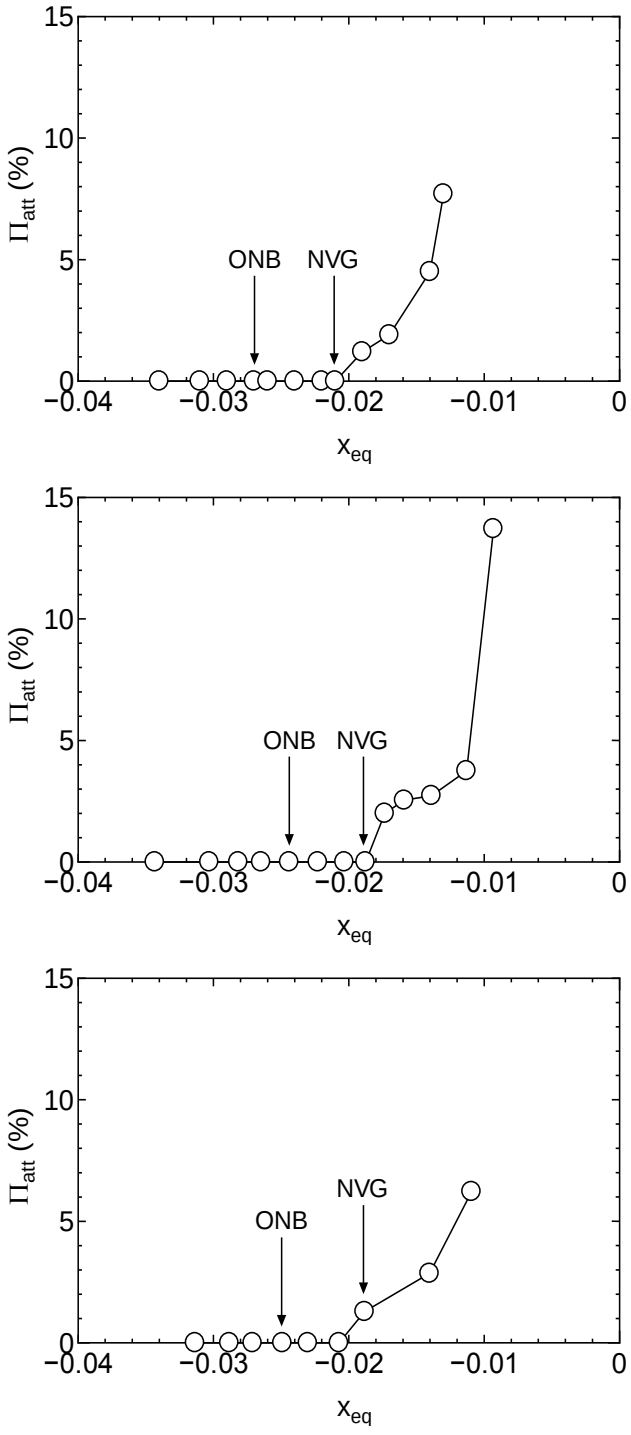

Fig. 4.7 Dependence of the bubble reattachment probability on the thermal-equilibrium vapor quality; (a) Exp. No. 1, (b) Exp. No. 2, and (c) Exp. No. 3

In order to investigate the contribution of the bubble reattachment to the increase of the void fraction quantitatively, the movie data were used to measure the amounts of vaporization and condensation for the individual bubbles nucleated within the visualization section. However, when the bubble is attached to the heated surface in subcooled flow boiling, vaporization at the wall side and condensation at the bulk liquid side occur simultaneously. It should hence be noted that accurate measurement of these phase change rates from the movie data was not always possible. Since the purpose of the image analysis was to reveal the contribution of the bubble reattachment to the increase of the void fraction, the following simplified methods were used in the present work. First, for the bubbles that were not reattached to the surface, the period between the nucleation and lift-off was regarded as the vaporization period and the period after the lift-off as the condensation period. The apparent masses of vaporization $\gamma_{\mathrm{V}}^{\mathrm{a}}$ and condensation $\gamma_{\mathrm{C}}^{\mathrm{a}}$ for each bubble were consequently defined by

$$\gamma_{\mathrm{V}}^{\mathrm{a}} = \rho_{\mathrm{g}} \frac{\pi d_{\mathrm{b,lift}}^3}{6} \tag{5}$$

$$\gamma_{\mathrm{C}}^{\mathrm{a}} = \rho_{\mathrm{g}} \frac{\pi}{6} (d_{\mathrm{b,lift}}^3 - d_{\mathrm{b,f}}^3) \tag{6}$$

where $d_{\mathrm{b,lift}}$ is the lift-off bubble diameter and $d_{\mathrm{b,f}}$ is the bubble diameter when the bubble vanishes from the visualization section. Since most bubbles were collapsed within the visualization section due to condensation if the reattachment did not occur, the value of $d_{\mathrm{b,f}}$ was usually zero. Next, for the bubbles that were reattached to the surface, only the mass of net vaporization was considered:

$$\gamma_{\mathrm{V}}^{\mathrm{a}} = \rho_{\mathrm{g}} \frac{\pi d_{\mathrm{b,f}}^3}{6} \tag{7}$$

$$\gamma_{\mathrm{C}}^{\mathrm{a}} = 0 \tag{8}$$

Since the bubbles slid along the surface after the reattachment, $d_{\mathrm{b,f}}$ was equal to the bubble size when the bubble left the visualization section. The apparent phase change rates $\Gamma_{\mathrm{V}}^{\mathrm{a}}$ and $\Gamma_{\mathrm{C}}^{\mathrm{a}}$ within the visualization section are calculated by

$$\Gamma_{\mathrm{K}}^{\mathrm{a}} = \frac{1}{V_0 t_0} \sum_{\mathrm{i=1}}^{N_{\mathrm{s}}} \sum_{\mathrm{j=1}}^{N_{\mathrm{b,i}}} (\gamma_{\mathrm{K}}^{\mathrm{a}})_{\mathrm{ij}} \tag{9}$$

where t_0 is the recording time, N_{s} is the number of active nucleation sites within the visualization section, $N_{\mathrm{b,i}}$ is the number of bubbles produced at the i-th nucleation site; the subscript K denotes V or C and the subscript ij refers the j-th bubble produced at the i-th nucleation site. The net vaporization rate Γ_{Net} is calculated by

$$\Gamma_{\mathrm{Net}} = \Gamma_{\mathrm{V}}^{\mathrm{a}} - \Gamma_{\mathrm{C}}^{\mathrm{a}} \tag{10}$$

Here, the superscript *a* was not attached to Γ_{Net} since the true values of γ_{V} and γ_{C} were indeterminate but the difference between γ_{V} and γ_{C} could be measured correctly from the time-elapsed bubble images. The values of $\Gamma_{\mathrm{V}}^{\mathrm{a}}$, $\Gamma_{\mathrm{C}}^{\mathrm{a}}$ and Γ_{Net} for Exp. Nos. 1-3 are plotted against x_{eq} in Figs. 4.8a-c, respectively. In all the three experimental conditions, $\Gamma_{\mathrm{V}}^{\mathrm{a}}$ tends to increase with x_{eq} after the ONB condition is reached. This implies that bubble ebullition from the heated surface was intensified gradually with decreased value of ΔT_{sub} even if the condition of NVG was not reached. However, almost all the bubbles

were collapsed within the visualization section due to condensation unless they were not reattached to the surface. Thus, between the conditions of ONB and NVG, both the values of Γ_V^a and Γ_C^a increase with x_{eq} and consequently the value of Γ_{Net} remains zero. It can be confirmed that the condition of NVG is eventually reached when Γ_{Net} takes nonzero values.

Equation 4 was used to investigate the effect of Γ_{Net} on $d\alpha/dx_{eq}$ quantitatively. In Fig. 4.9, the contribution of the new bubbles nucleated within the visualization section was calculated by substituting Γ_{Net} to the place of $\Gamma_V - \Gamma_C$ in Eq. 4 and compared with the actual increasing rate of the void fraction. The actual values of $d\alpha/dx_{eq}$ were simply calculated from the differences of α and x_{eq} between the two successive experiments listed in Tables 4.1-3. It would be interesting to note that the values of $d\alpha/dx_{eq}$ calculated by the two methods are in the same order of magnitude, indicating that the bubble reattachment followed by the formation of sliding bubbles was a key phenomenon to cause the rapid increase of $d\alpha/dx_{eq}$ at point of NVG in the present experiments.

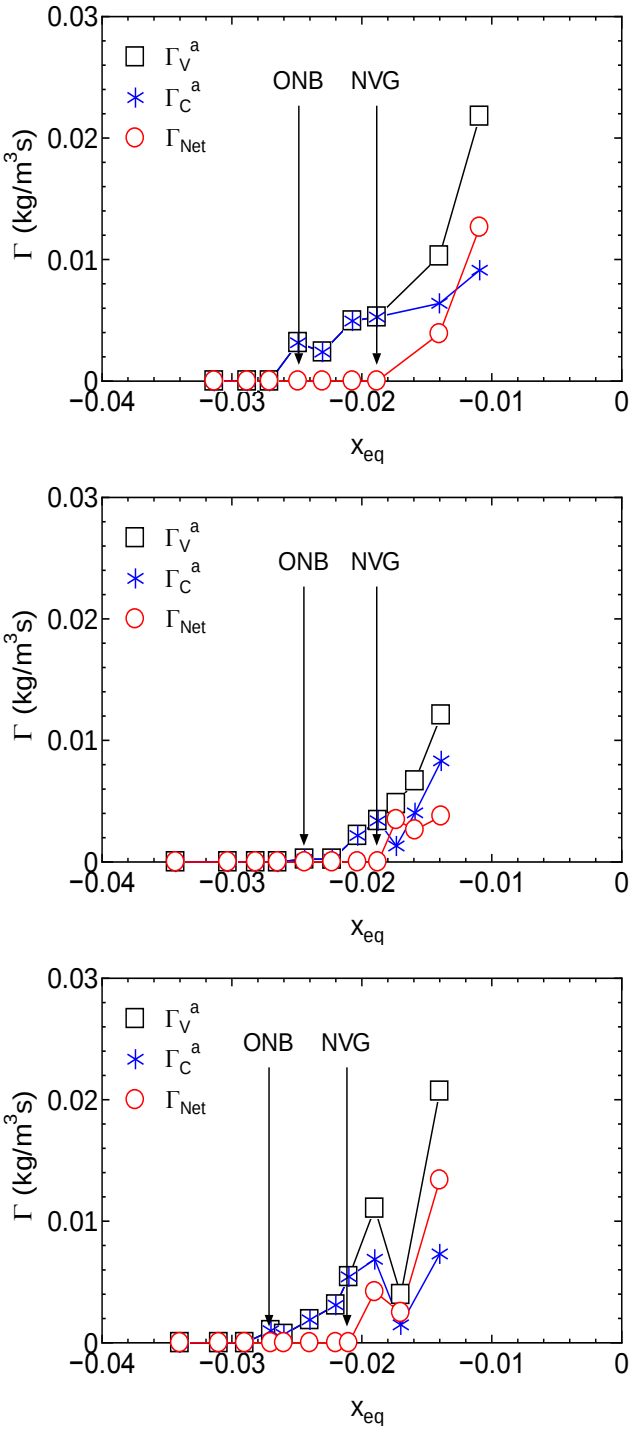

Fig. 4.8 Vaporization, condensation and net vaporization within visualization section; (a) Exp. No. 1, (b) Exp. No. 2, and (c) Exp. No. 3

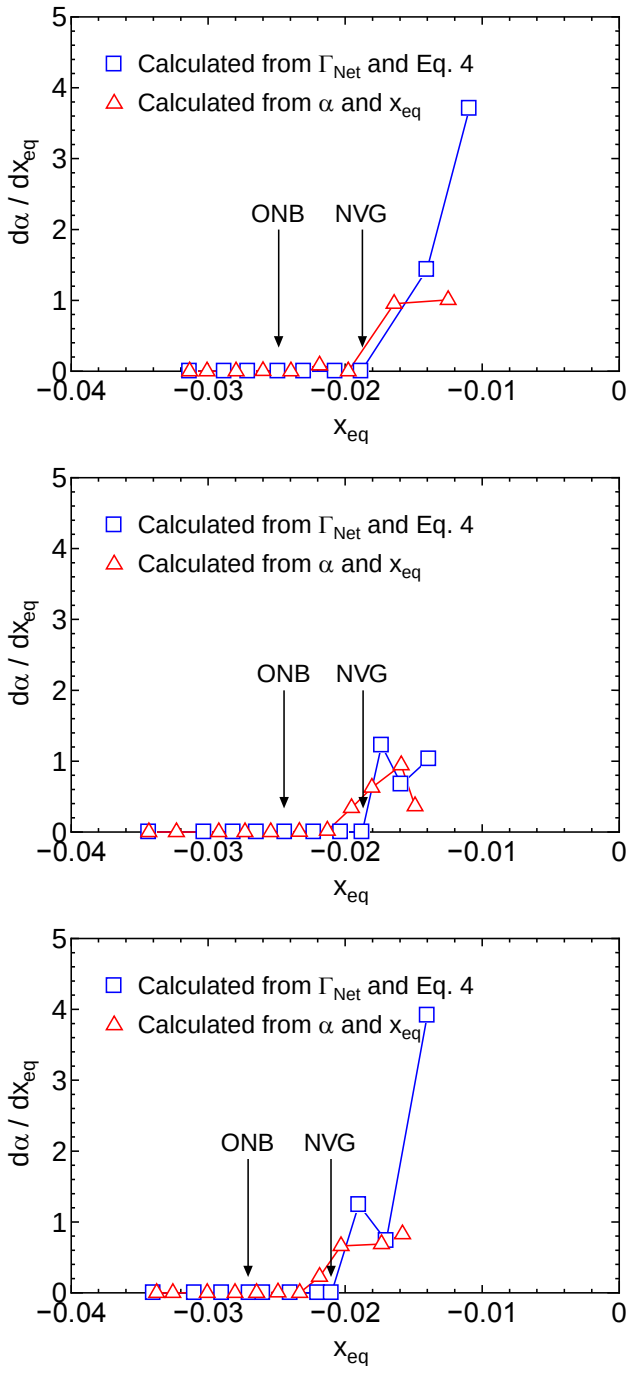

Fig. 4.9 Comparisons of the void gradients measured by the image analysis with those calculated from the void fractions measured in the two successive experimental conditions.

4.4. Conclusion

Bubble behavior in vertical upward subcooled flow boiling of water was studied to investigate the mechanisms triggering the net vapor generation at low pressure. In the present work, the inlet liquid subcooling was gradually decreased to change the thermal-equilibrium quality at the measuring section parametrically. At the high values of liquid subcooling near ONB, all the bubbles were lifted off the heated wall immediately after the nucleation and then collapsed in the subcooled bulk liquid. Since the condensation rate was nearly equal to the vaporization rate, a rapid increase in the vapor void fraction with an increase in the thermal-equilibrium quality was not permitted. It was found that some bubbles could be reattached to the surface when the subcooling was low enough. Since the bubbles slid along the vertical heated surface for a long distance after the reattachment, the occurrence of the bubble reattachment contributed to the increase of the void fraction. It was also confirmed that the increase of the void fraction caused by the bubble reattachment was in the same order of magnitude with the actual increase of the void fraction with increased value of the thermal-equilibrium quality. It can hence be said that the onset of the bubble reattachment followed by the formation of sliding bubbles played a particularly important role in causing NVG in the experimental conditions tested in the present work.

It should however be noted that the phenomenon triggering the NVG would be dependent on several factors. For instance, it is observed in preceding chapter that the bubbles in water subcooled flow boiling were not lifted off the surface at elevated pressures [14]. Furthermore, the lift-off of bubbles may be restricted to some extent if the heated surface is less hydrophilic [17]. When the bubbles are not lifted off the surface

after the nucleation, the bubble reattachment cannot be the main cause of NVG. Maity investigated the bubble dynamics in flow boiling using the channel orientation as a main experimental parameter [13]. In his work, the reattachment of bubbles was observed only in the experiments of vertical upflow, indicating that the flow direction would also affect the triggering mechanism of NVG. Another concern is the effect of mass flux. Saha and Zuber [8] indicated the possibility that the mechanism to cause NVG is different between low and high mass flux conditions and the boundary is expressed using the Peclet number. Since the present experiments were performed under the low mass flux condition in their notation, different phenomena might be of greater importance if the mass flow rate is increased. Although the main cause of NVG could be attributed to the bubble reattachment in present experiments, further studies are necessary to systematically understand the mechanisms causing the net vapor generation in subcooled flow boiling.

References

[1] S.C. Lee, S.G. Bankoff, Prediction of the onset of flow instability in transient subcooled flow boiling, Nuclear Engineering and Design 139 (1) (1993) 149-159.

[2] J.G. Collier, J.R. Thome, Convective Boiling and Condensation, third ed., Oxford University Press, Oxford, 1994. 325-374.

[3] P.G. Kroeger, N. Zuber, An analysis of the effects of various parameters on the average void fractions in subcooled boiling, International Journal of Heat and Mass Transfer 11 (2) (1968) 211-233.

[4] S.C. Lee, S.G. Bankoff, A comparison of predictive models for the onset of significant void at low pressures in forced-convection subcooled boiling, Journal of Mechanical Science and Technology 12 (3) (1998) 504-513.

[5] G.R. Warrier, V.K. Dhir, Heat transfer and wall heat flux partitioning during subcooled flow nucleate boiling–a review, Journal of Heat Transfer 128 (12) (2006) 1243-1256.

[6] R.W. Bowring, Physical model based on bubble detachment and calculation of steam voidage in the subcooled region of a heated channel, OECD Halden Reactor Project Report HPR-10, 1962.

[7] S. Levy, Forced convection subcooled boiling prediction of vapor volumetric fraction, International Journal of Heat and Mass Transfer 10 (7) (1967) 951-965.

[8] P. Saha, N. Zuber, Point of net vapor generation and vapor void fraction in subcooled boiling, Proceedings of the 5th International Heat Transfer Conference, Tokyo, 1974, pp. 175-179.

[9] J.T. Rogers, M. Salcudean, Z. Abdullah, D. McLeod, D. Poirier, The onset of significant void in up-flow boiling of water at low pressure and velocities, International Journal of Heat and Mass Transfer 30 (11) (1987) 2247-2260.

[10] G.E. Dix, Vapor void fraction for forced convection with subcooled boiling at low flow rates, Ph.D. Thesis, University of California, Berkeley, CA, 1971.

[11] E.L. Bibeau, M. Salcudean, A study of bubble ebullition in forced-convective

subcooled nucleate boiling at low pressures, International Journal of Heat and Mass Transfer 37 (15) (1994) 2245-2259.

[12] T. Okawa, T. Ishida, I. Kataoka, M. Mori, Bubble rise characteristics after the departure from a nucleation site in vertical upflow boiling of subcooled water, Nuclear Engineering and Design 235 (10-12) (2005) 1149–1161.

[13] Sandipan Maity, Effect of velocity and gravity on bubble dynamics, M.S. thesis, University of California, Los Angeles, 2000

[14] R. Ahmadi, T. Ueno, T. Okawa, Bubble dynamics at boiling incipience in subcooled upward flow boiling, International Journal of Heat and Mass Transfer 55 (1-3) (2012) 488-497.

[15] R. Situ, T. Hibiki, X. Sun, Y. Mi, M. Ishii, Flow structure of subcooled boiling flow in an internally heated annulus, International Journal of Heat and Mass Transfer 47 (24) (2004) 5351-5364.

[16] B.J. Yun, B.U. Bae, D.J. Euh, G.C. Park, C.-H. Song, Characteristics of the local bubble parameters of a subcooled boiling flow in an annulus, Nuclear Engineering and Design 240 (9) (2010) 2295-2303.

[17] T. Okawa, T. Harada, Y. Kotsusa, Photographic study on bubble motion in subcooled pool boiling, Journal of Engineering for Gas Turbines and Power 132 (10) (2010) Paper No. 102922.

CHAPTER 5 NET VAPOR GENERATION MECHANISM UNDER MODERATE PRESSURE CONDITION

5.1 Introduction

Prediction of the void fraction profile in the subcooled flow boiling region is of considerable practical importance in evaluating the two-phase flow instabilities in boiling channels and the neutron moderation and fuel burnup in nuclear reactor cores [1-5]. In a boiling channel, two-phase flow region is commenced at the point of the onset of nucleate boiling (ONB) where the wall temperature sufficiently exceeds the saturation temperature to permit the first bubbles to appear on the heated surface [1]. It is however known that the void fraction remains low within a certain region and it eventually starts to increase vigorously at the point further downstream from the point of ONB. Since the void faction just downstream from the ONB point is neglected in many cases, inception of the vigorous increase of the void fraction is commonly regarded as the onset of significant void (OSV) or the net vapor generation (NVG). Accurate evaluation of the point of NVG is an important step in predicting the void fraction profile in the subcooled boiling region [6-7].

In many models for the void fraction profile in subcooled flow boiling, the onset of NVG is associated with the behavior of vapor bubbles [7-12]. For instance, Levy postulated that the NVG occurs when the buoyancy and frictional forces attempting to remove the bubble overcome the surface tension force attempting to hold it on the heated surface [9]. Since the bubble behavior is of importance in evaluating the void fraction as well as the heat transfer [13], a number of visualization studies of subcooled flow boiling

were carried out so far in various configurations and different experimental conditions [14-27]. Although the behavior of vapor bubbles produced at the nucleation cavity is dependent on the surface wettability [15], bubble lift-off from the heated surface followed by the condensation in subcooled bulk liquid are observed in many experiments of water subcooled upward flow boiling particularly under low pressure conditions [15-24]. Whilst, the presence of bubbles sliding along the vertical heated surface for a long distance is also reported by several investigators [25-27]. The results of these visualization experiments are useful to correlate important parameters in subcooled flow boiling with fundamental ones such as the mass flux and heat flux. For instance, Prodanovic et al. [17] and Zeitoun and Shoukri [21] developed empirical correlations for the maximum and detachment bubble diameters and the Sauter mean bubble diameter, respectively. Numerical analyses of the void fraction in the subcooled flow boiling using a drift-flux model [28] and a two-fluid model [29-32] are also conducted. However, since the mechanisms of NVG have not been clarified sufficiently, fully empirical methods are still used to decide the onset of NVG [32].

In the preceding chapters, observation of the bubble behavior at ONB revealed that at elevated pressures, the bubbles slide along the heated surface after the departure from the nucleation site under the influence of the shear-induced lift force. Whilst, at low pressures close to the atmospheric pressure, they were lifted off the vertical heated surface immediately after the nucleation to collapse in the subcooled bulk liquid due to condensation. In consequence, bubble life-time at ONB was remarkably shorter in the low pressure experiments. It was discussed that the lift-off limit can be expressed in terms of the Jakob number since the distinct difference in the bubble behavior is mainly caused by the bubble growth rate after the nucleation [33]. The liquid subcooling was then parametrically changed to investigate the mechanisms causing the NVG. It was

found that at low pressures, all the bubbles collapsed in the subcooled bulk liquid at the ONB but some bubbles could be reattached to the heated surface when the liquid subcooling was low enough. Since the bubbles slid along the heated surface for a long distance after the reattachment, the bubble life-time was significantly extended and consequently the vaporization rate could noticeably be greater than the condensation rate. It was concluded that the bubble reattachment to the heated surface is a key phenomenon to cause the NVG in subcooled flow boiling [34]. Under the moderate pressure conditions, however, it was believed that different mechanisms are responsible for the onset of NVG since the bubbles are not lifted off the surface even at ONB. The mechanisms of NVG at elevated pressures are obviously of great importance from the engineering standpoint since most power plants are operated in high pressure conditions. Therefore, in the present work, series of experiments are conducted to explore the important mechanisms causing the NVG in subcooled flow boiling under elevated pressure conditions.

5.2 Experimental description

The heated surface was rather hydrophilic due to oxidization and its mean contact angle was measured 18º. In the present work, the measurements were carried out at the upper measuring section at 300 mm from the bottom. In the present experiments, the experimental procedure is the same as was discussed in previous chapter. Here, the visualization area of the photographic images captured with a high-speed camera was about 10 × 15 mm or 10 × 10 mm and the frame rate was set to 4000 or 6000 fps depending on the experimental conditions.

Four series of experiments (Cases I to IV) were conducted in this study; main experimental conditions are summarized in Tables 5.1 to 5.4, respectively. In each series of experiments, the values of P, G and the wall heat flux q_w were kept fairly constant and the liquid subcooling ΔT_{sub} was decreased step by step. The approximate ranges of P, G and q_w were 200-400 kPa, 400-1000 kg/m^{2}s and 200-320 kW/m^{2}s, respectively, and the range of ΔT_{sub} was selected so as to cover the conditions of ONB and OSV in each series. Typical bubble behavior observed at ONB is shown in Fig. 5.1. In all the experimental conditions tested in this work, Jakob numbers take low value; therefore bubbles produced under the condition of ONB slid along the vertical heated surface without being lifted off the surface as shown in the figure. In Tables 5.1-4, the wall superheat ΔT_w, the thermal equilibrium vapor quality x_{eq}, the cross-sectional area-averaged void fraction $<\alpha>$ and the experimental conditions under which the ONB and OSV occurred are also presented. The calculation method of $<\alpha>$ is described in the following section.

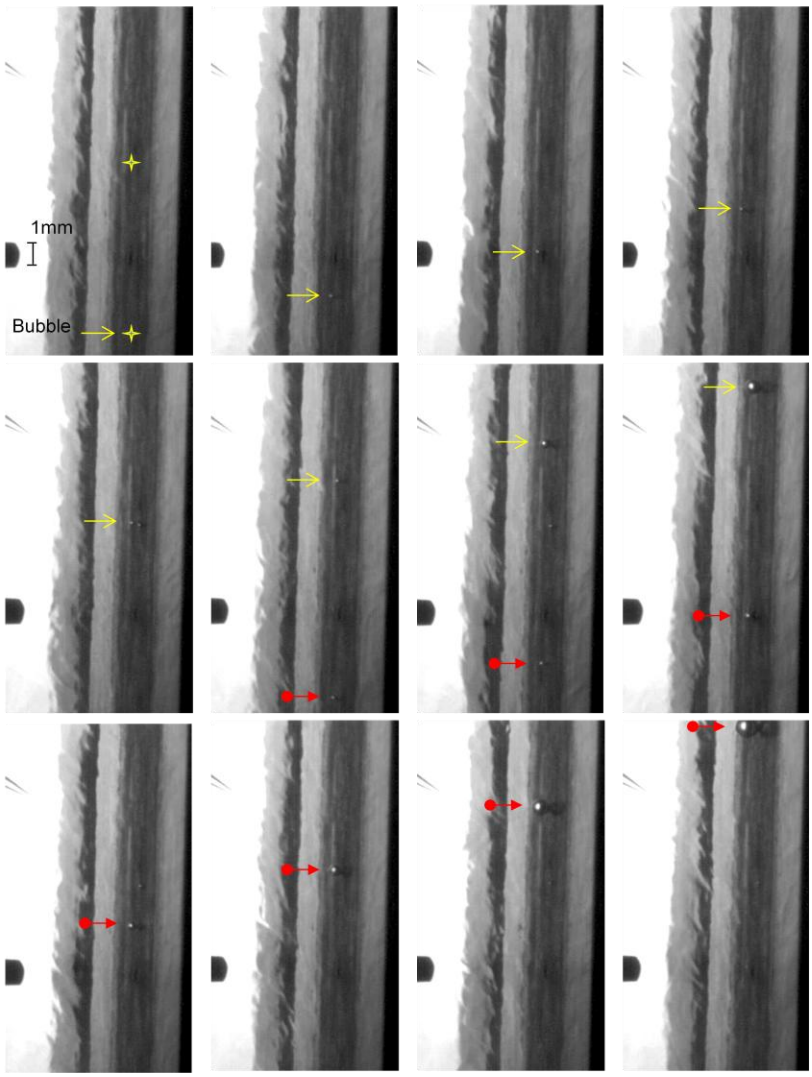

Fig. 5.1 Typical bubble behavior observed at ONB (Run 104, time interval = 10 ms)

Table 5.1 Main experimental conditions for Case I

Run	P (kPa)	G (kg/m^{2}s)	q_w (kW/m^2)	ΔT_{sub} (K)	ΔT_w (K)	x_{eq}	$\langle\alpha\rangle$	Ja
101	200	393	198	18.5	4.7	-0.0328	0.00000	7.65
102	200	395	196	16.7	6.3	-0.0295	0.00000	10.24
103	203	394	192	16.0	6.4	-0.0280	0.00000	10.26
104 (ONB)	200	394	192	14.8	7.4	-0.0256	0.00000	12.02
105	200	395	191	13. 6	8.2	-0.0233	0.00003	13.31
106	200	397	193	12.5	9.1	-0.0214	0.00009	14.76
107	201	396	196	11.7	9.3	-0.0197	0.00038	15
108 (OSV)	202	397	198	10.9	9.7	-0.0182	0.00069	15.57
109	202	399	195	9.8	9.8	-0.0161	0.00165	15.72
110	200	403	200	7.5	10.5	-0.0117	0.00504	16.97
111	200	403	199	5.4	10.8	-0.0077	0.00776	17.43
112	203	406	202	3.8	11.1	-0.0046	0.01633	17.66

Table 5.2 Main experimental conditions for Case II

Run	P (kPa)	G (kg/m^{2}s)	q_w (kW/m^2)	ΔT_{sub} (K)	ΔT_w (K)	x_{eq}	$\langle\alpha\rangle$	Ja
201	395	402	232	17.0	4.6	-0.0304	0.00000	4.035
202	402	401	232	16.7	5.1	-0.0298	0.00000	4.402
203	400	400	233	15.6	6.2	-0.0277	0.00000	5.372
204 (ONB)	399	400	237	14.7	7.5	-0.0259	0.00000	6.509
205	398	398	235	13.9	8.2	-0.0242	0.00000	7.129
206	400	398	236	12.9	8.7	-0.0221	0.00006	7.524
207 (OSV)	402	395	232	11.8	9.0	-0.0200	0.00007	7.743
208	401	391	228	10.7	9.2	-0.0180	0.00042	7.926
209	400	391	238	9.4	9.9	-0.0150	0.00104	8.541
210	400	386	241	8.9	10.1	-0.0141	0.00186	8.711
211	401	380	239	7.9	10.1	-0.0121	0.00261	8.685
212	402	382	243	5.9	10.4	-0.0080	0.00968	8.91
213	399	387	243	3.6	10.6	-0.0034	0.01758	9.128

Table 5.3 Main experimental conditions for Case III

Run	P (kPa)	G (kg/m^{2}s)	q_w (kW/m^2)	ΔT_{sub} (K)	ΔT_w (K)	x_{eq}	$\langle\alpha\rangle$	Ja
301	400	748	254	15.2	4.3	-0.0285	0.00000	3.725
302	399	747	256	14.1	5.7	-0.0263	0.00000	4.945
303	400	754	252	13.3	6.2	-0.0248	0.00000	5.363
304 (ONB)	399	750	250	12.1	7.1	-0.0225	0.00000	6.151
305	398	751	247	11.3	7.8	-0.0209	0.00000	6.769
306	398	755	252	10.6	8.7	-0.0194	0.00003	7.546
307 (OSV)	396	750	251	8.9	9.5	-0.0161	0.00009	8.268
308	398	753	252	8.0	9.9	-0.0143	0.00055	8.571
309	399	748	252	7.0	10.0	-0.0123	0.00173	8.632
310	397	749	256	6.0	10.5	-0.0101	0.00528	9.099
311	398	745	255	5.1	10.4	-0.0084	0.00905	8.986
312	400	740	259	4.2	10.7	-0.0066	0.02089	9.198
313	399	734	259	2.4	10.8	-0.0028	0.04284	9.293

Table 5.4 Main experimental conditions for Case IV

Run	P (kPa)	G (kg/m^{2}s)	q_w (kW/m^2)	ΔT_{sub} (K)	ΔT_w (K)	x_{eq}	$\langle\alpha\rangle$	Ja
401	305	983	312	15.1	6.6	-0.0230	0.00000	7.307
402	315	980	309	13.6	7.6	-0.0269	0.00000	8.163
403(ONB)	319	973	311	12.7	8.9	-0.0250	0.00000	9.445
404	316	979	319	11.7	10.2	-0.0231	0.00014	10.91
405	322	976	311	11.3	10.1	-0.0222	0.00014	10.62
406(OSV)	325	972	311	10.3	10.7	-0.0202	0.00023	11.15
407	338	977	325	9.8	11.0	-0.0195	0.00093	11.06
408	342	976	327	8.0	11.8	-0.0158	0.00359	11.72
409	349	963	327	7.6	11.9	-0.0151	0.00730	11.6

5.3 Experimental results

Snapshots obtained in each experimental run are displayed in Figs. 5.2a-d, in which the cross marks indicate the active nucleation sites. An important observation in these photos is that majority of the bubbles are located close to the vertical heated surface since most bubbles slid along the surface after the departure from the nucleation sites even when the condition of OSV is satisfied. It was also confirmed that bubbles are not attached to the nucleation sites in all the experimental conditions tested in this work. In addition, the snapshots indicate that in all the series of experiments, the bubble size and the number density of bubbles tended to increase with decreased value of ΔT_{sub} particularly when the OSV condition is reached. The results of quantitative investigations to explore the mechanisms causing OSV in subcooled flow boiling are presented below.

5.3.1 Void fraction measurement

The void fraction distributions in the lateral direction measured using the optical probe are shown in Figs. 5.3a-d; here, ΔT_{sub} is used as a parameter in each figure and y and α_{lta} represent the distance from the heated surface and the local time-average void fraction, respectively. It can be seen that the peak value of the void fraction as well as the bubble layer thickness tended to increase with a decrease of ΔT_{sub} in each series of experiments. The following equation was used to calculate the cross-sectional area-averaged void fraction $<\alpha>$ from α_{lta}:

$$\langle \alpha \rangle = \frac{l_h}{A_0} \int_0^{w_0} \alpha_{l\,t\,a} dy \tag{1}$$

Here, A_0, w_0 and l_h are the cross-sectional area (200 mm^2), the channel width (10 mm) and the width of the heated surface (10 mm), respectively. The thermal-equilibrium quality x_{eq} is calculated as a function of the axial coordinate z by

$$x_{eq}(z) = \frac{1}{h_{fg}} \left[\frac{q_w l_h}{G A_0} z - c_{pl} \Delta T_{sub} \right] \tag{2}$$

where h_{fg} is the latent heat of vaporization. The values of $<\alpha>$ are plotted against x_{eq} in Fig. 5.4 in which the conditions of ONB and OSV are indicated with arrows. It can be confirmed that the void fraction is negligibly small near the condition of ONB and a vigorous increase in the void fraction is permitted when x_{eq} is further increased. Lee and Bankoff [35] compared available OSV correlations with several experimental data obtained at low pressures to conclude that the experimental data agree with the Saha and Zuber correlation [7] well and the model of Levy [9] slightly overestimates the liquid subcooling at OSV. In Fig. 5.4, the conditions of OSV calculated using these correlations are also indicated with dotted lines. Comparisons of the present OSV data with these correlations are consistent with the analysis by Lee and Bankoff. It can also be seen that although the discrepancy from Levy's model is rather significant in low mass flux experiments (Cases I and II), fairly good agreement is obtained in higher mass flux experiments (Cases III and IV).

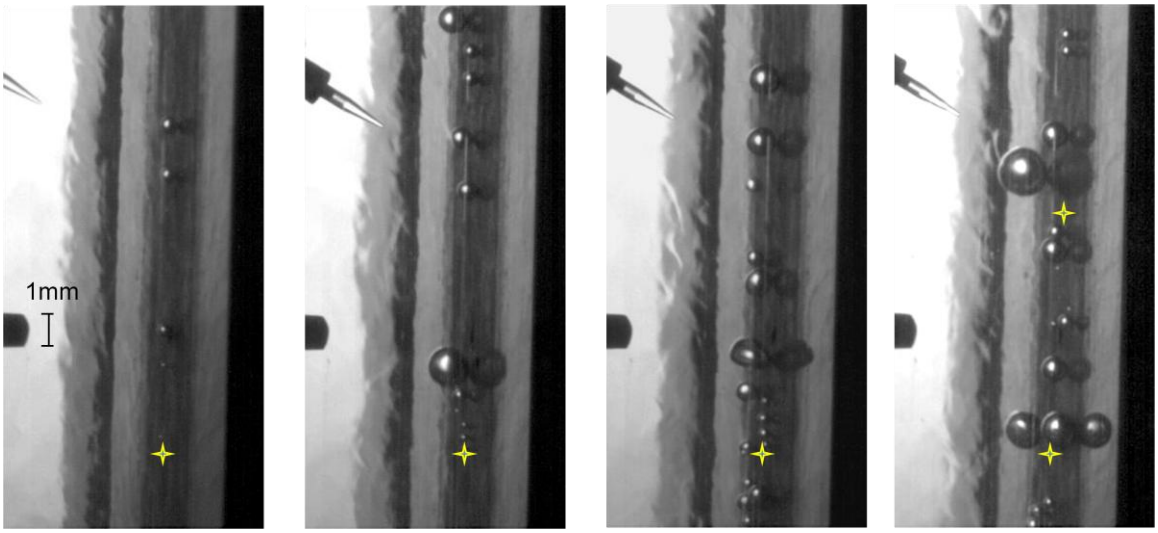

(a) Run 105 (b) Run 106 (c) Run 107 (d) Run 108 (OSV)

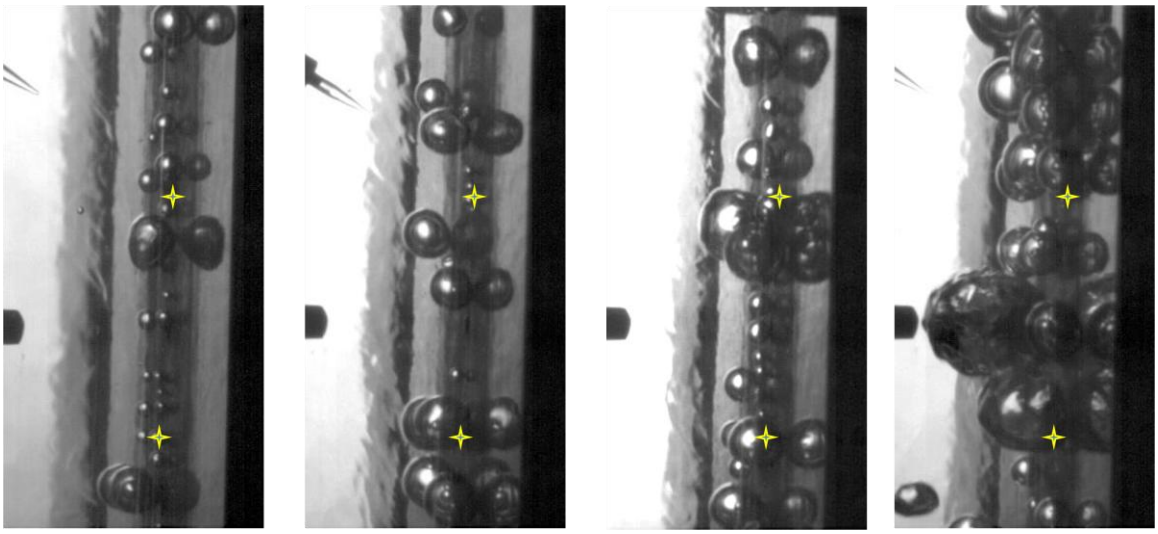

(e) Run 109 (f) Run 110 (g) Run 111 (h) Run 112

Fig. 5.2a Snapshots of bubbles at different values of subcoling in Case I

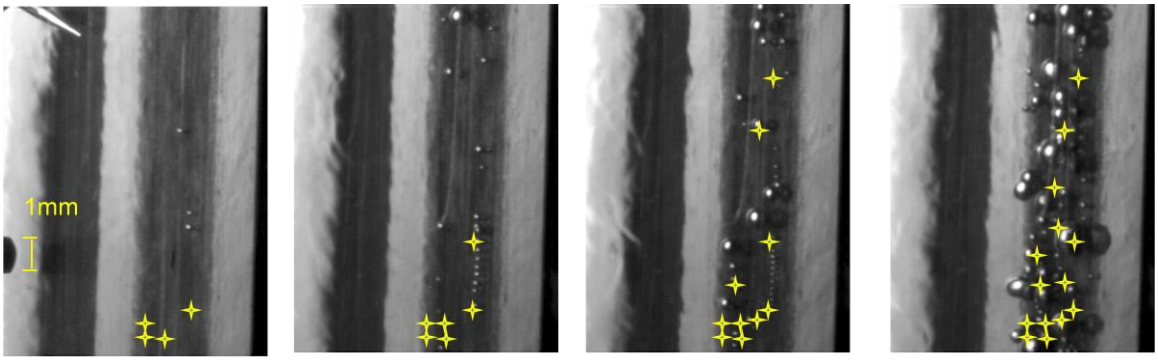

(a) Run 205 (b) Run 206 (c) Run 207 (OSV) (d) Run 208

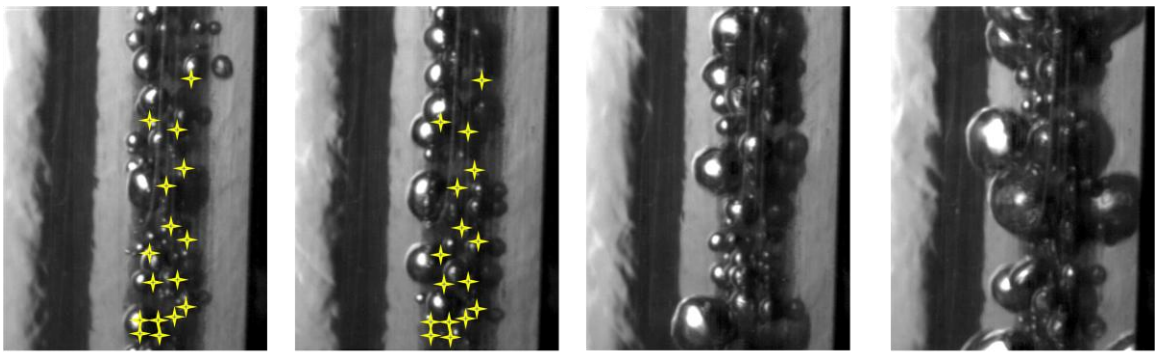

(e) Run 209 (f) Run 210 (g) Run 211 (h) Run 212

Fig. 5.2b Snapshots of bubbles at different values of subooling in Case II

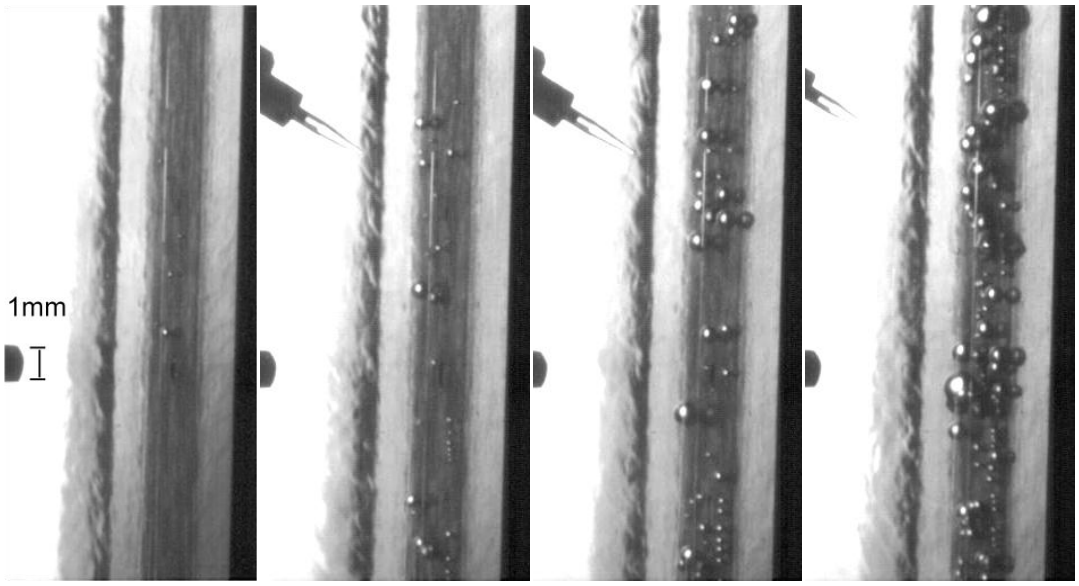

(a) Run 305 (b) Run 306 (c) Run 307 (OSV) (d) Run 308

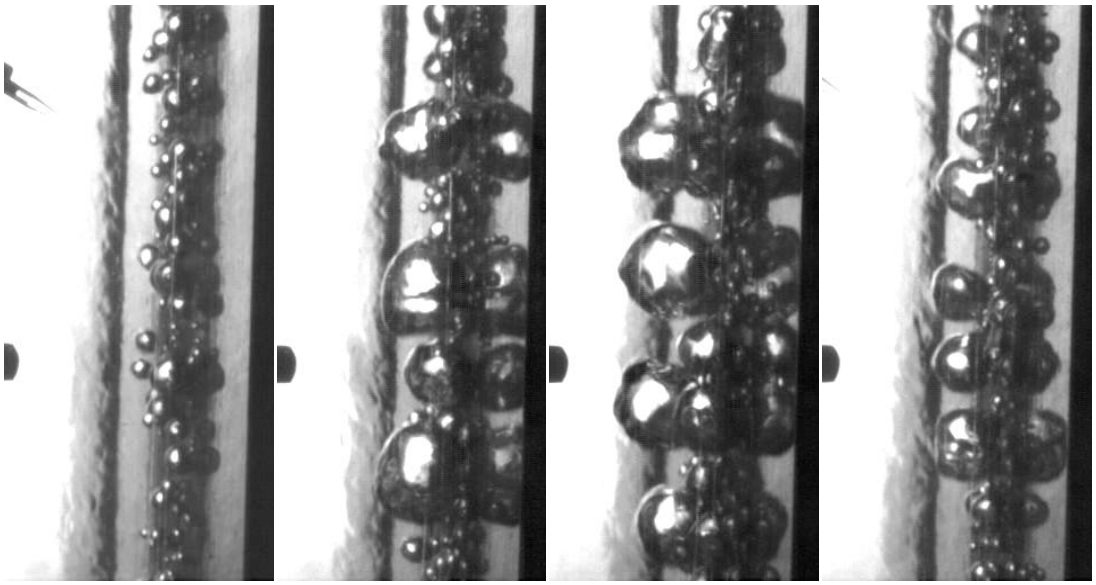

(e) Run 309 (f) Run 310 (g) Run 311 (h) Run 312

Fig. 5.2c Snapshots of bubbles at different values of subcoling in Case III

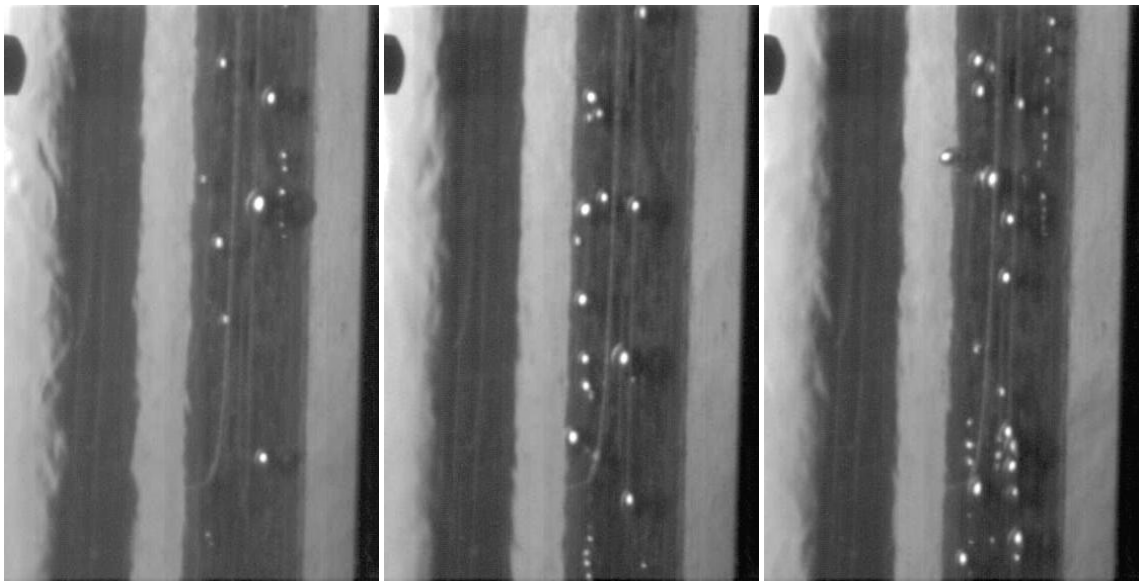

(a) Run 404 (b) Run 405 (c) Run 406 (OSV)

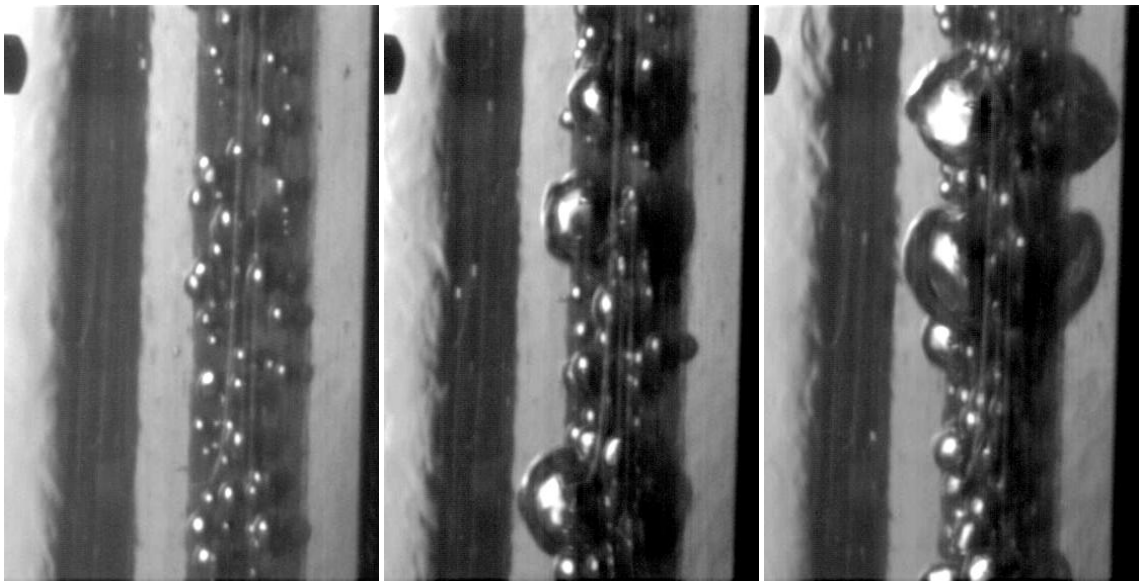

(d) Run 407 (e) Run 408 (c) Run 409

Fig. 5.2d Snapshots of bubbles at different values of subcoling in Case IV

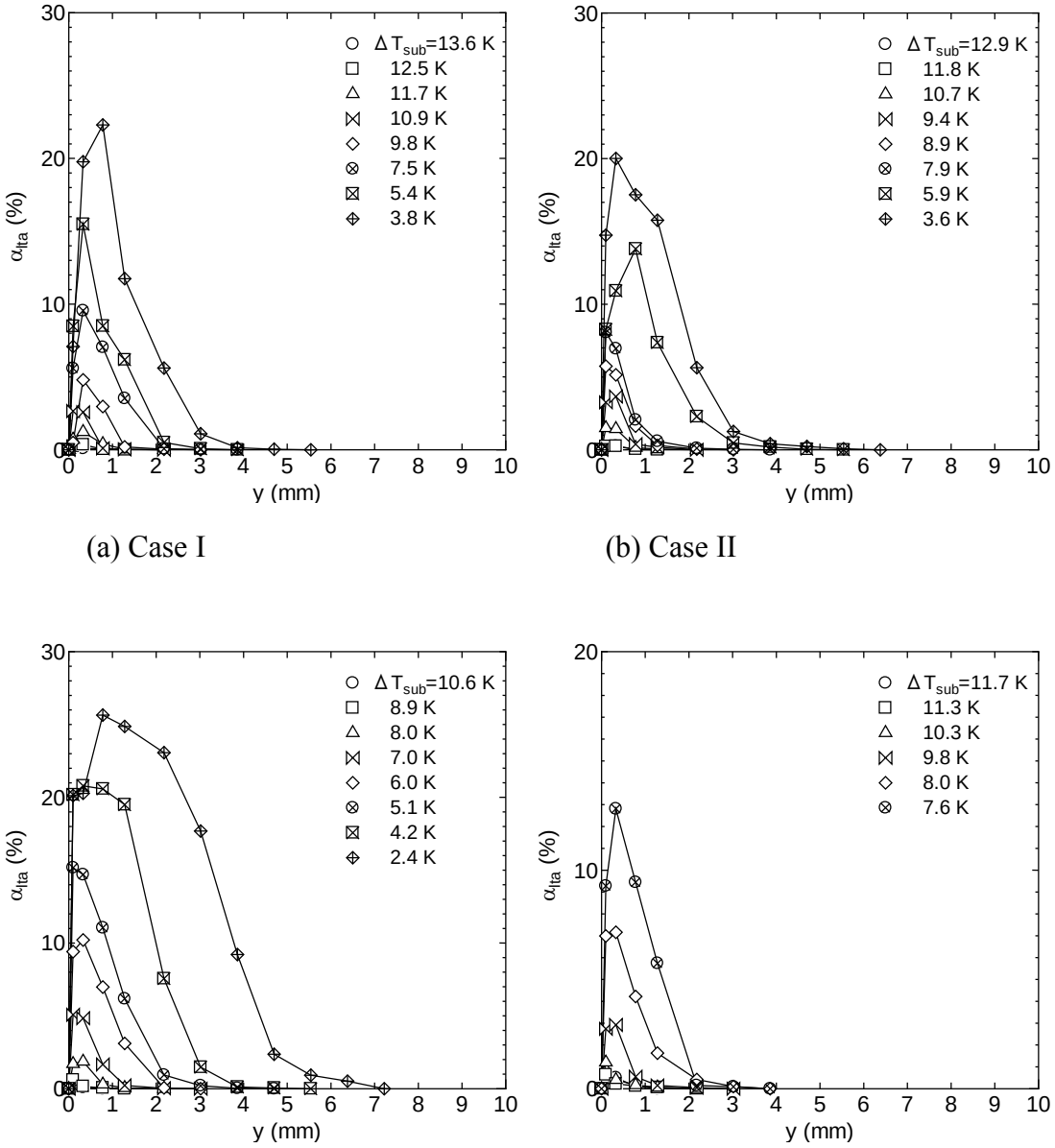

(a) Case I (b) Case II

(c) Case III (d) Case IV

Fig. 5.3 Dependence of the traverse void fraction distribution on the liquid subcooling; (a) Case I, (b) Case II, (c) Case III, and (d) Case IV

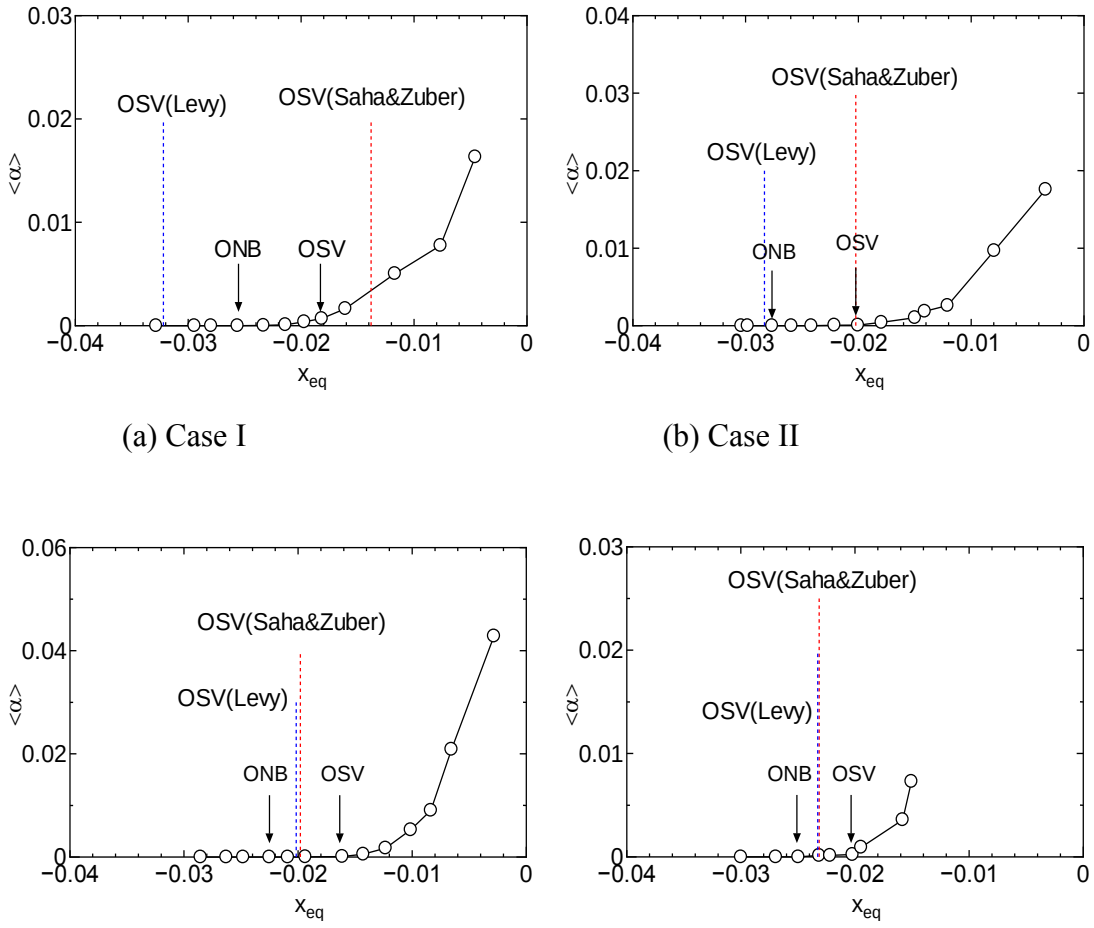

Fig. 5.4 Dependence of the time-average cross-sectional void fraction on the thermal-equilibrium vapor quality; (a) Case I, (b) Case II, (c) Case III, and (d) Case IV

5.3.2 Discussion on the onset of net vapor generation

To explore the mechanisms of NVG, the following mass conservation equation for the vapor phase based on the one-dimensional two-fluid model for the steady state is used.

$$\frac{\mathrm{d}}{\mathrm{d}z}(\alpha\rho_{\mathrm{g}}u_{\mathrm{g}}) = \Gamma_{\mathrm{V}} - \Gamma_{\mathrm{C}} \tag{3}$$

where Γ_{V} and Γ_{C} refer the vaporization rate and the condensation rate, respectively. If the vapor density ρ_{g} and the vapor velocity u_{g} are assumed to be fairly constant, Eq. 3 is transformed to

$$\frac{\mathrm{d}\alpha}{\mathrm{d}x_{\mathrm{eq}}} = \frac{Gh_{\mathrm{fg}}A_0}{q_{\mathrm{w}}l_{\mathrm{h}}\rho_{\mathrm{g}}u_{\mathrm{g}}}(\Gamma_{\mathrm{V}} - \Gamma_{\mathrm{C}}) \tag{4}$$

Here, the axial coordinate z is replaced by x_{eq}. This equation indicates that the net vaporization rate defined by $\Gamma_{\mathrm{Net}} = \Gamma_{\mathrm{V}} - \Gamma_{\mathrm{C}}$ should be large enough for α to increase rapidly with an increase in x_{eq}.

It was attempted to measure Γ_{V} and Γ_{C} separately from perceptible variation of the bubble size in the movie data. Three typical types of bubble behavior observed in the present experiments are illustrated in Fig. 5.5. The example of snapshots of the type-A bubble behavior was already depicted in Fig. 5.1. As shown in Fig. 5.5, the type-A bubbles travel for a long distance and grow asymptotically on the heated surface, the type-B bubbles coalesce with other preceding sliding bubbles in the course of sliding, and the type-C bubbles lose the contact to the heated surface during the sliding stage to be

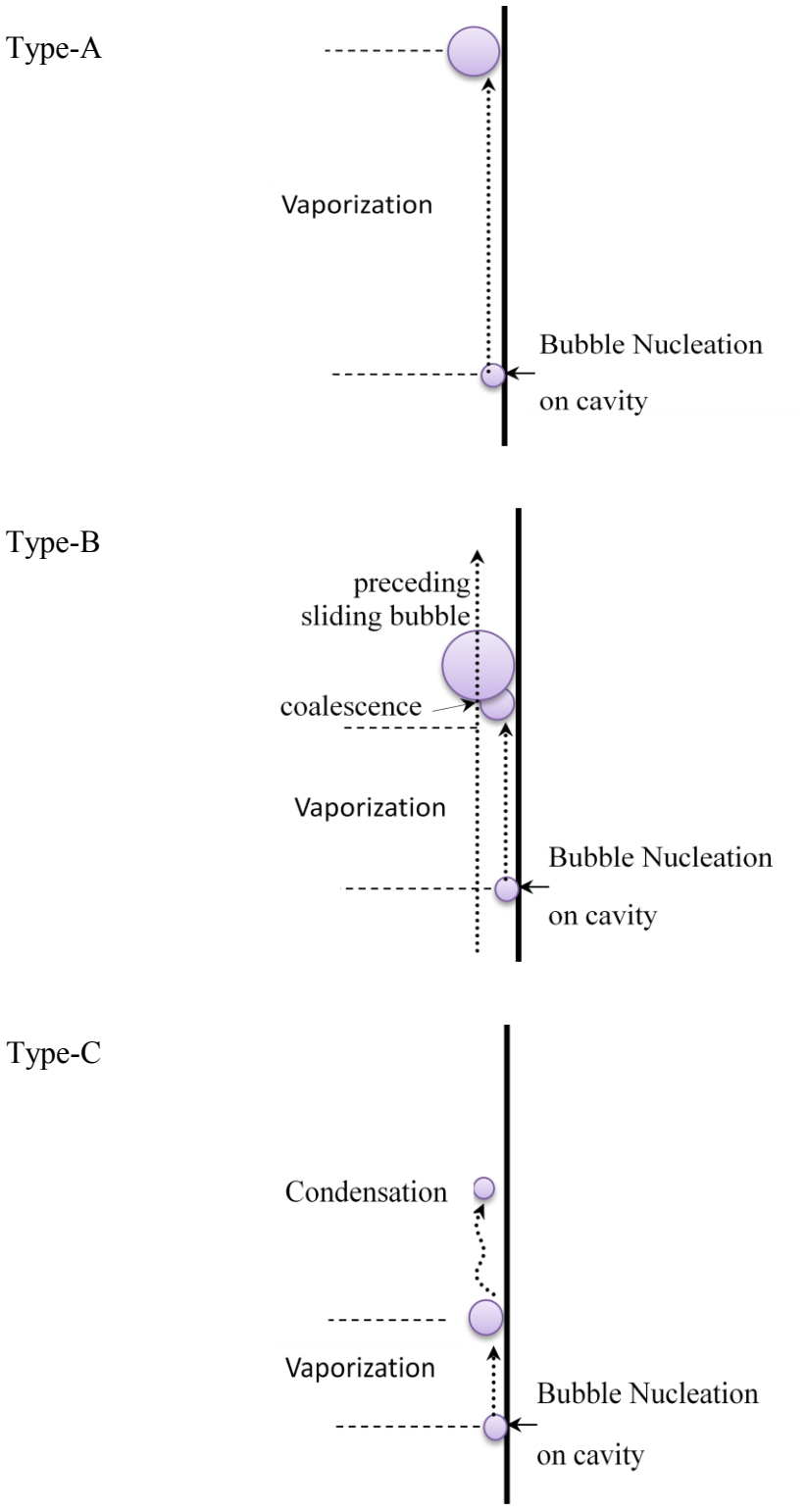

Fig. 5.5 Three types of typical bubble behavior after departure from active nucleation site

collapsed due to heat transfer with the subcooled bulk liquid. In order to deduce the information concerning Γ_{Net}, we measured the maximum bubble size $d_{\mathrm{b,max}}$ and the bubble size in the last image in the visualization window $d_{\mathrm{b,last}}$ for all the bubbles that were produced at the nucleation sites located within the visualization window. It is noted that the value of $d_{\mathrm{b,last}}$ was close to $d_{\mathrm{b,max}}$ for the type-A bubbles since the bubble size reached the quasi-equilibrium state at the moment of leaving the visualization window while it was zero for the type-C bubbles. The value of $d_{\mathrm{b,last}}$ for the type-B bubbles depends on the preceding sliding bubbles size, after coalescence. If the size of preceding bubble is increased due to coalescence, the value of $d_{\mathrm{b,last}}$ for the type-B bubbles is the bubble diameter at the moment of coalescence, unless it is zero. The apparent vaporization and condensation rates γ_V^{a} and γ_C^{a} are calculated for each bubble by

$$\gamma_{\mathrm{V}}^{\mathrm{a}} = \rho_{\mathrm{g}} \frac{\pi d_{\mathrm{b,max}}^3}{6} \tag{5}$$

$$\gamma_{\mathrm{C}}^{\mathrm{a}} = \rho_{\mathrm{g}} \frac{\pi}{6} (d_{\mathrm{b,max}}^3 - d_{\mathrm{b,last}}^3)_{\mathrm{t}} \tag{6}$$

The apparent phase change rates $\Gamma_{\mathrm{V}}^{\mathrm{a}}$ and $\Gamma_{\mathrm{C}}^{\mathrm{a}}$ within the visualization area are calculated by

$$\Gamma_{\mathrm{K}}^{\mathrm{a}} = \frac{1}{V_0 t_0} \sum_{\mathrm{i}=1}^{N_{\mathrm{s}}} \sum_{\mathrm{j}=1}^{N_{\mathrm{b,i}}} (\gamma_{\mathrm{K}}^{\mathrm{a}})_{\mathrm{ij}} \tag{7}$$

where V_0 is the volume of the visualization area, t_0 is the recording time, N_{s} is the number of active nucleation sites within the visualization area, $N_{\mathrm{b,i}}$ is the number of bubbles

produced at the i-th nucleation site; the subscript K denotes V or C and the subscript ij refers the j-th bubble produced at the i-th nucleation site. Finally, the net vaporization rate Γ_{Net} is calculated by

$$\Gamma_{\mathrm{Net}} = \Gamma_{\mathrm{V}}^{\mathrm{a}} - \Gamma_{\mathrm{C}}^{\mathrm{a}} \tag{8}$$

When the size of a sliding bubble is in the equilibrium state in subcooled flow boiling, it is expected that the evaporation on the wall side is balanced with the condensation on the bulk liquid side [4, 16, 17]. This implies that the measurements of true vaporization and condensation rates from simple bubble images are not possible and consequently the apparent phase change rate $\Gamma_{\mathrm{K}}^{\mathrm{a}}$ measured in this work is different from the true phase change rate Γ_{K}. Nonetheless, the value of Γ_{Net} can be calculated correctly by Eq. 8 because the underestimations of vaporization and condensation rates are canceled out each other. It was therefore assumed that the measurements of the apparent phase change rates are useful to understand the mechanisms of NVG in the present experiments.

It is noted that the measurements of $\Gamma_{\mathrm{V}}^{\mathrm{a}}$ and $\Gamma_{\mathrm{C}}^{\mathrm{a}}$ were conducted only for Case I and Case II since the overlapping of bubbles was too significant in other cases. The measurement results of the phase change rates are presented in Fig. 5.6. It can be seen that the values of $\Gamma_{\mathrm{V}}^{\mathrm{a}}$ and $\Gamma_{\mathrm{C}}^{\mathrm{a}}$ are kept low near the condition of ONB and only $\Gamma_{\mathrm{V}}^{\mathrm{a}}$ increases vigorously when the condition of OSV is reached. In consequence, the influence of $\Gamma_{\mathrm{C}}^{\mathrm{a}}$ is insignificant and the values of Γ_{Net} are nearly equal to the values of $\Gamma_{\mathrm{V}}^{\mathrm{a}}$ even after the condition of OSV is reached. In Fig. 5.6, the values of $\Gamma_{\mathrm{V}}^{\mathrm{a}}$ and $\Gamma_{\mathrm{C}}^{\mathrm{a}}$ were derived from the images of bubbles that were produced at the nucleation sites located within the visualization window. Therefore, the measured data of $\Gamma_{\mathrm{V}}^{\mathrm{a}}$ and $\Gamma_{\mathrm{C}}^{\mathrm{a}}$ were substituted to Eq. 4 to calculate $\mathrm{d}\alpha/\mathrm{d}x_{\mathrm{eq}}$, and the results were compared with the

values of $d\alpha/dx_{eq}$ calculated from the probe data presented in Fig. 5.4. The results of comparison are displayed in Fig. 5.7. It is noted that the value of x_{eq} in Run 209 is close to the value in Run 210, in Case II. Since the small uncertainty in measuring of α can cause big uncertainty in the value of $d\alpha/dx_{eq}$, Run 210 is neglected for the probe measurement data in Fig. 5.7. It can be seen that the values of $d\alpha/dx_{eq}$ derived from the probe data and image analysis are fairly in the similar trend. It was therefore assumed that the increase of Γ_{Net} found in Fig. 5.6 reflects the vigorous increase of α after the condition of OSV is reached.

5.3.3 Propose triggering mechanisms of NVG

As shown in Fig. 5.1, in this experimental study bubble departure from the active nucleation sites is commenced as the condition of ONB is satisfied. After departure, some bubbles grow while sliding on the heated surface (type-A), some bubbles slide and then coalesce with other preceding sliding bubbles (type-B), and some others slide shortly and then collapse in the subcooled liquid (type-C). As depicted in Fig. 5.6, the condensation rates are essentially insignificant in the present experiments. The distribution of measurement results of Γ_V^a and Γ_C^a are plotted against the maximum bubble diameter $d_{b,max}$ in Fig. 5.8a and b for two series of experiments. For all experimental conditions, these figures confirm that the volume of the collapsing bubbles consist a small fraction of whole bubbles volume, owing to their small size. Therefore, it is concluded that the collapsing bubbles can be neglected in the investigation of void evolution.

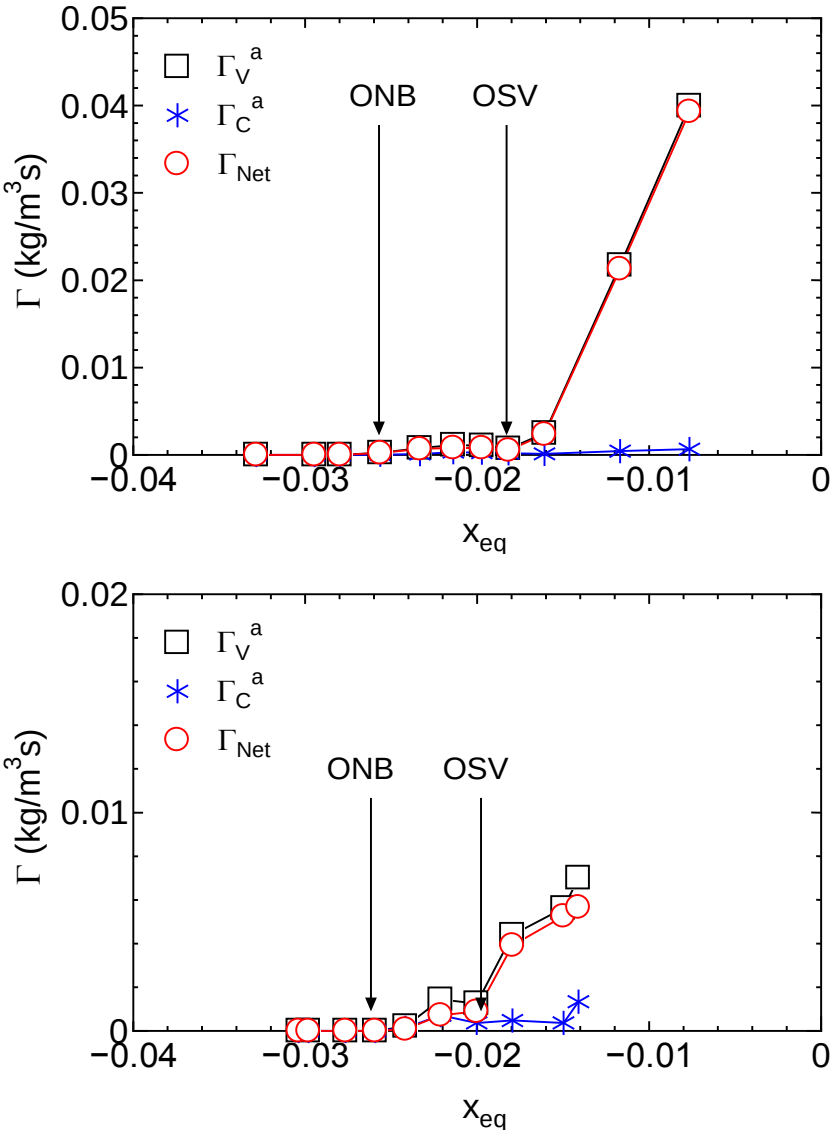

Fig. 5.6 Vaporization, condensation and net vaporization rates within the visualization section; (a) Case I, (b) Case II

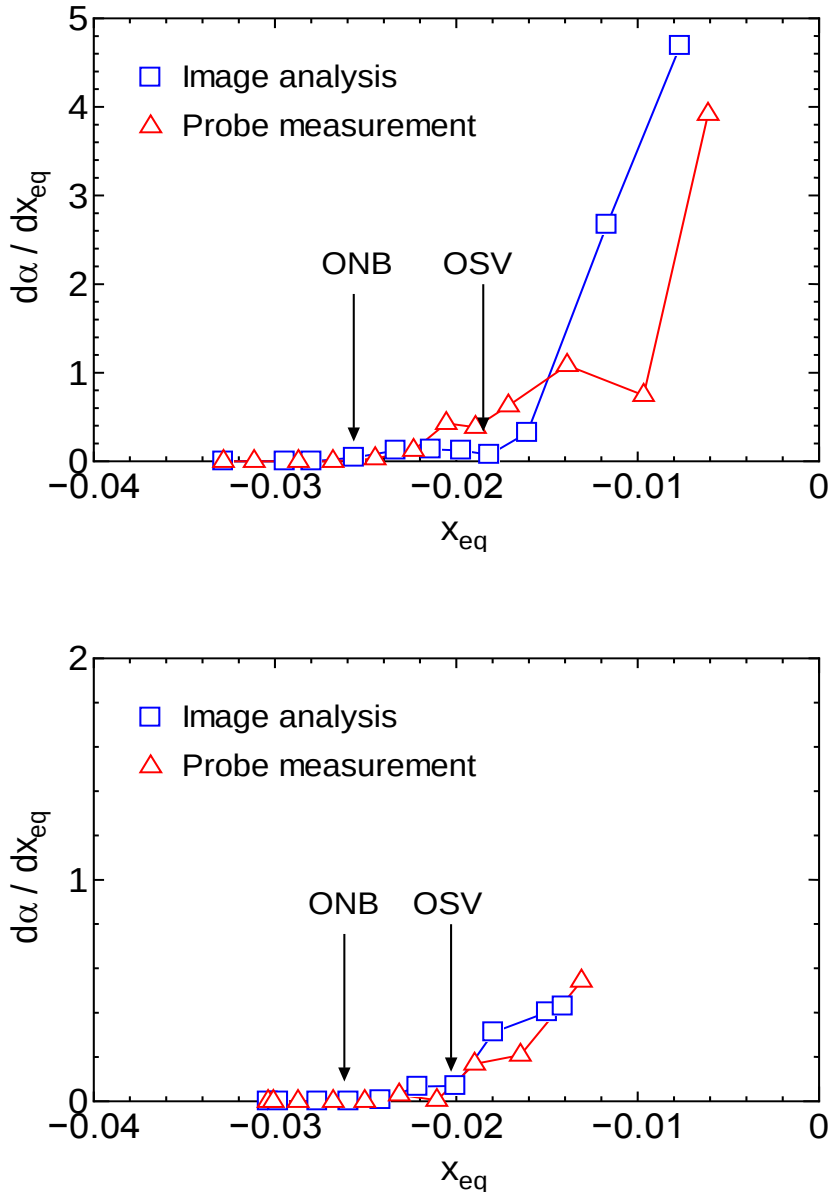

Fig. 5.7 Comparisons of the void gradients measured by the image analysis with those measured by void probe; (a) Case I, (b) Case II

The observations show that when the type-B bubbles coalesce with the preceding sliding bubbles, the size of the preceding sliding bubbles is commonly increased. Therefore, the type-B bubbles are as non-collapsing bubbles. The net vapor generation rate is fundamentally influenced by two parameters: the number of non-collapsing sliding bubbles released from the heated surface into the channel and the maximum bubbles size. By considering non-collapsing sliding bubbles as type-A and type-B bubbles, the net vaporization rate can be express as

$$\Gamma_{Net} = \frac{1}{V_0 t_0} \sum_{i=1}^{N_s} \sum_{j=1}^{N_{b,i}} \frac{1}{6} \pi \left(d_{b,\max}^3 \right)_{ij} \rho_g = n \overline{f} \overline{V_b} \frac{A_h \rho_g}{V_0} \tag{9}$$

The definitions of the three variables of nucleation site density n, mean bubble release frequency $\overline{f}$ and mean bubble volume $\overline{V_b}$ can be seen in the following equation clearly

$$\Gamma_{Net} = \underbrace{\left[\frac{N_s}{A_h} \right]}_{n} \underbrace{\left[\frac{\sum_{i=1}^{N_s} N_{b,i}}{N_s t_0} \right]}_{\overline{f}} \underbrace{\left[\frac{\frac{1}{6} \pi \sum_{i=1}^{N_s} \sum_{j=1}^{N_{b,i}} \left(d_{b,\max}^3 \right)_{ij}}{\sum_{i=1}^{N_s} N_{b,i}} \right]}_{\overline{V_b}} \frac{A_h \rho_g}{V_0} \tag{10}$$

Here, A_h and $(d_{b,max})_{ij}$ are heated area and the maximum size of the j-th bubble created at the i-th nucleation site, respectively.

As depicted in Figs. 5.2a and b, in Case I only one or two nucleation sites are activated during subcooled flow boiling, and in Case II the number of active nucleation site increases with the increase of x_{eq}. In consequence, the number of sliding bubbles released from each nucleation site is counted in a period of time to obtain mean bubble

release frequency $\overline{f}$. Therefore, the total number of sliding bubbles released from the heated surface into the channel can be obtained by $n \times \overline{f}$. In order to realize the influence of both parameters of the number of sliding bubbles and the bubble size on the vapor generation, the distributions of $n \times \overline{f}$ were plotted against bubble size in Figs. 5.9a and b for two series of experiments. In these figures Γ_{Net} is further divided into $\Gamma_{Net,WA}$ and $\Gamma_{Net,NWA}$ ($\Gamma_{Net} = \Gamma_{Net,WA} + \Gamma_{Net,NWA}$); here, the subscription WA and NWA denote the wake-affected and non-wake-affected bubbles, respectively, and their definition are given later. As depicted in Fig. 5.9a, in Case I net vaporization is commenced with the few releasing of small bubbles at Run 104, corresponding to ONB condition. In the conditions before Run 108, since both parameters of the bubbles size and the numbers of sliding bubbles are low, the net vaporization rates are kept low. However, after Run 108, which corresponds to the conditions after OSV, the wide ranges of bubbles size are produced in the channel, which the particular increase of the number of bubbles is for small bubbles.

Since Γ_{Net} is proportional to the third power of the bubble size, the bigger bubbles have a high impact on the increase of net vaporization rates. Correspondingly, the measurement results of Case II in Fig. 5.9-b reveal that the bubbles size and the number of sliding bubbles significantly increase right after the OSV condition. Therefore, it is concluded that the few production of big sliding bubbles contributed to the increase of void fraction vigorously after the condition of OSV is reached.

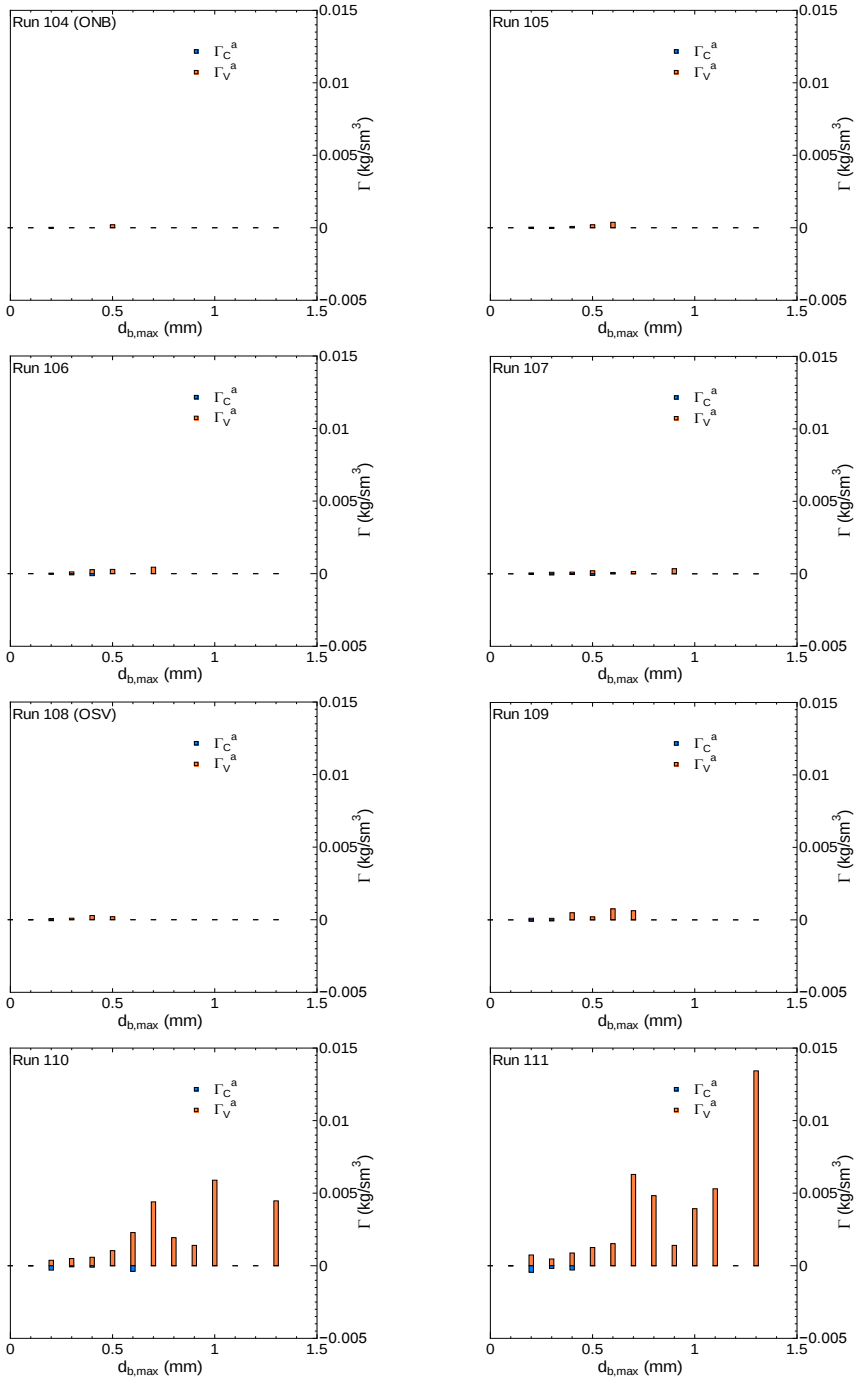

Fig. 5.8a Discrete distribution of Vaporization and condensation against maximum bubble diameter in Case I

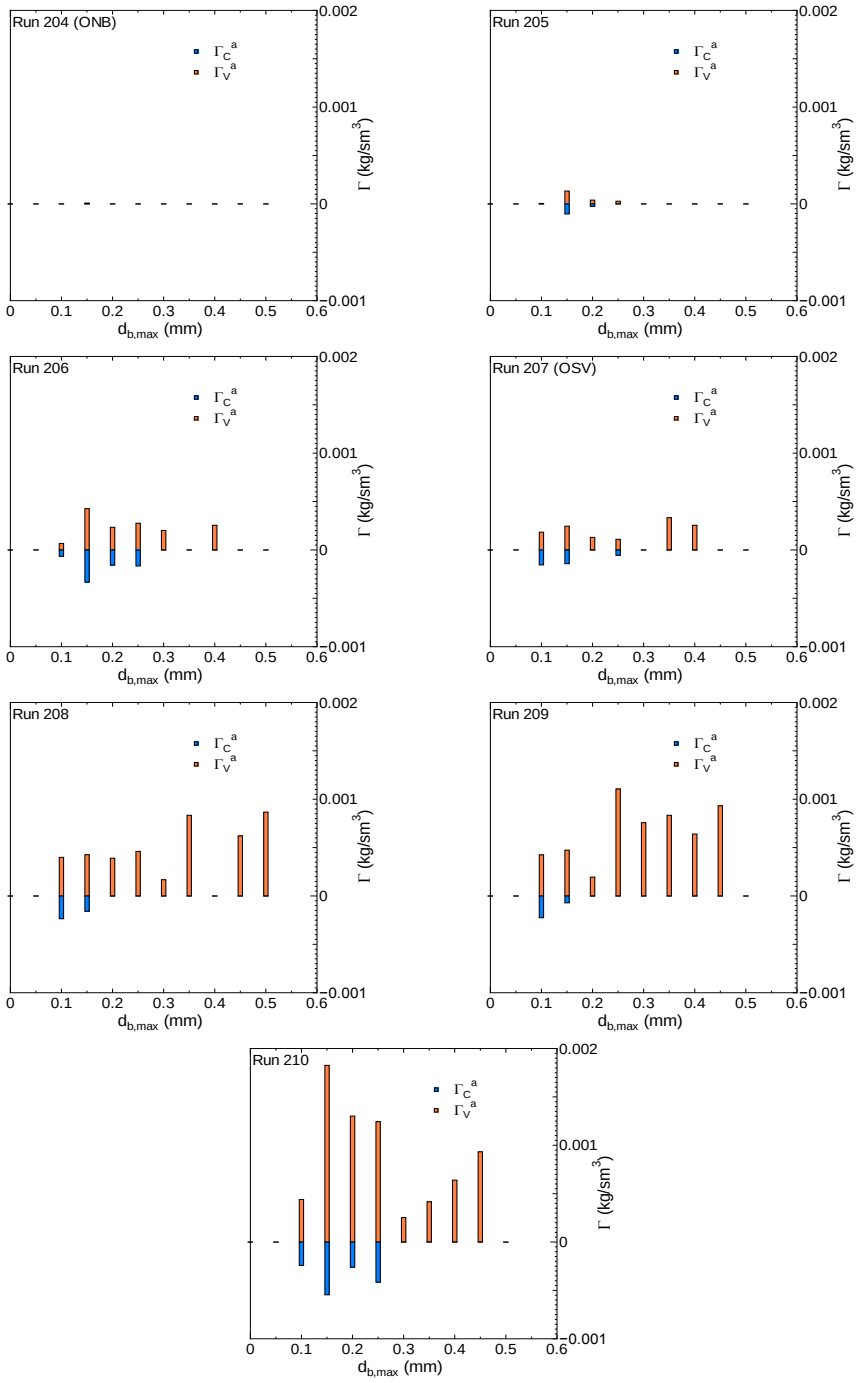

Fig. 5.8b Discrete distribution of Vaporization and condensation against maximum bubble diameter in Case II

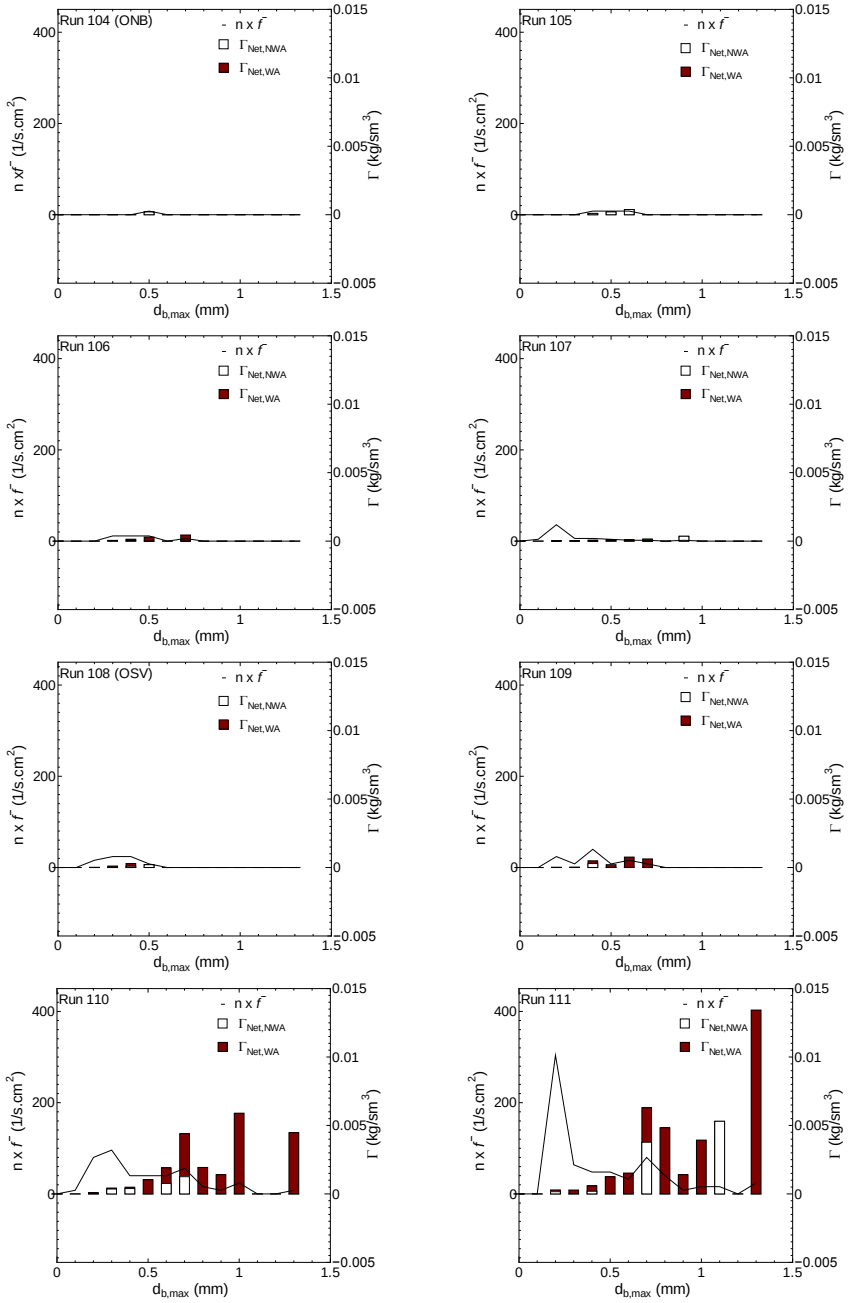

Fig. 5.9a Discrete distribution of wake-effected and non-wake-effected net vaporization rates and the number of non-collapsing bubble generation against maximum bubble diameter in Case I

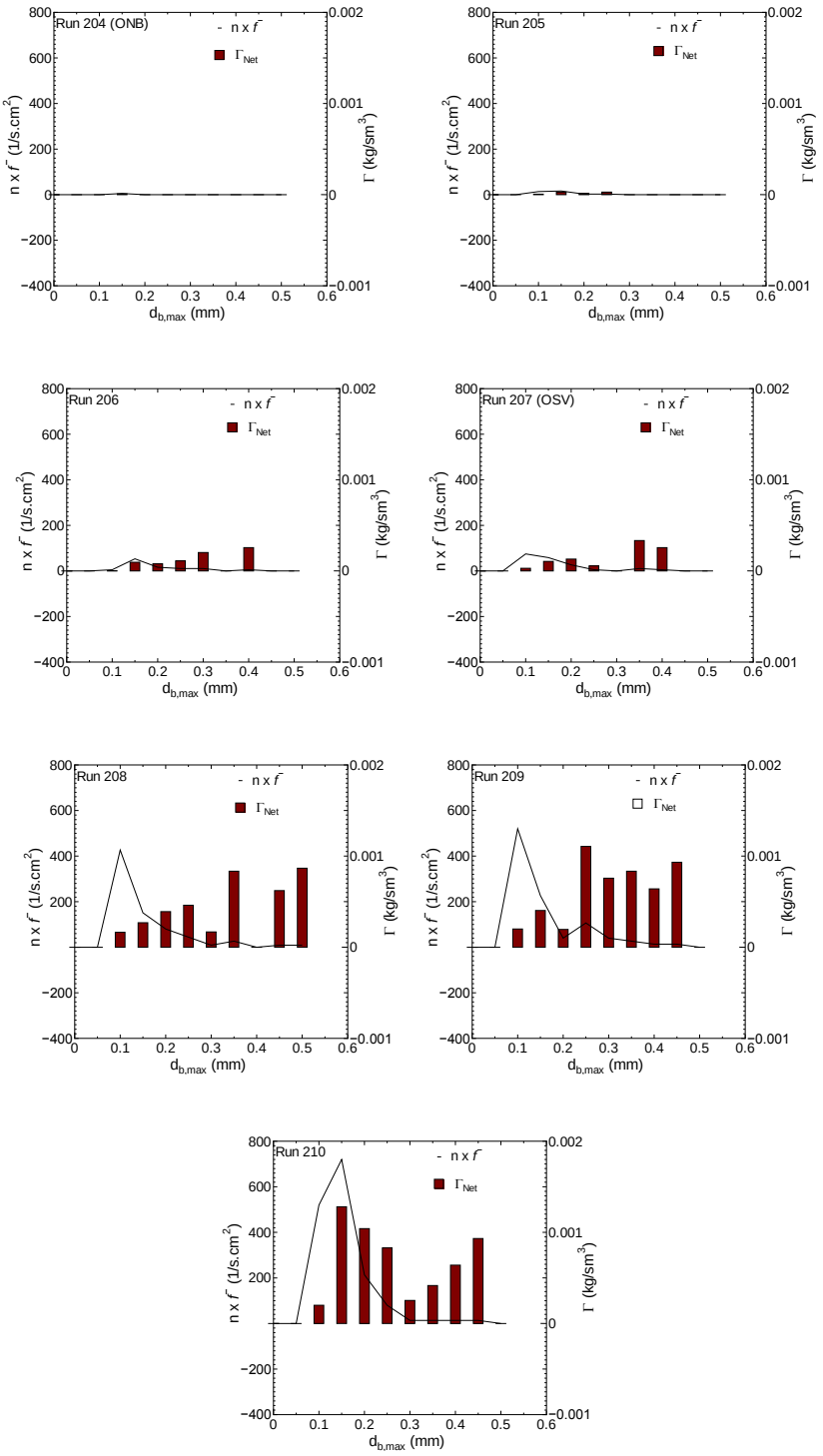

Fig. 5.9b Discrete distribution of net vaporization rates and the number of non-collapsing bubble generation against maximum bubble diameter in Case II

The important part of this study is devoted to the exploring of phenomena causing extensive production of non-collapsing big sliding bubbles, which are mainly produced after the OSV condition. In low void fraction condition close to ONB condition, because bubble number density is very low, some isolated bubbles slide and grow discretely, without influence of other sliding bubbles. However, when subcooling temperature is low enough, bubbles are created in the presence of many sliding bubbles which come from upstream flow. The visual investigation reveals that the preceding sliding bubbles which come from upstream flow affect bubble generation within visualization window. It is observed that when a big sliding bubble is passing over an active nucleation site a chain of nucleated bubbles are created immediately in the wake region of this big sliding bubble and then some of them gain volume very fast. In this study, this process of vapor formation in a transient condition is referred to as 'wake-effect' of preceding sliding bubbles.

Figure 5.10 illustrates an example of wake-effect process which causes several big sliding bubbles be created in a short time. Four sliding bubbles which come from downside of the visualization window are followed by different arrows. It is observed that when sliding bubble passes over the nucleation site, chain of bubbles are created at the nucleation site and slide in the wake of the preceding sliding bubble. In Fig. 5.10 the growing stages of one nucleated bubble which is indicated by circle are followed from the moment of creation at 10 ms until leaving visualization window. This bubble is created when preceding sliding bubble number 2 passes over the nucleation site. The nucleated bubble goes afterward of the sliding bubble number 2 and grows up. It is observed that when bubble is leaving visualization window at 39 ms, the bubble size become considerably big because of wake-effect. In order to confirm the influence of wake-effect on the nucleated bubble size, the value of $d_{b,max}$ of bubbles that were

produced at the nucleation sites located within the visualization window are measured. In addition, the dimensionless distance from the preceding bubble at nucleation site $dz/d_{b,p}$ was considered; here, dz is the distance of preceding sliding bubble from the nucleation site at the moment of nucleation and $d_{b,p}$ is the diameter of the preceding bubble. Figure 5.11 demonstrates $d_{b,max}$ against $dz/d_{b,p}$ for Runs 109 and 110. It can clearly be seen that bubble growth occurs mainly when the dimensionless distance is smaller than 3.

Because of flow separation in the rear side of the sliding bubbles, the significant turbulence of liquid flow, pressure and temperature are formed in the wake region. Therefore, understanding the effect of the wake on the increase of the bubbles size is not possible just via observation. It would however be assumed that due to two-phase heat transfer between the preceding sliding bubbles and subcooled liquid the local liquid subcooling is reduced in the wake region of the sliding bubbles. Therefore, a possible explanation for the distinct increase of the bubbles size after OSV is that large bubbles are mainly produced in the wake region of lower subcooling which is prepared by the preceding sliding bubbles.

In order to understand the influence of wake-effect on net vaporization rate, the non-collapsing bubbles are divided into the two district subgroups: wake-affected bubbles which are produced afterward of the preceding sliding bubbles, and non-wake-affected bubbles which are produced freely. In this study, the wake-affected bubbles are distinguished from the non-wake-affected bubbles by assuming a wake length of preceding sliding bubble. Hence, in an active nucleation site the wake-affected bubbles are the bubbles which are formed in a period of time which a preceding sliding bubble moves over active nucleation site and far from it for a wake length. In accordance with the results obtained in Fig. 5.11, the wake-length is assumed as three times of the preceding sliding bubble‘s diameter.

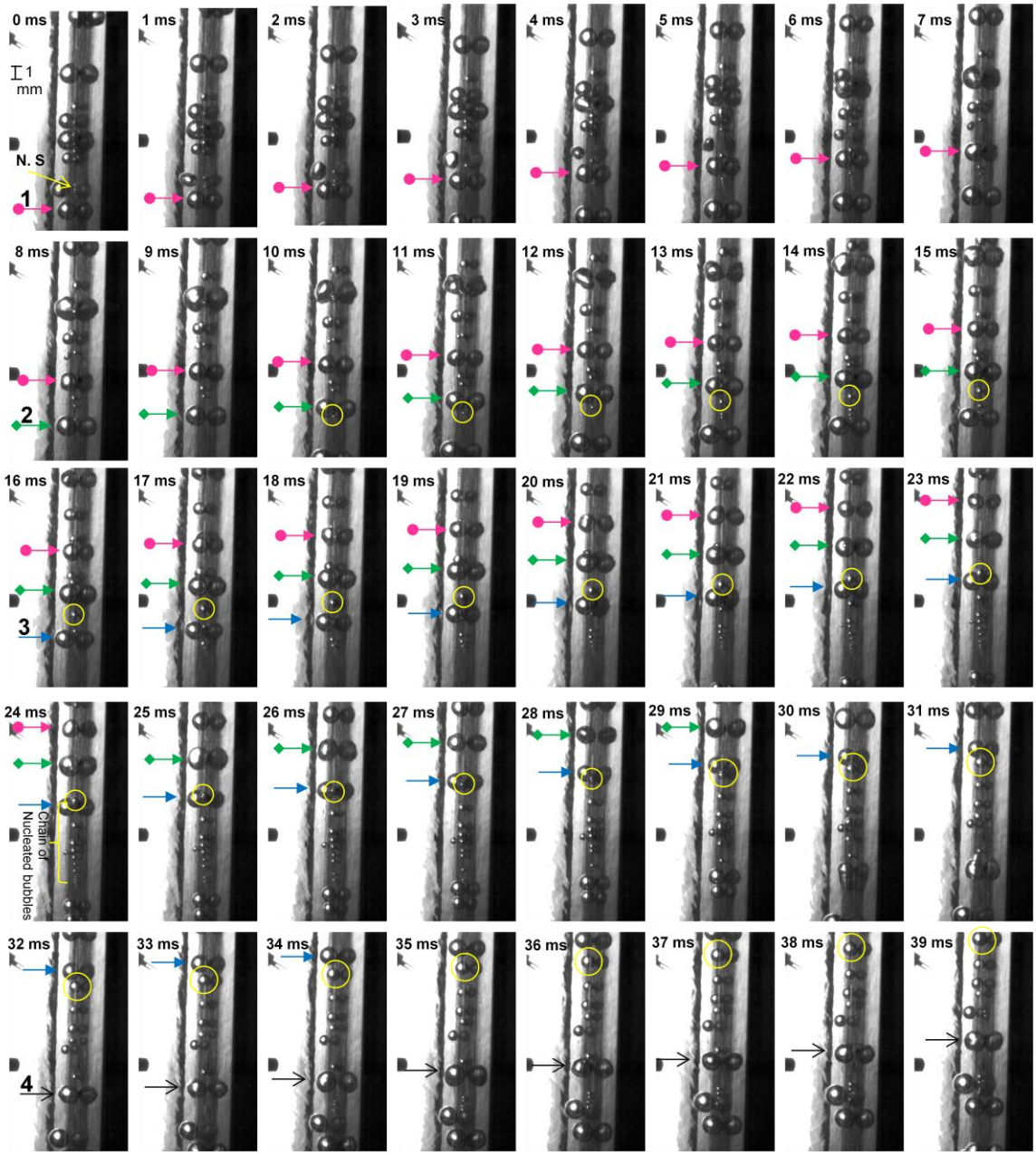

Fig. 5.10 Example of wake-effect of preceding sliding bubbles on bubble generation and bubble size in Case I- Run 110

With considering two types of wake-affected and non-wake-affected bubbles, net vaporization rates are measured and depicted in Fig. 5.9a for Case I. This evidence is an example which confirms that the most of the net vaporization rates are made by the big bubbles which are formed by the wake-effect of preceding sliding bubbles, particularly after the condition of OSV. Moreover, the number of non-collapsing bubbles and the number of wake-affected bubbles is depicted in Fig. 5.12 for Case I. It is obviously seen that the number of non-collapsing bubbles sharply increased after the OSV condition. The important result is that the major part of these non-collapsing bubbles is formed by the wake-effect process. For other experimental conditions in this study, because nucleated bubbles are very tiny and bubble number density is high, it is impossible to separate and measure accurately two types of wake-affected and non-wake-affected bubbles. However, a visual observation through movie data is carried out to be certain that the bubble generation rate and their growing is enhanced in the wake region of preceding sliding bubbles when the OSV condition is reached.

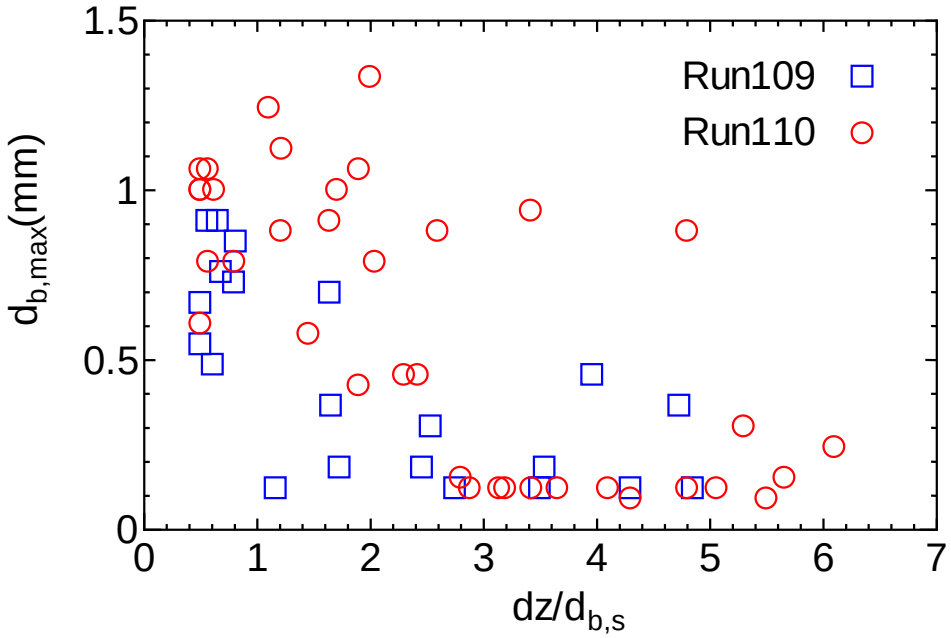

Fig. 5.11 $d_{b,max}$ against dimensionless distance from nucleation site $dz/d_{b,p}$ at the moment of bubble nucleation for Runs 109 and 110.

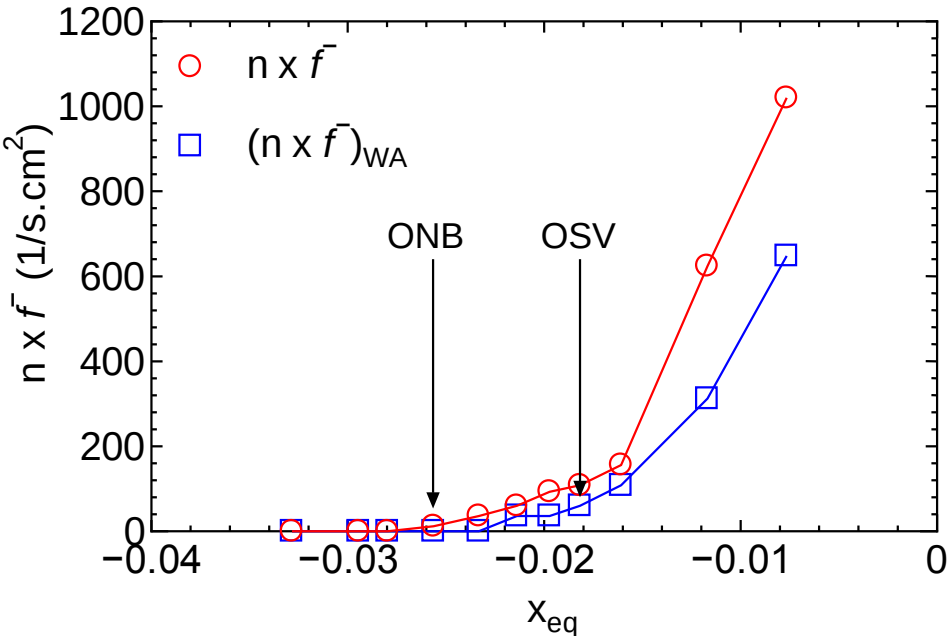

Fig. 5.12 The number of total and wake-affected of non-collapsing bubble generation on the thermal-equilibrium vapor quality in Case I

5.4 Conclusion

Visual experimental study of bubble generation in vertical, upward subcooled flow boiling is carried out using a high-speed camera to explore mechanism of net vapor generation. A rather hydrophilic surface of copper is used as a heated surface which is mounted in a part of the one side of the rectangular channel. Experiments are conducted under moderate pressure and wide ranges of mass flux, injecting water from high subcooling temperature to near saturation condition, step by step. Bubble departure from active nucleation site is initiated from ONB condition when first bubble appears on the heated surface. Throughout the present experiments, because Jakob numbers are low, bubbles after departure typically slide on the heated surface [33]. Therefore, it is concluded that the former mechanisms of bubble departure or bubble lift-off from nucleation site or heated surface does not appear to explain the NVG phenomenon for the present experimental conditions.

The triggering mechanism of NVG is investigated by considering one-dimensional mass conservation for the vapor phase with measuring of the apparent vaporization and condensation rates by image analysis process. Three typical bubble behaviors are observed in this study: some bubbles are growing while sliding for a long distance (type-A), some bubbles slide and then coalesce with some preceding sliding bubbles (type-B) and some others collapse in the subcooled liquid (type-C). Close to the condition of ONB, since few small bubbles are created on the heated surface, the vaporization rates and therefore void fraction are low. It is found that the few production of big sliding bubbles mainly contributed to the significant increase of void fraction at the condition of OSV. The visual investigation reveals that the sliding bubbles which come

from upstream flow affect bubble generation and bubble growth rate in the downstream flow, particularly in the conditions after OSV. It is observed that when a big sliding bubble passes over the active nucleation site a chain of nucleated bubbles immediately is created in the wake region of this sliding bubble and then some of them gain volume very fast. It can be assumed that, due to two-phase heat transfer between the preceding sliding bubbles and subcooled liquid the subcooling temperature is diminished in the wake region of sliding bubbles. Therefore, a possible explanation for the increase of the bubbles size after OSV is that, the bubbles are mainly formed in the lower subcooling condition which is prepared by the preceding sliding bubbles' wake. Therefore, the wake-effect of the preceding sliding bubbles plays an important role to increase void fraction significantly after OSV condition by enhancing vaporization rate.

References

[1] J.G. Collier, J.R. Thome, Convective Boiling and Condensation, third ed., Oxford University Press, Oxford, 1994. pp. 325–374.

[2] S.C. Lee, S.G. Bankoff, Prediction of the onset of flow instability in transient subcooled flow boiling, Nuclear Engineering and Design 139 (1) (1993) 149–159.

[3] A. Hainoun, E. Hicken, J. Wolters, Modeling of void formation in the subcooled boiling regime in the ATHLET code to simulate flow instability for research reactors, Nuclear Engineering and Design 167 (1996) 175–191.

[4] S.M. Ghiaasiaan, Two-Phase Flow, Boiling, and Condensation in Conventional and Miniature Systems, Cambridge University Press, New York, 2008. pp. 341–346.

[5] A. Satou, Y. Maruyama, H. Nakamura, A new model for onset of net vapor generation in fast transient subcooled boiling, Journal of Power and Energy Systems 5 (3) (2011) 263-278.

[6] P.G. Kroeger, N. Zuber, An analysis of the effects of various parameters on the average void fractions in subcooled boiling, International Journal of Heat and Mass Transfer 11 (2) (1968) 211-233.

[7] P. Saha, N. Zuber, Point of net vapor generation and vapor void fraction in subcooled boiling, Proceedings of the 5th International Heat Transfer Conference, Tokyo, 1974, pp. 175-179.

[8] R.W. Bowring, Physical model based on bubble detachment and calculation of steam voidage in the subcooled region of a heated channel, OECD Halden Reactor Project Report HPR-10, 1962.

[9] S. Levy, Forced convection subcooled boiling prediction of vapor volumetric fraction, International Journal of Heat and Mass Transfer 10 (7) (1967) 951-965.

[10] F.W. Staub, The void fraction in subcooled boiling: Prediction of the initial point of net vapor generation. Journal of Heat Transfer 90 (1968) 151–157.

[11] J.T. Rogers, M. Salcudean, Z. Abdullah, D. McLeod, D. Poirier, The onset of significant void in up-flow boiling of water at low pressure and velocities,

International Journal of Heat and Mass Transfer 30 (11) (1987) 2247-2260.

[12] Z. Rouhani, E. Axelsson, Calculation of void volume fraction in the subcooled and quality boiling regions, International Journal of Heat and Mass Transfer 13 (1970) 383–393.

[13] G.R. Warrier, V.K. Dhir, Heat transfer and wall heat flux partitioning during subcooled flow nucleate boiling–a review, Journal of Heat Transfer 128 (12) (2006) 1243-1256.

[14] F.C. Gunther, photographic study of surface-boiling heat transfer to water with force convection, J. Heat Transfer 73 (1951) 115–123.

[15] T. Okawa, T. Harada, Y. Kotsusa, Photographic study on bubble motion in subcooled pool boiling, Journal of Engineering for Gas Turbines and Power 132 (10) (2010) Paper No. 102922.

[16] E.L. Bibeau, M. Salcudean, A study of bubble ebullition in forced-convective subcooled nucleate boiling at low pressures, International Journal of Heat and Mass Transfer 37 (15) (1994) 2245-2259.

[17] V. Prodanovic, D. Fraser, M. Salcudean, Bubble behavior in subcooled flow boiling of water at low pressures and low flow rates, International Journal of Multiphase Flow 28 (2002) 1–19.

[18] T. Okawa, T. Ishida, I. Kataoka, M. Mori, An experimental study on bubble rise path after the departure from a nucleation site in vertical upflow boiling, Experimental Thermal and Fluid Science 29 (3) (2005) 287–294.

[19] T. Okawa, T. Ishida, I. Kataoka, M. Mori, Bubble rise characteristics after the departure from a nucleation site in vertical upflow boiling of subcooled water, Nuclear Engineering and Design 235 (10-12) (2005) 1149–1161.

[20] M. Akiyama, F. Tachibana, Motion of vapor bubble in subcooled heated channel, Bulletin of JSME 17 (1974) 241-247.

[21] O. Zeitoun, M. Shoukri, Bubble behavior and mean diameter in subcooled flow boiling, Journal of Heat Transfer 118 (1996) 110–116.

[22] R. Situ, Y. Mi, M. Ishii, M. Mori, Photographic study of bubble behaviors in forced

convection subcooled boiling, International Journal of Heat and Mass Transfer 47 (2004) 3659–3667.

[23] A.H. Abdelmessih, F.C. Hooper, S. Nangia, Flow effects on bubble growth and collapse in surface boiling, International Journal of Heat and Mass Transfer l5 (1972) 115-126.

[24] S. Maity, Effect of velocity and gravity on bubble dynamics, M.S. thesis, University of California, Los Angeles, 2000.

[25] G.E. Dix, Vapor void fraction for forced convection with subcooled boiling at low flow rates, General Electric Report NEDO-10491 (Ph.D. thesis, University of California, Berkeley), 1971.

[26] H.C. Unal, Determination of the initial point of net vapor generation in flow boiling systems, International Journal of Heat and Mass Transfer 18 (1975) 1095-1099.

[27] G.E. Thorncroft, J.F. Klausner, R. Mei, An experimental investigation of bubble growth and detachment in vertical upflow and downflow boiling, International Journal of Heat and Mass Transfer 41 (1998) 3857–3871.

[28] O. Zeitoun, M. Shoukri, Axial void fraction profile in low pressure subcooled flow boiling, International Journal of Heat and Mass Transfer 40 (1997) 869–879.

[29] L.W. Hu, C. Pan, Prediction of void fraction in convective subcooled boiling channels using a one-dimensional two-fluid model, Journal of Heat Transfer 117 (1995) 799–803.

[30] A. Hainoun, E. Hicken, J. Wolters, Modeling of void formation in the subcooled boiling regime in the ATHLET code to simulate flow instability for research reactors, Nuclear Engineering and Design 167 (1996) 175–191.

[31] J.Y. Tu, G.H. Yeoh, On numerical modeling of low-pressure subcooled boiling flows, International Journal of Heat and Mass Transfer 45 (2002) 1197–1209.

[32] J.L. Xu, T.N. Wong, X.Y. Huang, Two-fluid modeling for low-pressure subcooled flow boiling, International Journal of Heat and Mass Transfer 49 (2006) 377–386.

[33] R. Ahmadi, T. Ueno, T. Okawa, Bubble dynamics at boiling incipience in subcooled upward flow boiling, International Journal of Heat and Mass Transfer 55 (1-3)

(2012) 488-497.

[34] R. Ahmadi, T. Ueno, T. Okawa, Experimental identification of the phenomenon triggering the net vapor generation in upward subcooled flow boiling of water at low pressure, International Journal of Heat and Mass Transfer 55 (21-22) (2012) 6067–6076

[35] S.C. Lee, S.G. Bankoff, A comparison of predictive models for the onset of significant void at low pressures in forced-convection subcooled boiling, Journal of Mechanical Science and Technology 12 (3) (1998) 504-513.

CHAPTER 6 INFLUENCE OF SURFACE WETTABILITY ON BUBBLE DYNAMICS AND VOID EVOLUTION

6.1 Introduction

The point of net vapor generation is mainly known as position which bubbles can depart from the wall. It has been proposed that this condition is controlled either hydrodynamically or thermally. Among the early proposals for thermally controlled departure are those by Griffith et al. [1], Bowring [2] and Dix [3]. These three criteria are based on the assumption that at OSV the wall heat flux is balanced by heat removal due to liquid subcooling. Levy [4] introduced a hydrodynamically based model, assuming that the bubble detachment is primarily the result of drag (or shear) force overcoming the surface tension force. Saha and Zuber [5] postulated that both the hydrodynamic and the heat-transfer mechanisms may apply. In addition, in some study OSV was defined a point where bubble was lifted off from the heated surface [6].

For all the addressed models the crucial processes are similar in their treatment and were fundamentally based on bubble behavior. Many experimental studies were carried out to observe bubble behavior in various configurations and different experimental conditions. As expressed in detail in chapter 3 to 5, close to atmospheric pressure, bubbles typically depart from nucleation sites and after short sliding tend to lift off from the wall and then immediately collapse in subcooled liquid. In some experimental study at elevated pressure, bubbles depart from nucleation site and slide on the heated surface. Moreover, in some experimental conditions bubbles may be restricted to some extent if the heated surface is less hydrophilic [7].

The influence of surface property on bubble dynamics and void fraction was few considered in subcooled flow boiling. It is understood that, heat transfer is improved with an increase in surface wettability [8]. A decrease in contact angle decreases the population of bubble nucleation sites by reducing the effective radii of individual site [9]. The distribution of cavities of different sizes and shapes strongly depends on the manufacturing conditions and the procedure that is used to polish the surface [10]. Basu et al. [10] expressed that bubble nucleation is contingent upon two conditions: the corresponding cavity is available on the surface, and the cavity is not flooded i.e., it contains gas or vapor. He argued that flooding of cavities depends on the shape of the cavities and the wettability of the surface. As contact angle inclines to zero all the cavities will be flooded and therefore number of active nucleation site diminishes.

John ID. Bernardin et al. [12] studied dependence of contact angle on temperature. They used a polished aluminum surface. Two distinct temperature-dependent regimes were reported. They measured contact angle below 120°C at relatively constant value of 90°. In the high temperature regime, above 120°C, the contact angle decreased in a fairly linear manner.

On the hydrophilic surface, regard with the bubble behavior at boiling incipience different mechanisms of void evolution at OSV was proposed, in chapter 4 and 5. In atmospheric pressure conditions, since all bubbles after nucleation were lifted off into the subcooled bulk liquid and collapsed completely near their origin of formation, it was observed that void cannot increase downstream of ONB. It was expressed that reattachment of the lift-off bubbles toward heated surface in proximity of OSV led to bubbles grew up while sliding on heated surface, and hence contributed sharply increase of void fraction in that condition. In consequence, mechanism of void evolution for sliding bubbles under moderate pressure was investigated with similar approach in

chapter 5. In this condition, the significant increase of the void fraction at OSV is contributed to the formation of extensive big sliding bubbles which is induced by the wake-effect of the preceding sliding bubbles.

The present study aims to understand effect of surface contact angle on bubble dynamics and void evolution in subcooled flow boiling.

6.2 Experimental Description

It is found in chapter 3 that system pressure is dominant parameter that influence behavior of bubbles created on the hydrophilic surface with low contact angle. Therefore, in this chapter, to identify influence of contact angle on bubble dynamics heated surface with different contact angle is used in low and high pressure. Experiment data are accumulated in upper measuring section, and the experimental procedure is the same as introduced in chapter 4 and 5.

Various contact angles can be achieved by different surface finishes, oxidation, or coatings. The metal ions combine with oxygen to form metal oxides that precipitate around the mouth of the cavities or at the base of bubbles, where high heat and mass transfer gradients exist [11]. In chapter 3 to 5 the oxidized surface was used as heated surface; therefore, contact angle was rather low of 18°. In present experimental work, heated surface is treated using Pikal paste for polishing copper surface, which it does not scratch heated surface. Static advancing contact angle of the heated surface was measured before and after each series of experiment at ambient temperature. In order to measure contact angle, heater block was dismantled from rectangular test section. An instrument with PG-X (FIBRO system AB) model was used to measure contact angle as a way to

measure surface wettability. A liquid droplet applied on a solid substrate will interact with the surface. This interaction can be described as wetting, when the liquid droplet spreads across the surface without penetration. A digital image of the droplet profile was analyzed manually to derive the static contact angle.

In present work, experiments are performed in low mass flux and three categories of system pressures of 100, 200 and 400 kPa. In each system pressure, several series of experiment are carried out with different surface contact angle. In each series of experiment, the value of P, G and q_w are fairly kept constant throughout all series of experiment and the only parameter of liquid subcooling ΔT_{sub} is decreased, step by step. The range of subcooling covers the subcooled flow boiling region from close to ONB condition to near saturation boiling. For all stages of the experiments wall superheat temperature ΔT_w, thermal equilibrium quality x_{eq} and time-average cross-sectional void fraction $<\alpha>$ were calculated and represented in the tables 6.1 to 6.7. In these tables, φ_1 and φ_2 represent contact angle value before and after experiment, respectively.

In the present experiment, when heated surface is polished contact angle is around 90°. However, when surface is heated during experiment, contact angle is changed quickly. The change rate of contact angle when surface temperature is high at elevated pressure is faster. For example, contact angle at Exp. P1.1 under 100 kPa pressure changes from 97° to 81°, but in Exp. P4.1 under 400 kPa contact angle changes from 94° to 57°.

Table 6.1 Main experimental conditions for Exp. P1.1 (φ_1=97°, φ_2=81°)

Run	P (kPa)	G (kg/m^{2}s)	q_w (kW/m^2)	ΔT_{sub} (K)	ΔT_w (K)	x_{eq}	$\langle\alpha\rangle$	Ja
1101	100	419	222	10.8	9.9	-0.01662	0.00015	30.19
1102	103	419	220	10.3	9.8	-0.01573	0.00019	29.08
1103	103	419	216	7.5	10.2	-0.01057	0.00467	30.22
1104	104	414	220	4.8	9.9	-0.00544	0.01259	29.02

Table 6.2 Main experimental conditions for Exp. P1.2 (φ_1=94°, φ_2=70°)

Run	P (kPa)	G (kg/m^{2}s)	q_w (kW/m^2)	ΔT_{sub} (K)	ΔT_w (K)	x_{eq}	$\langle\alpha\rangle$	Ja
1201	99	409	203	16.8	4.0	-0.02799	0.00000	12.35
1202 (ONB)	102	425	207	13.3	7.9	-0.02157	0.00000	23.69
1203	102	427	200	11.6	8.6	-0.01851	0.00052	25.77
1204	100	432	205	9.0	10.0	-0.01363	0.00188	30.46
1205	101	436	205	8.2	10.2	-0.01217	0.00217	30.78
1206	102	430	207	7.6	10.7	-0.01099	0.00377	31.99
1207	106	427	205	6.6	10.9	-0.00913	0.00880	31.44
1208	107	430	204	4.8	10.4	-0.00582	0.00975	29.71
1209	111	427	207	3.7	10.6	-0.00370	0.01557	29.26

Table 6.3 Main experimental conditions for Exp. P1.3 (φ_1=57°, φ_2=56°)

Run	P (kPa)	G (kg/m^{2}s)	q_w (kW/m^2)	ΔT_{sub} (K)	ΔT_w (K)	x_{eq}	$\langle\alpha\rangle$	Ja
1301	99	414	211	10.4	12.2	-0.01599	0.00000	37.54
1302	100	408	213	9.7	12.3	-0.01461	0.00020	37.49
1303	102	405	208	7.2	12.5	-0.01003	0.00208	37.36
1304	100	413	206	4.0	12.7	-0.00414	0.01171	38.58

Table 6.4 Main experimental conditions for Exp. P2.1 (φ_1=94°, φ_2=70°)

Run	P (kPa)	G (kg/m^{2}s)	q_w (kW/m^2)	ΔT_{sub} (K)	ΔT_w (K)	x_{eq}	$\langle\alpha\rangle$	Ja
2101	196	430	220	17.3	4.0	-0.03026	0.00000	6.626
2102	196	430	214	15.0	5.4	-0.02588	0.00000	8.933
2103 (ONB)	198	429	216	13.1	7.3	-0.02238	0.00000	11.95
2104	198	430	215	12.3	8.0	-0.02073	0.00002	13.09
2105	198	428	217	11.3	8.6	-0.01875	0.00008	14.06
2106	198	430	218	10.3	9.0	-0.01697	0.00029	14.71
2107	197	429	220	9.1	9.3	-0.01456	0.00079	15.26
2108	199	430	219	8.3	9.3	-0.01312	0.00180	15.11
2109	198	428	221	7.2	9.6	-0.01086	0.00529	15.66
2110	197	427	223	6.1	10.0	-0.00876	0.00757	16.37
2111	196	428	227	3.8	10.2	-0.00426	0.01503	16.75
2112	197	430	226	1.9	10.6	-0.00061	0.02289	17.31

Table 6.5 Main experimental conditions for Exp. P2.2 (φ_1=94°, φ_2=57°)

Run	P (kPa)	G (kg/m^{2}s)	q_w (kW/m^2)	ΔT_{sub} (K)	ΔT_w (K)	x_{eq}	$\langle\alpha\rangle$	Ja
2201	198	410	221	12.3	8.5	-0.02041	0.00001	13.91
2202	198	411	221	10.2	9.1	-0.01639	0.00016	14.87
2203	200	414	222	7.5	9.6	-0.01145	0.00264	15.52
2204	196	399	219	3.8	8.8	-0.00398	0.01192	14.45

Table 6.6 Main experimental conditions for Exp. P2.3 (φ_1=57°, φ_2=57°)

Run	P (kPa)	G (kg/m^{2}s)	q_w (kW/m^2)	ΔT_{sub} (K)	ΔT_w (K)	x_{eq}	$\langle\alpha\rangle$	Ja
2301	198	415	216	11.9	9.4	-0.01998	0.00005	15.38
2302	200	419	217	11.2	9.9	-0.01863	0.00019	16.04
2303	200	418	217	10.4	10.1	-0.01717	0.00050	16.36
2304	200	410	219	7.2	10.6	-0.01089	0.00323	17.13
2305	201	417	220	4.4	10.9	-0.00547	0.01385	17.5

Table 6.7 Main experimental conditions for Exp. P4.1 (φ_1=94°, φ_2=57°)

Run	P (kPa)	G (kg/m^{2}s)	q_w (kW/m^2)	ΔT_{sub} (K)	ΔT_w (K)	x_{eq}	$\langle\alpha\rangle$	Ja
4101	393	385	246	11.8	8.4	-0.01976	0.00008	7.376
4102	403	384	241	8.8	8.8	-0.01381	0.00037	7.538
4103	398	387	246	5.2	10.1	-0.00655	0.00435	8.727
4104	404	373	245	2.0	10.3	0.00013	0.01737	8.761

6.3. Experimental results

6.3.1. Bubble dynamics

Close to ONB condition, on the hydrophilic surface with low contact angle two types of bubble behavior are observed, in chapter 3. Close to atmospheric pressure when Jakob number is high, bubbles after formation on the nucleation sites lift off from surface and then collapse immediately in the subcooled liquid. In elevated pressure Jakob number is low; in this condition bubbles leave nucleation sites and slide on the heated surface. In the present experiment, on the surface with high contact angle bubbles typically stick to their nucleation sites close to ONB condition. The typical behavior of bubbles close to ONB condition is shown in Fig. 6.1a and b, for experiments with high contact angle. It is observed that no bubble lifts off from surface or slide on the surface, and bubbles just grow and shrink at which they are formed. The behavior of bubbles at ONB condition alters from attachment to detachment as surface property turns to the wettable state. For instance, in the experiments performed under pressure 100 kPa, all bubbles stick to nucleation sites in Exp. P1.1, some bubbles stick to nucleation sites and some bubbles lift

off from surface in Exp. P1.2, and all bubbles lift off from surface in Exp. P1.3, in the condition close to ONB.

For more understanding of the influence of contact angle in subcooled flow boiling, data of three series of experiments which are investigated in previous chapters with low surface contact angle of 18° will be considered with the present experimental series. These are Exp. No. 1 in chapter 4, experiments Case I and Case II in chapter 5; which they are considered in the pressure class of 100, 200 and 400 kPa, respectively.

Close to ONB condition, the measurement results of nucleation site density are shown in Fig 6.2, for two system pressure of 100 and 200 kPa. On the surface with low contact angle, the effective radii of individual sites are small [9], and even if many cavities are available some of them may not work as active nucleation sites due to flooding [10]. Therefore, in Fig. 6.2 it is seen that with the decrease of surface contact angle population of nucleation site density decreases for both system pressure. In this figure, the average contact angle of the values measured before and after each experiment is assumed as contact angle quantity. Because in low contact angle active nucleation site is rare, higher wall superheat is needed to nucleation site be able to produce vapor bubbles. Wall superheat temperature for experiments under 100 and 200 kPa are measured and are shown in Fig 6.3. In each system pressure four series of experiment with different surface contact angle are considered. This figure confirmed that at experiment with lower contact angle the wall superheat temperature is higher.

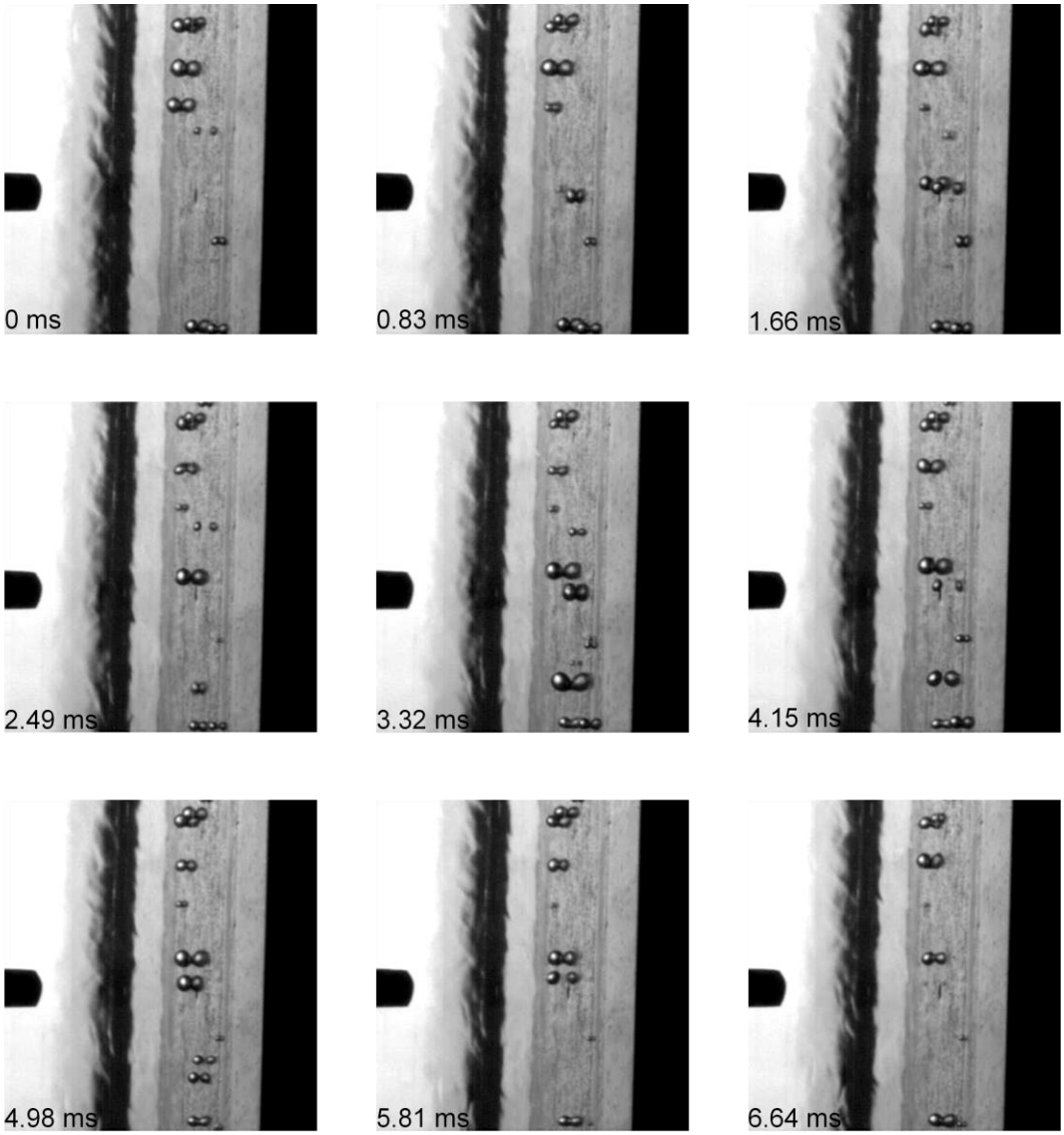

Fig. 6.1a Typical bubble behavior observed close to ONB condition in Exp. P1.1 with high contact angle (Run 1101)

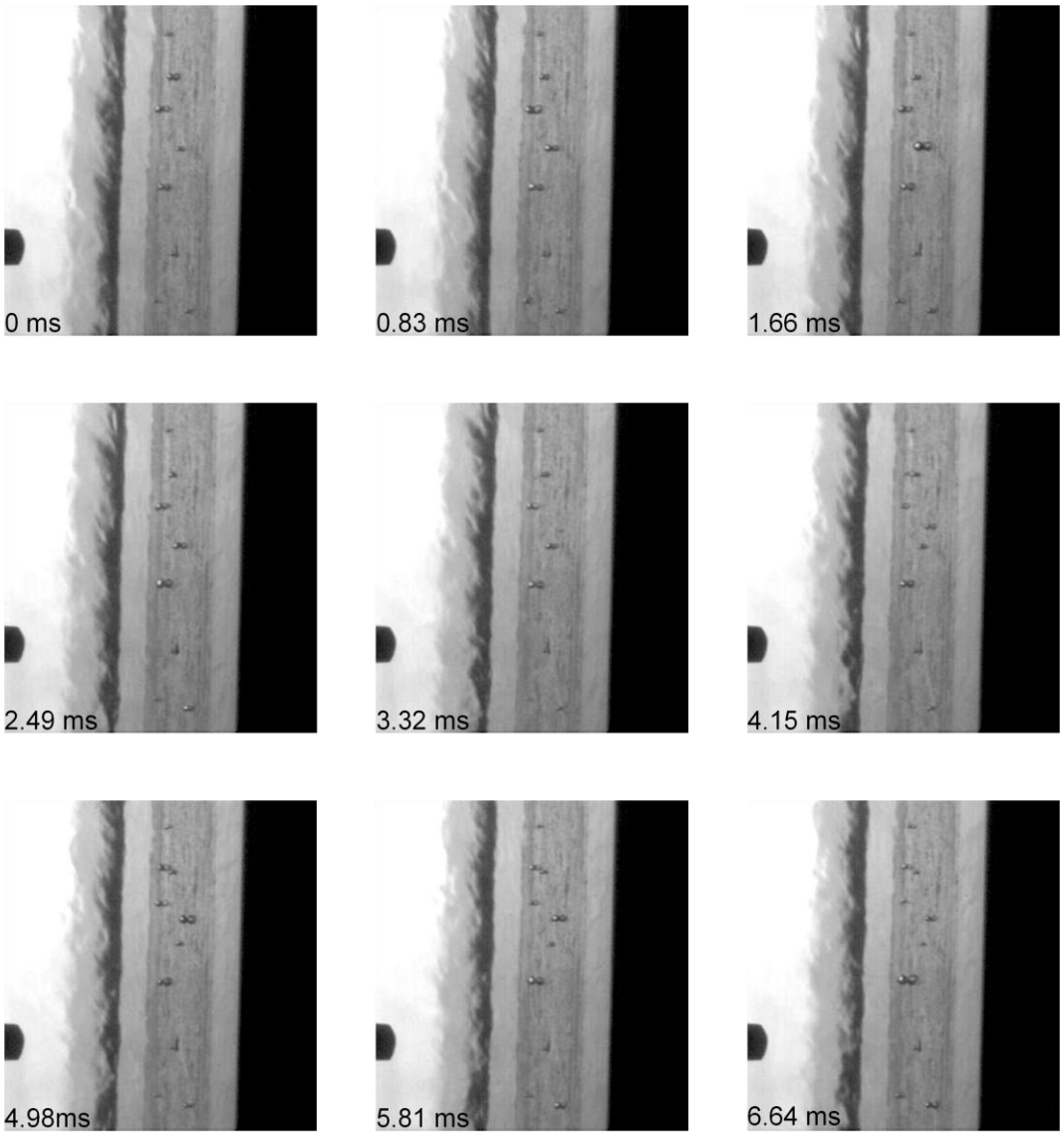

Fig. 6.1b Typical bubble behavior observed close to ONB condition in Exp. P2.2 with high contact angle (Run 2201)

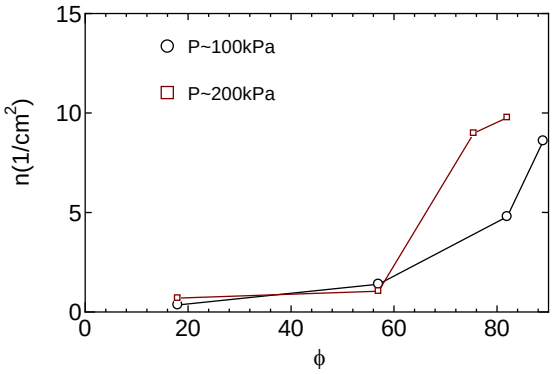

Fig. 6.2 Dependence of nucleation site density to surface contact angle

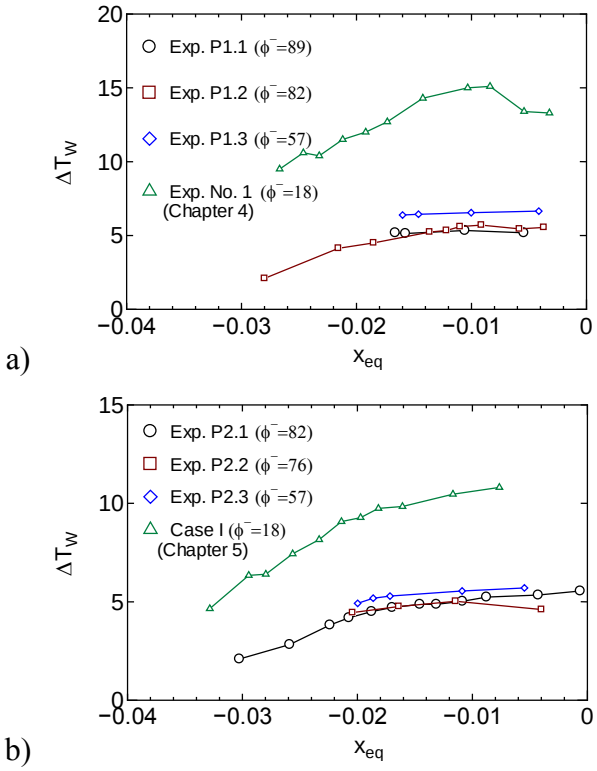

Fig. 6.3 Superheat temperature during subcooled flow boiling at different surface contact angle (a) experiments at P~100 kPa, and (b) experiments at P~200 kPa

6.3.2. NVG mechanism

In the present experimental series, the subcooled liquid temperature is gradually decreased to increase thermal equilibrium quality in the channel. The status of the void content in the channel is monitored during subcooled flow boiling using high speed camera. Using movie data, the average void fraction can be easily estimated by

$$<\alpha>=\frac{1}{V_0 N_{\mathrm{im}}}\sum_{\mathrm{i=1}}^{N_{\mathrm{im}}}\sum_{\mathrm{j=1}}^{N_{\mathrm{b,i}}}V_{\mathrm{b,ij}} \tag{3}$$

where V_0 is the volume of the visualization area, N_{im} is the number of images considered in the void measurement, and $N_{b,i}$ is the number of bubbles within i-th image. The number of images considered in the void fraction measurements is so as the relative error of measured void fraction is small enough.

The measurement results of average void fractions are shown for all experimental condition in three categories of system pressure, in Fig 6.4a-c. In this figure, ONB and OSV condition is indicated only for experiments Exp. No. 1, Case I and Case II. It is seen that the void fraction trends are similar in their increment in each pressure class; void fraction increases significantly at OSV condition indicated in each figure. It is noted that, if bubble stick to nucleation site, it in fact hinders bubble generation on the nucleation site for the period of attachment. In this case, bubble departure from nucleation site is a preliminary condition to bubble generation be continues on the heated surface. However, as was observed in chapter 4 and 5 bubble departure from nucleation sites is not sufficient condition to void fraction increase in the channel.

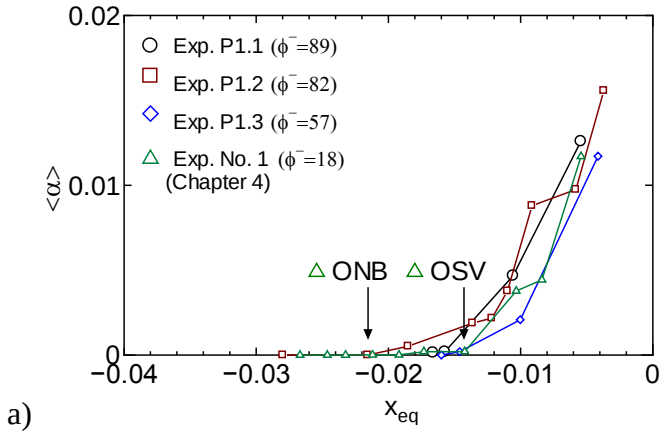

a)

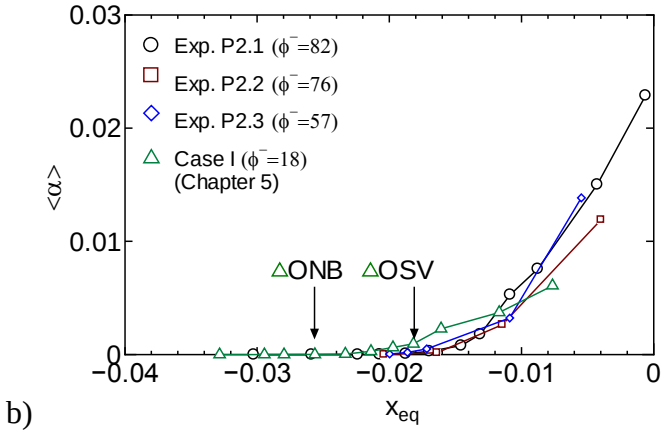

b)

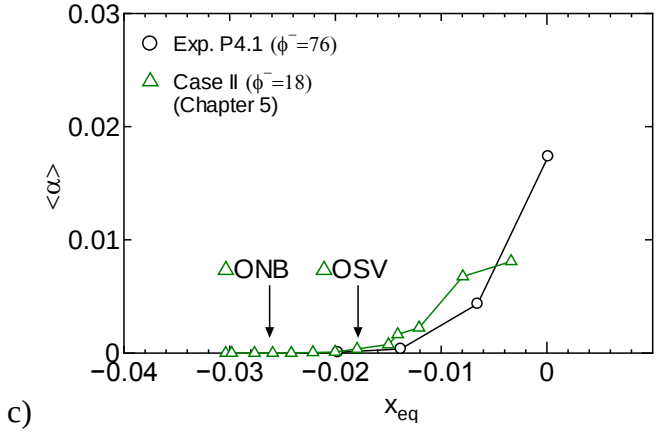

c)

Fig. 6.4 Dependence of the time-average cross-sectional void fraction on the thermal-equilibrium vapor quality; (a) experiment at P~100 kPa, (b) experiment at P~200 kPa, and (c) experiment at P~400 kPa.

In the present experiments on surface with high contact angle or low wettability, it is observed that the bubble detachment occurs in proximity of OSV condition. In the atmospheric pressure, bubbles although tend to lift off from surface after departure, some reattachment of bubbles takes place at the moment of lift off. Figure 6.5 demonstrates example of reattachment of lift-off bubble close to OSV condition, in Exp. P1.1 Run 1102. The reattached bubbles are indicated in the circles. On the surface with high contact angle, bubbles are held strongly to nucleation site by surface tension force. Therefore, bubbles do not move far away from heated surface while they lift off from surface with low velocity. As the result, bubble reattachment takes place coincident with bubble departure close to the condition OSV. Hence, it is concluded that in hydrophobic surface bubble departure followed by bubble reattachment to contribute void fraction increase sharply at the condition of OSV reaches, in atmospheric pressure.

In elevated pressure, when bubbles depart from nucleation sites with high contact angle, they slide on the heated surface. Because nucleation site density on the surface with high contact angle is higher than low contact angle, when a bubble departs from nucleation site and slides on the heated surface, it can affect many nucleation sites. Sliding bubbles can merge with attached bubbles on other nucleation sites. Moreover, sliding bubbles can induce nucleation sites to produce new bubbles and grow up in the wake region of sliding bubbles. An example of effect of preceding sliding bubbles on the bubble generation on nucleation site is shown in Fig. 6.6, for Exp. P2.2 Run 2202. In this figure, two sliding bubbles which come from down slide over a nucleation site, and cause to produce big sliding bubbles in the wake region. Therefore, in elevated pressure bubble departure coincides with the wake-effect of preceding sliding bubble to cause void fraction significantly increase at OSV, in the hydrophobic surface.

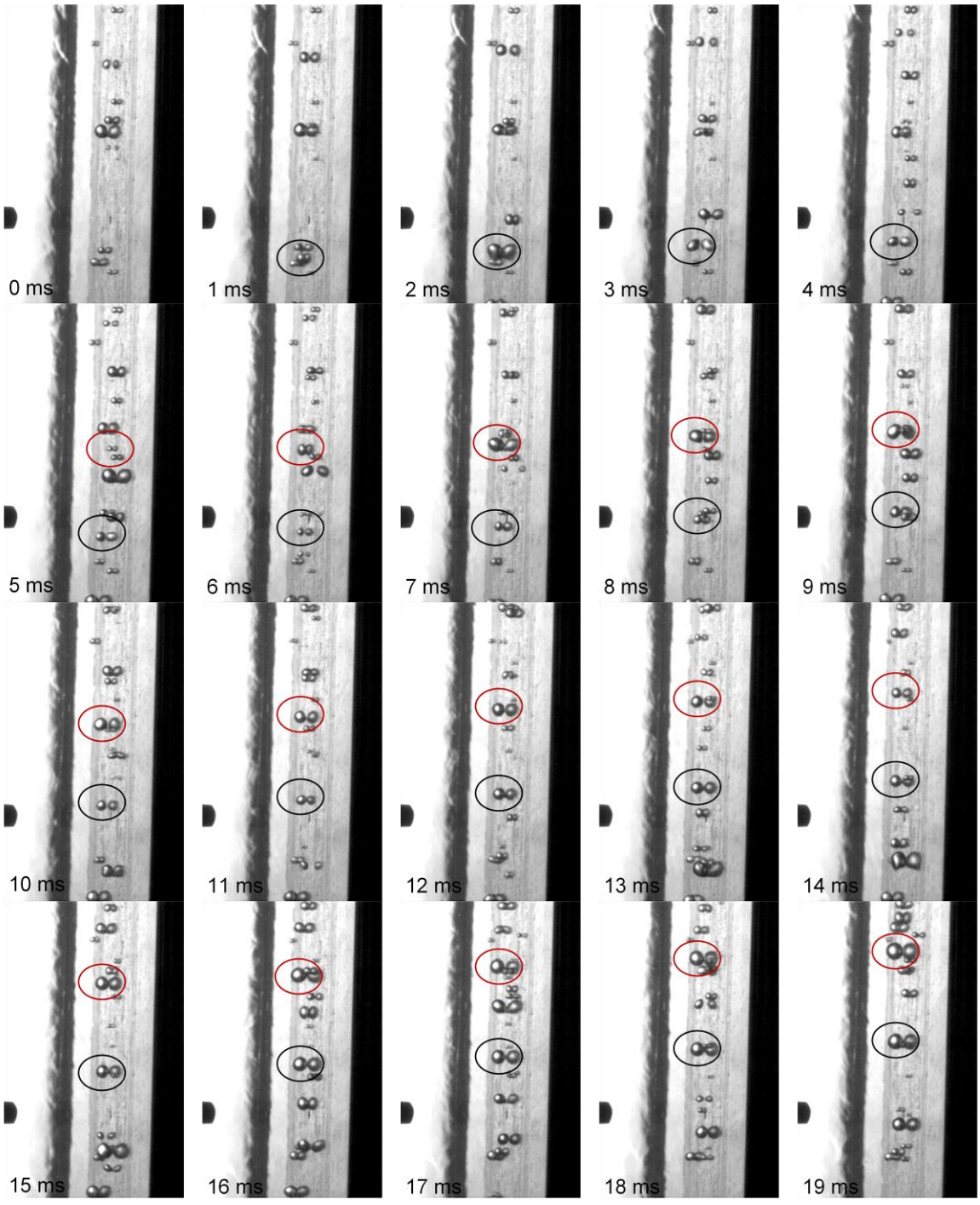

Fig. 6.5 Example of bubble reattachment close to OSV condition in Exp. P1.1, Run 1102

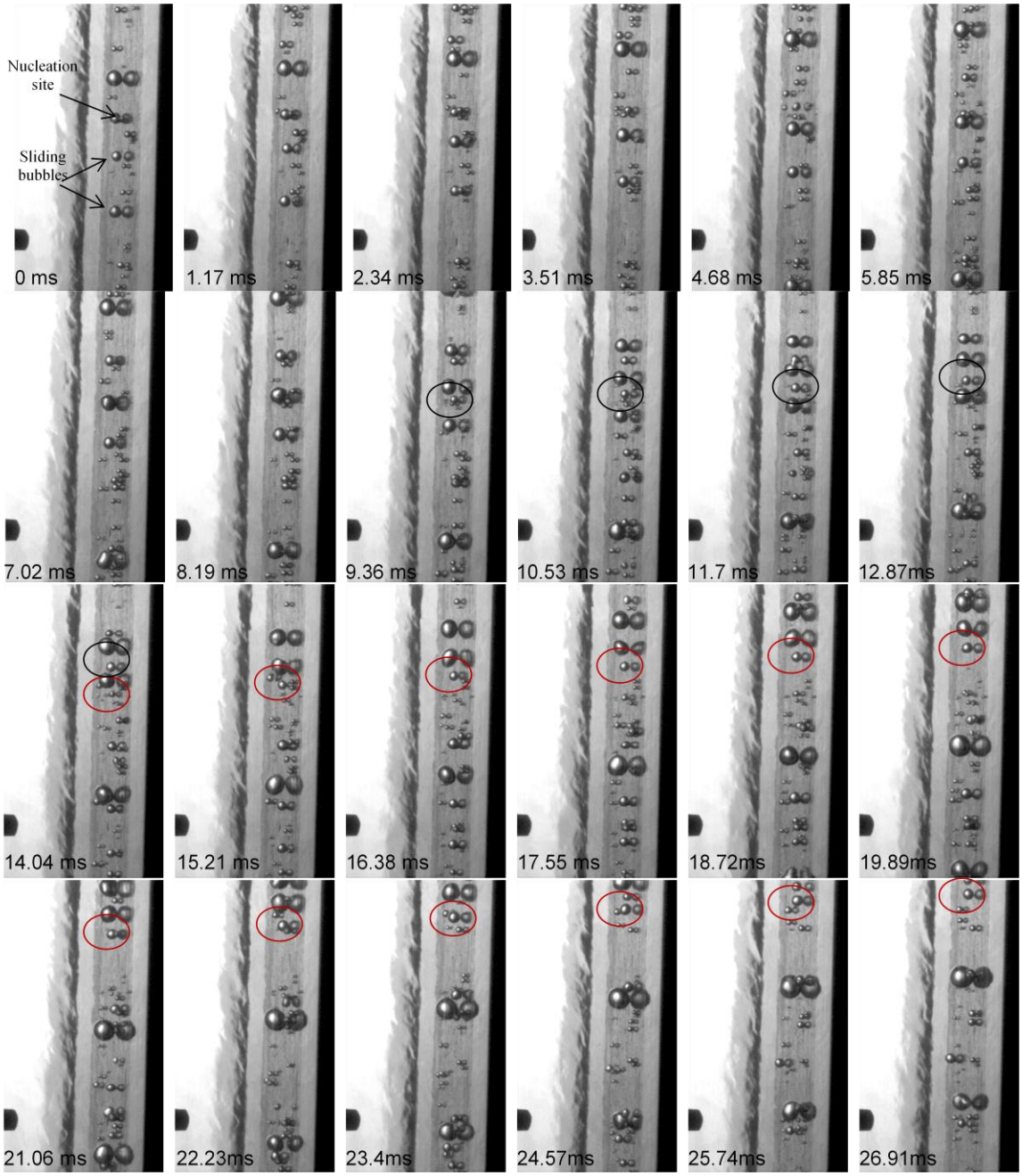

Fig. 6.6 Example of bubble generation in the wake region of preceding sliding bubbles close to OSV condition in Exp. P2.2, Run 2202

6.4. Conclusion

In the present work, influence of contact angle on bubble dynamics and void evolution is investigated with visual method. Close to ONB condition, it is observed that bubble behavior is substantially different in different surface contact angle. Bubbles stick to nucleation site in hydrophobic surface, and they depart from nucleation site in hydrophilic surface. In hydrophilic surface, bubble departure follows with lift-off from surface under atmospheric pressure, and sliding on heated surface under elevated pressure. OSV mechanism was considered for hydrophilic surface, in chapter 4 and 5. In hydrophobic surface, it is observed that the bubble detachment occurs in proximity of OSV condition. It is noted that bubble departure causes to new bubbles can be able to create on the nucleation site. In atmospheric pressure condition, it is observed that in some nucleation sites bubble departure follows by bubble reattachment to contribute void fraction increase sharply when the condition of OSV reaches. In elevated pressure, bubble departure coincides with the wake-effect of preceding sliding bubble to cause void fraction significantly increase at OSV.

References

[1] Griffith, P. J., Clark, A., and Rohsenow, W. M. Void Volumes in Subcooled Boiling Systems. ASME paper 58-HT-19, 1958.

[2] R.W. Bowring, Physical model based on bubble detachment and calculation of steam voidage in the subcooled region of a heated channel, OECD Halden Reactor Project Report HPR-10, 1962.

[3] G.E. Dix, Vapor void fraction for forced convection with subcooled boiling at low flow rates, Ph.D. Thesis, University of California, Berkeley, CA, 1971.

[4] S. Levy, Forced convection subcooled boiling prediction of vapor volumetric fraction, International Journal of Heat and Mass Transfer 10 (1967) 951–965.

[5] P. Saha, N. Zuber, Point of net vapor generation and vapor void fraction in subcooled boiling, Proceedings of the 5th International Heat Transfer Conference, Tokyo, 1974, pp. 175-179.

[6] G.R. Warrier, V.K. Dhir, Heat transfer and wall heat flux partitioning during subcooled flow nucleate boiling–a review, Journal of Heat Transfer 128 (12) (2006) 1243-1256.

[7] T. Okawa, T. Harada, Y. Kotsusa, Photographic study on bubble motion in subcooled pool boiling, Journal of Engineering for Gas Turbines and Power 132 (2010) art. no. 102922.

[8] Liaw, S. P., and Dhir, V. K., Effect of surface wettability on transition boiling heat transfer from a vertical surface, Proceedings of the Eighth International Heat Transfer Conference, San Francisco, CA., Vol. 4, (1989) pp. 2031–2036.

[9] R.I. Eddington, and D.B.R. Kenning, The effect of contact angle on bubble nucleation, International Journal of Heat and Mass Transfer 22 (1979) 1231–1236.

[10] N. Basu, G.R. Warrier, V.K. Dhir, Onset of nucleate boiling and active nucleation site density during subcooled flow boiling, Journal of Heat Transfer 124 (2002) 717–728.

[11] S.G. Kandlikar, M. Shoji, V.K. Dhir, Handbook of Phase Change: Boiling and

Condensation, Taylor & Francis, London, 1999.

[12] John ID. Bernardin et al., Contact angle temperature dependence for water droplets on practical aluminum surfaces, International Journal of Heat and Mass Transfer 40 (1996) 1017–1033.

CHAPTER 7 CONCLUSION

7.1 Summarizes and Conclusions

Visual experimental investigations are carried out in subcooled upward flow boiling to explore bubble dynamics and phenomenological mechanisms causes the significant increase of void fraction at onset of significant void (OSV) condition. Because of practical use of wettable surface, bubble dynamics is first investigated on a hydrophilic heated surface at the onset of nucleate boiling in water subcooled flow boiling. The flow direction is vertical upward. The pressure, mass flux and liquid subcooling are used as the main experimental parameters. The main conclusions found from the investigation on bubble dynamics are summarized as follows:

(1) The size and behavior of bubbles were significantly dependent on the pressure. The difference of the typical bubble diameter was greater than one order of magnitude between the experiments performed under the atmospheric and elevated pressures. In the experiments under the atmospheric pressure, most bubbles lifted off the heated surface within a short time after nucleation. Since the bubbles were collapsed rapidly in subcooled bulk liquid after the lift-off, the bubble lifetime was generally short. In contrast, bubbles usually slid along the vertical heated surface in the experiments under the elevated pressures. In this case, most bubbles traveled long distance, although some bubbles condensed to disappear during sliding in the experiments of high liquid subcooling.

(2) The wall superheat at the onset of nucleate boiling was higher in the experiments under the atmospheric pressure mainly due to low vapor density. In consequence, the

Jakob number based on the wall superheat decreased with an increase in the pressure. It was shown that the boundary between the lift-off and sliding in the present experiments can be determined in terms of the Jakob number. It was also indicated that the bubble size scaled by the superheated layer thickness tended to increase with increased value of the Jakob number.

(3) The unsteady growth force, the time variation of the bubble shape and the condensation at the sidewall of the bubble were considered as the possible mechanisms to cause the bubble lift-off. It was considered that the bubble behavior observed in this work could be characterized in terms of the Jakob number since the three effects mentioned above are intensified with an increase in this dimensionless parameter.

From results found in above, it is concluded that for wettable surface neither bubble departure nor bubble lift-off from nucleation site or heated surface is triggering mechanism of NVG. Therefore, in next stage, NVG mechanism is investigated for the condition that bubbles lift off from surface at ONB condition. Under atmospheric pressure condition, the inlet liquid subcooling was gradually decreased to change the thermal-equilibrium quality at the measuring section parametrically. At the high values of liquid subcooling near ONB, all the bubbles were lifted off the heated wall immediately after the nucleation and then collapsed in the subcooled bulk liquid. Since the condensation rate was nearly equal to the vaporization rate, a rapid increase in the vapor void fraction with an increase in the thermal-equilibrium quality was not permitted. It was found that some bubbles could be reattached to the surface when the subcooling was low enough. Since the bubbles slid along the vertical heated surface for a long distance after the reattachment, the occurrence of the bubble reattachment contributed to the increase of the void fraction. It was also confirmed that the increase of the void fraction

caused by the bubble reattachment was in the same order of magnitude with the actual increase of the void fraction with increased value of the thermal-equilibrium quality. It can hence be said that the onset of the bubble reattachment followed by the formation of sliding bubbles played a particularly important role in causing NVG in the experimental conditions tested under atmospheric pressure.

It should however be noted that the phenomenon triggering the NVG would be dependent on several factors. For instance, it is reported in chapter 3 that the bubbles in water subcooled flow boiling were not lifted off the surface at elevated pressures. Therefore, NVG mechanism was investigated under the conditions that bubbles depart from nucleation sites at ONB condition and slide on the heated surface. Experiments are conducted under moderate pressure and wide ranges of mass flux, injecting water from high subcooling temperature to near saturation condition, step by step. A rather hydrophilic surface is used as a heated surface. Bubble departure from active nucleation site is initiated from ONB condition when first bubble appears on the heated surface. Throughout these experiments, because Jakob numbers are low, bubbles after departure typically slide on the heated surface. The triggering mechanism of NVG is investigated by considering one-dimensional mass conservation for the vapor phase with measuring of the apparent vaporization and condensation rates by image analysis process. Close to the condition of ONB, since few small bubbles are created on the heated surface, the vaporization rates and therefore void fraction are low. After the OSV condition, it is observed that wide ranges of bubble sizes are produced in the channel, which the majority number of bubbles is for small bubbles and minor for large bubbles. It is conclude that the creation of large bubbles contributed to the significant increase of vaporization rate, when the OSV condition is reached. The visual investigation reveals that the sliding bubbles which come from upstream flow affect bubble generation and

bubble growth rate in the downstream flow, particularly in the conditions after OSV. It was found that the large bubbles were mostly produced when other sliding bubbles passed over the active nucleation sites. Although complex thermal-hydraulic field formed around the sliding bubbles was not measured in this experiment, it was expected that liquid subcooling was locally reduced in the wake region of the sliding bubbles due to the enhancement of mixing. It was hence supposed that the production of large bubbles in the wake region of lower subcooling that was prepared by the preceding sliding bubbles was a key phenomenon in permitting the rapid increase of the vaporization rate as well as the void fraction at NVG.

The influence of contact angle on bubble dynamics and void evolution is investigated with visual method. Close to ONB condition, it is observed that bubble behavior is substantially different as surface contact angle is changed. Bubbles stick to nucleation site in hydrophobic surface, and they depart from nucleation site in hydrophilic surface. In hydrophobic surface, bubble departure as preliminary condition for NVG mechanism is observed in this work. In atmospheric pressure condition, it is observed that in some nucleation sites bubble departure follows by bubble reattachment to contribute void fraction increase sharply when the condition of OSV reaches. In elevated pressure, bubble departure coincides with the wake-effect of the preceding sliding bubble to cause void fraction significantly increase at OSV.

PUBLICATIONS

Journals:

1. R. Ahmadi, T. Ueno, T. Okawa, Bubble dynamics at boiling incipience in subcooled upward flow boiling, *International Journal of Heat and Mass Transfer*, Vol. 55, No. 1-3, pp. 488-497 (2012).
2. R. Ahmadi, T. Ueno, T. Okawa, Experimental identification of the phenomenon triggering the net vapor generation in upward subcooled flow boiling of water at low pressure, *International Journal of Heat and Mass Transfer*, Vol. 55, No. 21-22, pp. 6067-6076 (2012).

International Conferences:

1. R. Ahmadi, T. Ueno, T. Okawa, Influence of mass flux on bubble interaction during upward subcooled flow boiling, *7th Japan-Korea Symposium on Nuclear Thermal Hydraulics and Safety*, Paper No. N7P0026 (2010).
2. T. Okawa, Y. Yamagoe, R. Ahmadi, Void fraction evolution in subcooled flow boiling under low-pressure and low-flow condition, *14th International Topical Meeting on Nuclear Reactor Thermalhydraulics*, Paper No. 117 (2011).
3. R. Ahmadi, T. Ueno, T. Okawa, Bubble behavior in subcooled flow boiling in a vertical rectangular channel, *19th International Conference on Nuclear Engineering*, Paper No. 43556 (2011).

4. R. Ahmadi, T. Ueno, T. Okawa, Vapor bubble dynamics in upward subcooled flow boiling during void evolution, *World Academy of Science, Engineering and Technology*, Vol. 69, pp. 1133-1140 (2012).
5. R. Ahmadi, T. Ueno, T. Okawa, Visualization of bubble dynamics in water subcooled flow boiling at low pressure, *20th International Conference on Nuclear Engineering*, Paper No. 54727 (2012).
6. R. Ahmadi, T. Ueno, T. Okawa, Effect of surface wettability on void development in forced-convective subcooled nucleate boiling, *4th Korea-Japan Seminar on Nuclear Thermal Hydraulics and Safety for Students and Young Researchers* (2012)

Domestic Conferences:

1. R. Ahmadi, Y. Yamagoe, T. Okawa, Bubble coalescence effect on axial development of void fraction in subcooled flow boiling, *Annual Meeting of the Japanese Society for Multiphase Flow* (2010).
2. T. Okawa, Y. Yamagoe, R. Ahmadi, A study on axial development of vapor void fraction in subcooled flow boiling, *Annual Meeting of the Japanese Society for Mechanical Engineers* (2010).
3. T. Okawa, R. Ahmadi, T. Ueno, Mechanism of void fraction determination in subcooled flow boiling, *Annual Meeting of the Atomic Energy Society of Japan* (2010).
4. R. Ahmadi, T. Okawa, Bubble dynamics in subcooled flow boiling under low void fraction condition, *Annual Meeting of the Atomic Energy Society of Japan* (2011).

5. T. Ueno, T. Okawa, R. Ahmadi, Experimental study on bubble behavior at ONB in subcooled flow boiling, *Annual Meeting of the Japanese Society for Multiphase Flow* (2011).
6. R. Ahmadi, T. Ueno, T. Okawa, Experimental study on void fraction in low-pressure subcooled flow boiling, *Annual Meeting of the Atomic Energy Society of Japan* (2011).
7. T. Okawa, R. Ahmadi, T. Ueno, Mechanisms of void evolution in subcooled flow boiling, *15th Organized Multiphase Flow Forum* (2011).
8. R. Ahmadi, T. Ueno, T. Okawa, Visual investigation of void in the course of development in subcooled flow boiling, *Annual Meeting of the Japanese Society for Multiphase Flow* (2012).
9. T. Ueno, R. Ahmadi, T. Okawa, Reattach of the bubble in subcooled flow boiling under low pressure, *Annual Meeting of the Japanese Society for Multiphase Flow* (2012).
10. R. Ahmadi, T. Ueno, T. Okawa, Visualization Study to Investigate the NVG Mechanisms in Subcooled Flow Boiling, *Annual Meeting of the Japanese Society for Mechanical Engineers* (2012).